**High Frequency Behavior of Electrical Contact Subjected to
Vibration Induced Fretting Corrosion**

by

Haoyue Yang

A dissertation submitted to the Graduate Faculty of
Auburn University
in partial fulfillment of the
requirements for the Degree of
Doctor of Philosophy

Auburn, Alabama
Dec 17, 2017

Keywords: electrical contacts, fretting corrosion, vibration,
surface impedance, high-frequency applications

Approved by

George T. Flowers, Chair, Professor of Mechanical Engineering
Zhongyang Cheng, Professor of Materials Engineering
Robert N. Dean Jr., McWane Professor of Electrical and Computer Engineering
Michael C. Hamilton, Associate Professor of Electrical and Computer Engineering
Jeffery C. Suhling, Quina Distinguished Professor and Chair of Mechanical Engineering

Abstract

Vibration induced fretting corrosion is generally recognized as one of the major causes of failures for electrical connector systems. The major driver of fretting damage is micro-scale relative motion at contact interface which produces material displacement and transfer. For non-precious metal plated contact interfaces, this fretting motion serves to repeatedly expose fresh metal to atmospheric oxidation. This results in a rapid and substantial increase in contact resistance due to localized buildup of an insulating layer. Relative motion between contact surfaces can be induced by thermal expansion/contraction, mechanical vibration, or by a combination of these two mechanisms. Recently there has been considerable work on this topic, including experimental investigations and model development work. Much of the previous work has been focused on the increase of electrical resistance between the blade and receptacle of power and signal connectors. As the speed of data transmission increases, however, not only the contact resistance, but also the contact impedance is supposed to be considered a significant quantity in the high frequency data transfer. The physical separation of two sides of the contact interface by the corrosion products produces a capacitive effect that has not been comprehensively studied before. The present study seeks to explore this phenomenon and develop an understanding of its significance.

In the author's work, the first project investigated the influence of vibration induced fretting corrosion to contact impedance. With a higher degradation level, a remarkable capacitive characteristic was observed at fretted contacts. A corresponding statistical model was developed

to account for the fashion of development of contact capacitance. The second project studied the impact of fretting corrosion to signal transmission at a radio frequency spectrum. As contact resistance increased, the metallic contact gradually lost the transmission capability especially at a low frequency range. Using a network model, this phenomenon was explained by the capacitive property of degraded contacts as a result of build-up of insulating layer at the contact interface. In the last study, it was revealed that the dynamics of fretting motion influenced AC signals through the oscillation of contact resistance. Due to non-uniform accumulation of corrosion products at a contact area, contact resistance tends to have higher values at ends of a fretting track. This behavior resulted in intermodulation products when an AC signal passing through an electrical contact at the occurrence of fretting motion. Through this series of studies, experiments and simulation have been performed to investigate the phenomenon and to develop an understanding of the way fretted electrical contact influences RF data transmission. Of particular interest is the effect on signal phase and frequency response across the contact interface and how these effects might be employed to monitor the health of connector systems used for communication signals.

Acknowledgments

Firstly, I would like to express my sincere gratitude to my advisor Dr. George T. Flowers for his generous support of my Ph.D. study and this research work in Auburn University. His profound knowledge, wise suggestion and whole-heartedly encouragement helped me in all the time of research and writing of this dissertation. I could not have imagined having a better advisor and mentor for my Ph.D. study.

Besides my advisor, I would like to thank my advisory committee members, Dr. Michael C. Hamilton, Dr. Zhongyang Cheng, Dr. Robert N. Dean Jr. and Dr. Jeffery C. Suhling not only for their insightful comments and guidance, but also for the hard questions which incented me to widen my research from various perspectives. I also thank Dr. Michael J. Bozack for his valuable comments and corrections, and for his great help for being my outside reader.

My sincere thanks also goes to all my friends, especially Dr. Chong Li, Dr. Thomas Stegeman, Dr. Yang Tong, Dr. Simin Zou, Dr. Zhangming Zhou, Dr. Yang Xu and Dr. Xianzhang Wang for their support and cooperation in the last four years.

Last but not the least, I would like to thank my parents, Donghai Yang and Jie Wen, and my grandparents whose love and perpetual support have been invaluable for the completion of this degree (Doctor of Philosophy in Mechanical Engineering) and for my life.

Table of Contents

List of Tables

List of Figures

List of Abbreviations

AMC   Amphenol RF Micro Coaxial

BNC   Bayonet Neill-Concelman

CPW   Coplanar Waveguide

CPWG   Coplanar Waveguide with Ground

DUT   Device under Test

ECR   Electrical Contact Resistance

EDAX   Energy Dispersive Analysis of X-rays

EDX   Energy-dispersive X-ray Spectroscopy

EPMA   Electron Microprobe

FEA   Finite Element Analysis

FFT   Fast Fourier Transform

FIB   Focused Ion Beam

ICP   Intrinsically Conducting Polymers

MSRS   Multi-scale Sinusoidal Rough Surface

PCB   Printed Circuit Board

PRC   Parallel Resistor-Capacitor

RF   Radio Frequency

SAM   Scanning Auger Microprobe

SEM   Scanning Electron Microscopy

SIMS   Secondary Ion Mass Spectroscopy (SIMS)

SMA   SubMiniature version A

SNA   Scalar Network Analyzer

SRL   Series Resistance-Inductance

TEM   Transmission Electron Microscopy

TCR   Thermal Contact Resistance

VNA   Vector Network Analyzer

CHAPTER 1   INTRODUCTION AND LITERATURE REVIEW

Fretting corrosion is widely recognized a major cause of failures of electrical connectors. In last several decades, a lot of researchers have contributed to understanding causes, mechanisms, behaviors and prediction of the fretting corrosion. As the fundamental factor of such degradation, the chemical reactions of contact surface materials in the corrosive environments around them, like oxygen and chlorine, have been deeply studied and well understood. From the mechanical engineering prospective, dynamic and thermal research has been performed since they trigger fretting motion between contact surfaces, and considerable efforts have been devoted to tribology research because the characteristic of contact areas is a sensitive factor that influences the behavior of the proceeding of this degradation.

1.1 Fretting Corrosion

Fretting refers to a special wear process and sometimes corrosion damage at asperities of contact surfaces which are subjected to load and repeated relative motion [1]. The amplitude of the such slip motion generally ranges from micrometers to millimeters, but also can be as low as 3 to 4 nanometers. This relative motion between two sides of contact surfaces usually results from mechanical vibration, changing temperatures, load relaxation and junction heating as the power is switched on and off.

Fretting motion causes mechanical wear and material transfer at the contact surface, which serves to expose fresh non-precious metal from surface layer to atmospheric oxidation. With the surface wear, oxidation of metallic debris and fresh exposed surfaces tend to produce

1

increased surface roughness and micropits which downgrades the surface layer quality [1]. In fretting, adhesion, abrasion and delamination wears proceed to result in the wear and oxidized debris. The formation of pits and grooves along with various corrosion products surrounding them discolor the metal surface [2]. For example, with a surface containing iron, "Reddish brown debris" was found at the contact area [3]. The corrosion process is detrimental to dimensional accuracy and satisfactory tolerance, which may bring about seizing or clogging for moving parts. In addition, fretting is deleterious to fatigue strength of material of components under cycling stress. Fretting leads fatigue crack to initiate in the fretting zone and to propagate into the material afterwards [4].

There have been various failures caused by fretting corrosion in suspension springs, bolt and rivet heads, king pins in auto steering mechanisms, jewel bearings, variable- pitch propellers, shrink fits, contacts of electrical relays, connecting rods, and other parts of vibrating machinery. Multiple Bridges have collapsed due to fretting at essential parts of the bridge design. Discoloration of metal sheets may be caused by it during shipment. As one reason of the substitute of artificial hips every nine years, fretting corrosion loosens femoral stems. One of the earliest documented examples of this corrosion was about automobiles shipped by railroad from Detroit to the West Coast. Because ball- bearing races of wheels were severely pitted by fretting, the automobiles were not operable on arrival. Based on its significance and influences, fretting corrosion is one of the topics under research at the Corrosion Technology Laboratory at the NASA Kennedy Space Center.

Multiple environmental factors have been investigated by laboratory experiments. Based on a study on steel contact, rather than moisture, oxygen was found the requirement of fretting corrosion. Even moist air causes less corrosion damages compared to dry air, and nitrogen

atmosphere considerably decreases the rate of progression of fretting corrosion. Since more damages were found with a lower temperature, the fretting mechanism is not believed electrochemical in nature. In the absence of lubricants in the contact interface, increased load and slip lead to more severe damage. A lower frequency of fretting motion for the same number of cycles tends to worsen damage [5].

1.2 Mechanism of Fretting Corrosion
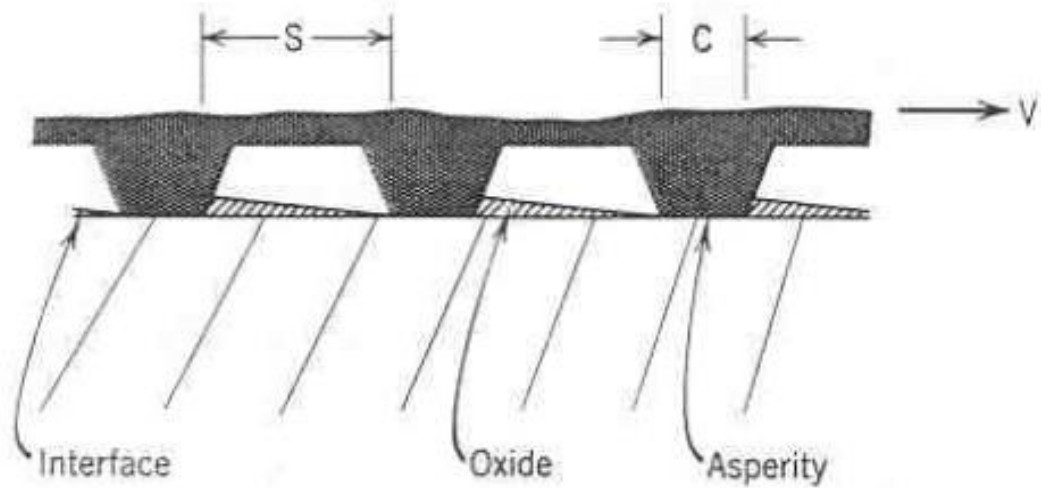
Figure 1-1: Idealized Model of Fretting Action [6]

While two surfaces are compressed to touch each other, the actual contact occurs between asperities. Therefore the real contact area is much smaller than the nominal/apparent contact area. During relative motion of the surfaces, asperities rub clean tracks on the opposite surface. The track may oxidize superficially. By the repeated slip, the oxides are wiped off by the asperities. This slip activates a repeated conversion from metal to oxides, which is wiped off in turn, forming another fresh metal track. As shown in Figure 1-1, the oxide particles moving relatively to the metal surface fret the contact surface after a run-in period [6]. Thus electrical resistance between the surfaces increases from a low value and remains high.
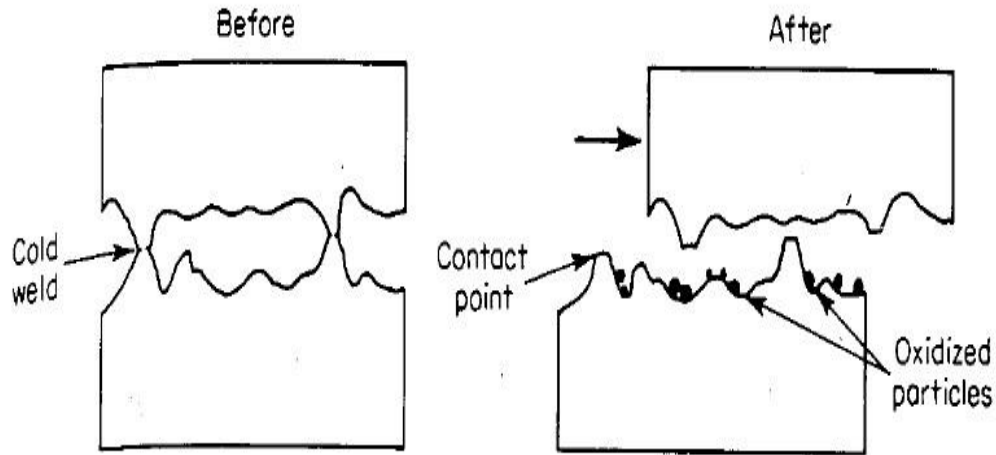
Figure 1-2: Mechanics of Wear-Oxidation Theory [2]
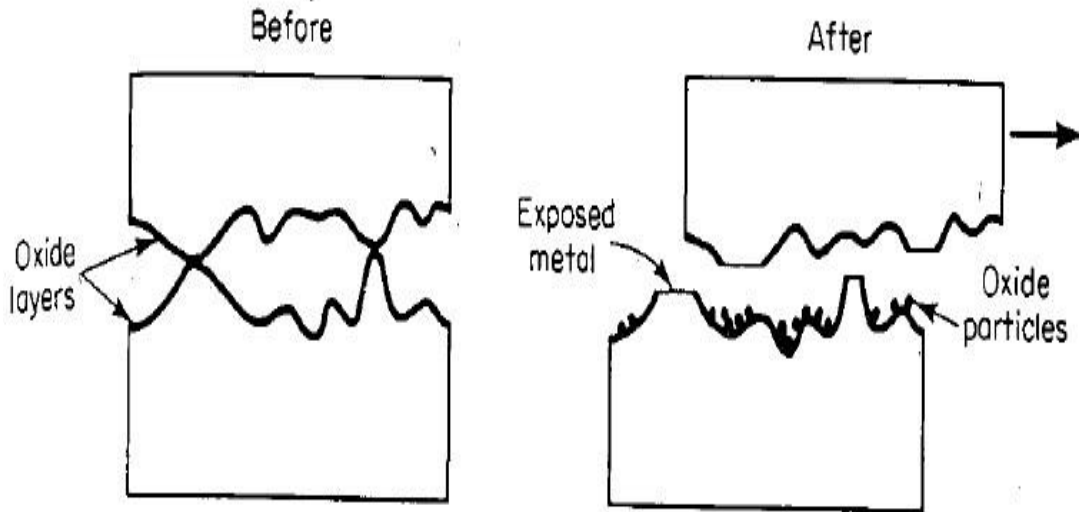
Figure 1-3: Mechanics of Oxidation-Wear Theory [2]

Oxidation usually takes place at interfaces of metallic surfaces that relatively slip. Two mechanisms called wear-oxidation and oxidation-wear theories are used to explain how oxidation occurs. As shown in Figure 1-2 which illustrates the wear-oxidation theory, the oxidation of particles is caused by the asperities that are broken by frictional forces. The oxidation-wear theory shown in Figure 1-3 is the opposite of wear-oxidation theory. It is

believed that the wear-oxidation theory takes place first with the alternate occurrence of these theories after that [2].
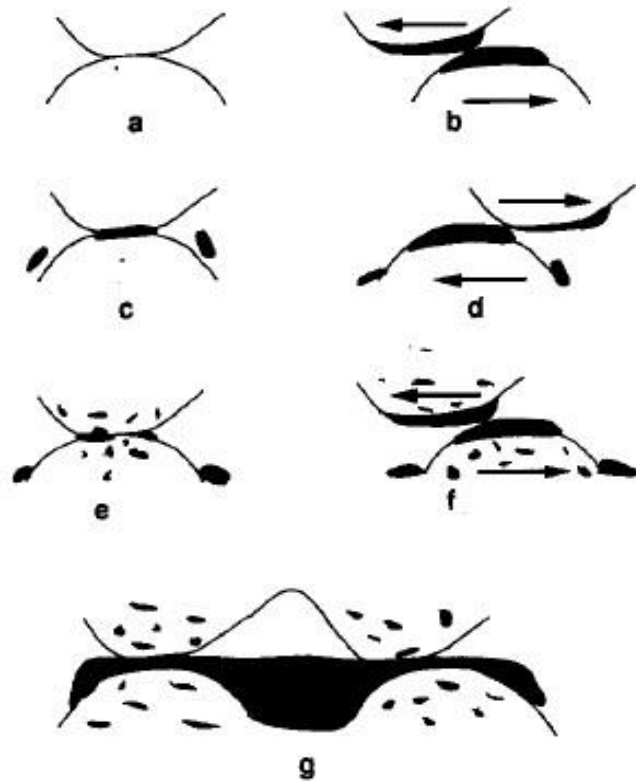
Figure 1-4: Mechanism of Connector Degradation due to Fretting [7]

As shown in Figure 1-4, Bryant introduced a mechanism of fretting corrosion in electrical contacts [7]. During the process of fretting, the initial rubbing of asperities is ignored. Fretting motions expose the asperity contacts to corrosive attack and films are formed. The reversal fretting motions shears off corrosive layers and/or drag layers into contact. Further motion exposes contact to repeated corrosive attack. After a while, fretting motions induce plastic deformation of asperities, breaking the corrosive layers between the contacting asperities and mix this corroded material with the asperity metal. The asperities become contaminated with corrosion product and electrical resistance increases. Finally, after this series of events, the connector fails.

5

Corrosive gases, such as oxygen, are considered a key factor causing fretting corrosion. Sakmann et al performed a series of tests on the same pairs of materials in different gaseous environments [8]. Under the identical condition of load and slip motion, the fretting test was performed in air, in oxygen, in helium and in vacuum. The debris formation and severity of the damage were found considerably less in vacuum and helium than experiments conducted in air or oxygen.

1.3 Literature Review of Fretting Corrosion in Electrical Contacts

Fretting corrosion is a significant problem that affects performance of various electrical and electronic equipments that contain expensive components. The detrimental influence of fretting to the electrical connections was not widely recognized until some failures of electrical connectors and Bock and Whitley's subsequent work [9] in 1974. In their work, commonly used non-noble contact materials experienced large increases of electrical resistance during fretting actions in electrical contacts as a result of vibration, mechanical motion or differential thermal expansion. Lubricants were proved to be able to exclude oxygen and other oxidizing gases from the contacts, thus preventing oxidation of the wear. With the applications of lubricants, rather than followed an increasing trend, contact resistance slightly fell off due to a loss of contact material during fretting.

Multiple lubricants were evaluated in terms of volatility and ability to prevent fretting degradation on tin-to-solder contact, considering spreading properties, thermal degradation characteristics and effects on contact resistance [10]. It was found that lubricants generally slowed down progress of wear and finally led to a less weight loss. Because all lubricants performed poorly when applied sparsely, a minimum level of about 0.1 mg per cm^2 was

6

recommended, and it was best that blade and receptacle could be both lubricated. Antioxidants was expected to be included in the formulation with respect to the useful life of lubricants. Lubricant viscosity was realized not correlated with fretting behavior. In multiple works afterwards, it was observed that many fluid lubricants contributed to a low and stable contact resistance in different scenarios when a thick coating layer was applied [11] [12] [13], even if the coating layer was made of nickel which caused severe damage and extensive exchange of materials [14].

In the complex process of fretting corrosion, mechanical and thermal parameters including normal load, slip amplitude, frequency and surrounding temperature, are considered significant factors. In 1982, Antler et al. performed a study on palladium to palladium contact of which the results indicated that a higher contact force tended to decrease contact resistance [15]. In the range from 10 um to 160 um, a larger fretting amplitudes resulted in a more rapid increase of electrical resistance [16]. Increase rate of resistance was independent of cycling rate in the spectrum from 1 to 8 Hz. In addition, it was found that electrical resistance was the highest at the ends of the wear track due to more corrosive product accumulation. This phenomenon was duplicated and the explanation was supported by a latter study on tin plated contacts [17]. Compared to the contact resistance at rest, the resistance value transients might be significantly higher. In a pair of solder coated contacts, decrease of normal force and increase of slip length ranging from 10 um to 240 um were found to worsen the fretting condition; fretting rate was independent of cycling frequency between 0.17 to 8 Hz [11]. However it is supposed to be noticeable that a high contact load would rise the wear rate, though it was favor of a decreased and stabilized electrical resistance [18]. In respect to this phenomenon, Malucci drew a point of view that higher contact force led to more asperity deformation which allowed heavier surface

damage, but tended to stabilize the oxide film between contact surfaces [19]. Regarding the classical explanation of effect of wiping amplitude, a larger fretting amplitude leads to a higher rate of debris removal which expedite the formation of new metallic contacts and attenuate contact damage. Nevertheless, fretting behavior is not well supported by it since the wear mechanism varies in different amplitude ranges. With a low amplitude, plastic deformation of coating material absorbs the relative motion; attrition is important while the amplitude is "large"; within the range between, the fretting phenomenon takes place with a mixture of adhesive, abrasive and corrosive wear. The mechanisms were later explained by the category of fretting process based on regimes [20]. Stick regime happens for motions of approximate 1 μm according to the contacting material, geometry and other factors. In this regime, relative motion between contact surfaces is accommodated by elastic deformation of the parts near contact regions. Not until the parts are separated, the asperities are joined and there is no surface damage. Mixed stick-slip regime occurs with central stick areas surrounded by ring slip regions at which crack formation, fretting fatigue and wear debris may take place. In gross slip regime with 10 to 100 μm movement of contact surfaces, all asperity contacts are broken and asperities rub others of the opposing surface during each cycle. Fretting corrosion occurs in reciprocating sliding regime with large displacements of surface movement more than 100 to 200 μm. In research of Hannel et al. [21], the relative motion is divided into partial slip and gross slip conditions. The stabilized partial slip sliding condition allows direct metal/metal interactions to operate where inner stick domain maintains low and stable contact resistance. Under the stabilized gross slip condition, the wear produces oxidized debris, and generates an insulating oxide layer. Stable metal/metal interactions are no longer possible and the electrical contact resistance becomes high and unstable, which is controlled by random oxide debris movement through the interface. During

the gross slip process, the coating is necessary to display noble properties to prevent the formation of oxide debris and a high wear resistance. Because tin would soften and cause an increase in the thickness of oxidation film, [22] tin plated copper was not suggested under high temperatures over 85°C. A study on a clad material (65Au21Pd14Ag) and electroplated gold over palladium coating showed that increased temperature has a deleterious effect on anti-fretting performances of coatings [23]. Similarity was observed on lead free alloy and tin alloy coatings that fretting corrosion was marginally increased under a higher temperature condition [24]. In thermal induced fretting corrosion, a larger range of temperature swing tended to amplify and to accelerate the fretting corrosion since a longer fretting amplitude was produced [19].

Gold is recognized the most reliable coating material in electrical contacts since it does not react with oxygen at temperatures [25]. In Consideration of its high price, a lot of research was focused on the influences of different non-precious materials as coatings of the contact surfaces. Song et al. indicated that there was a strong correlation between the rate of wear and lifetime of electrical contacts [26]. Compared to solder-to-solder contact, the solder versus cobalt gold-plated contact pair showed a more rapid rise in contact resistance [11]. This was explained by differences in the mechanics of oxide film fracture. When contact materials differing in hardness are mated, the harder side partially supports the softer and prevents oxide cracks which are necessary for a low contact resistance. The contact with similar hardness extends facture of the oxide layer and superimposes oxide cracks, which contributes to the establishment of metallic contact. Dissimilar coating behaviors were investigated on non-lubricated interfaces composed of Sn-Au, SnPb-Au, Au-Au and SnPb-SnPb. The similar metal interfaces were proved much more reliable than dissimilar contact pairs again under low level vibrations [27]. The rise of resistance occurred after the tin oxide deposits became thicker than 200 Å, and no gold

intermetallics were found in the deposits. Silver was recognized a reliable coating material with a thickness in 150 pm. However in the range 7 to 15 pm, its performance varies largely with intermediate coating layers[18]. Tin is a good alternative for silver under low amplitude (<5 um) fretting motion. Because of its low hardness, indentation resulted in large contact area and low contact resistance. And low melting point facilitated welding and plastic deformation absorbed relative displacements. The oxidation of tin, however, was easy to trigger under the fretting motion with a large amplitude. Whereas if lubricant was applied, the performance of Sn-Sn contact was comparable to that of Au-Au pair [28]. In a later work focused on mateability of tin with other coating materials, Sn-Sn interface behaved similarly to Sn-Ag interface, which was much better than Sn-Au and An-Pd combinations [29]. This work indicated that tin was susceptible of fretting corrosion no matter which material it combined with, in the absence of anti-fretting contact lubricants. Nickel is not preferred to act as a coating material because its high hardness and electrical resistivity causes a quite high static resistance and fast degradation. However nickel performs well as an underplating regarding its high hardness which improves the durability of gold plating that undergoes depletion under fretting condition [16]. Alloy of noble and non-noble materials is another idea to improve the anti-fretting capability of coating layer. The alloy of palladium and gold was investigated, and it showed a better performance with a higher portion of gold content [30]. A new silver alloy containing Li and La was developed with more satisfactory property as a anti-fretting contact coating compared to traditionally used AgCd1 that contained 1% of cadmium. It did not only show low contact resistance, abrasion resistance and arc resistance, but also maintained favorable characteristics of silver including chemical stability, cost efficiency and workability [31]. An alloy comprising 65% Au, 21% Pd and 14% silver was developed with outstanding anti-fretting performances in a temperature

range from 20 ℃ to 200 ℃ [23]. A comparison between SnAgCu PbSn and SnCu was conducted at various temperatures [32]. BNi-Au contact pair was proved able to replace Au-Au contact pair under limited conditions of short fretting lifetime with several thousand cycles [33]. And it was worse for BNi to be used as coupon than as probe where contact pair displayed rather low and stable fretting resistance within thousands of cycles that was longer than BNi(coupon)-Au(probe). Effects of N+ and In+ Ion-implantation on anti-fretting performance of silver-copper alloy contacts was investigated. The deleterious effects of fretting corrosion were significantly reduced with N+ Ion-implantaion, whereas no influence was found using In+ ion-implantation. It was impressive that processed AgCu-AgCu contacts did not suffer any detrimental effects from fretting [34]. Based on the enhanced mechanical and tribological characteristics, the beneficial effects of nanocrystalline materials were rationalized. In presence of nanocystalline coatings, notably Pd, Pd-Ag and Pd-Y films, the fretting damage to the contact areas was significantly inhibited. As a result, the low and stabilized contact resistance was maintained under fretting conditions [35][36]. Fouvery et al. stated the reason and mechanism that noble coatings like gold and silver last longer than non- noble material like tin [37]. It was concluded that electrical contact endurance under established gross slip conditions was controlled by the kinetics of oxide debris layer formation and by the evolution of its composition of the debris. For non-noble coatings, like tin, the electrical conductivity decays as soon as the debris layer fully separates the interface, which was resulted from the high current resistivity of tin oxides. And for noble materials, electrical failure is controlled by the progressive elimination of the noble element from the oxide debris layer. When the content of noble atoms in the lay has been low, the conductivity of the interface decreases and the electrical contact fails. As the coating layer was continuously wiped due to fretting, fresh barrier or base layer with different micro-hardnesses tended to

gradually be exposed. Around the moment that the coating was depleted and the fresh inner layer was exposed, the increase of contact resistance would be disturbed and dropped to a bottom value. As the oxidation of barrier and base material proceeded, resistance rose again and eventually reached the latter stage with large scale of fluctuation [38].

The damage of contact zone was observed using various techniques, such as scanning electron microscopy (SEM), secondary ion mass spectroscopy (SIMS), scanning Auger microprobe (SAM) and energy dispersive analysis of X-rays (EDAX). During fretting motion, serious material transfer caused by several mechanisms including adhesion, abrasion, arching/melting and delamination wear [39]. Surfaces with different tin coating thicknesses were examined based on SEM [40]. The cross section photographs showed that tin coatings were comprised of a white layer, a soft layer of tin, and an uneven intermetallic compounds in light grey color. EPMA mapping was used to analyze corrosion products in the vicinity of contact area at the whole area of which oxidation took place. FIB, Focused Ion Beam, TEM, EDX and electron diffraction measurement were performed for cycles of tin plated contacts [38]. At the initial state of 10 cycles, 100 nanometer-size granular structures and continuous crystal-lattice fringes were observed in the tin coating layer. Sharp diffraction spots in electron diffraction pattern suggested that the part of tin coating near the surface had high crystallinity. It was concluded that the tin plated layer did not oxide near the contacting surface. After 30 to 100 cycles, resistance had not increased. It was observed that size of granular structure reduced to 10 nanometer scale and crystal-lattice fringes turned to be discontinuous. The crystallinity of tin coating became finer, and a large number of anisotropic micro crystals appeared. Besides, oxygen and tin was found using EDX mapping simultaneously, which indicated a high oxidation level than 10 cycle fretting. At the further fretting stage of 160 to 300 cycles, discontinuous and

anisotropic crystal-lattice fringes were observed and a higher level of oxygen was detected than early stages. Using FIB-SEM technique, three dimensional observations were performed on tin plated fretting contacts [41]. The layers with rich and poor oxidation were observed in tin oxidized layer and intermetallic compound layer, and voids in the oxidized layer were also found.

With the development of conducting polymer, Swingler and McBride firstly introduced extrinsic conducting polymer into the electrical contacts to come out a study on polymer-tin interface [42]. This interface behaved significantly better than Sn-Sn contact, and several features were observed. Like the Sn-Sn contact, the electrical resistance of polymer-tin contact decreased at the very beginning and increased thereafter under fretting corrosion. Resistance fluctuation was also found at during fretting motion. However, it was noticeable that the resistance of polymer-tin interface was the lowest at the ends of wear track, which was reverse to the Sn-Sn contact having a highest value there. This was explained that the polymer terminal was being further compressed to decrease the electrical resistance. Intrinsically conducting polymers (ICP) were implemented as the interface coating in a later work. The optimum conductivity level of ICPs were found relatively lower than that of extrinsic conducting polymers and metal. An outstanding elastic characteristic, however, minimized the influences of micro scale relative movements at contacting interfaces by absorbing and dispersing the kinetic energy though material. During the test, no scratches or wear marks were observed after compressive actions between contact surfaces. Negative temperature coefficient of resistance was found in ICP material of PEDOT/PSS and its blends with DMF. Moreover as DMF was doped with a higher level, fretting tended to lower the electrical resistance. This phenomenon was discussed in regard to three causes: change of the internal structure of the material, change of geometry and change at the surfaces and interfaces [43].

Besides, the effect of electrical factors, such as current passing through contact interface, to fretting corrosion have also been investigated. It was revealed that a high open circuit voltage contributed to less variation of contact resistance because of the fritting of insulating films. High-current contacts, nonetheless, can lead resistive heating to occur, and then cause the early contact failure [16]. According to a research of current influence on fretting of tin-pated copper alloy, the contact resistance was similar with and without electrical load for the very early stage. For the increasing fretting periods, higher currents slightly augment resistances due to higher contact temperature. At the further stage, a higher current gave a lower resistance plateau and a longer plateau can be brought about by a higher circuit voltage [32]. The influence of voltage and current to tin coated contacts was studied over a current sourcing range from 0.1mA to 100mA, and a voltage range from 1 to 12V. The presence of melting and current sintering of corrosive debris was observed at the high power sourcing [44]. Gagnon et al. performed a study focused on effects of AC and DC current to fretting corrosion on Cu-Cu interface [45]. Regarding the resistance behavior, no considerable difference was found for AC and DC current conditions. Nevertheless there was significant variation in the morphology at contact zones subjected to fretting corrosion. Under DC current, fretting formed loose and flake-like debris scattered at the periphery of fretting area; debris that are more compacted and adhering to the surface was structured under AC current condition.

For predicting contact resistance behavior of electrical contacts under fretting corrosion, modeling work are necessary but difficult to be developed. In 1990, a multispot model was proposed by Malucci in terms of surface features to account for long term corrosion of stationary contacts. A third level of multispot constrictions were introduced on each asperity. Asperity deformation and film growth were found essential in delaying fretting corrosion. Statistic data

14

provided by this model showed an increased variation of resistance as fretting proceeded which was often observed experimentally [46]. Incorporating normal force, micro-hardness of surface, real and nominal contact areas, a statistic model was proposed for surface profile characterization and density calculation of contact spots formed as rough surfaces were compressed. The influences of the parameters to contact spots and asperity deformation were calculated and the results were used to evaluate the effects on electrical behaviors of degraded contacts [47]. Using these two models, a Monte Carlo analysis of aged copper contacts was performed to value the effects of fretting parameters such as film thickness, contact force and surface micro-hardness and geometry. Material properties and design variables were employed in the statistic model of degradation. Using a power law model that described concentration of oxides, the calibrated degradation model was able to come out with results in a good agreement with laboratory data [48]. This model was further modified by considering electrical resistivity of asperities a random variable and shear force produced by wipe to deform asperities additionally [49]. Later, the two previous models were refined combined into a single analytical model to predict the impact of contact force and fretting amplitude. The modeling results were well correlated with the experimental observation that lower contact force and larger amplitude were favorable to a more dramatic resistance increase [19]. A model depicting thermal induced fretting was developed in terms of experimental data of thermal cycling tests and material aging. Parameters including thermal swing width, dwell time and cycling number were incorporated to account for aging processes. Three processes, fretting corrosion, oxidation and stress relaxation, were successfully simulated. Oxidation rate and stress relaxation per cycle reveal significant influence to the rate of temperature induced fretting degradation [50]. A model combining the tribological properties of contact surfaces and the chemical reaction of such corrosion was also put forward by Bryant [7].

This comprehensive model is able to predict the contact resistance during specific fretting cycles and the lifetime of the ultimate failure of contacts. In this model, contact wipe, fretting vibration amplitude and frequency, contaminant chemistry, material properties, plating thickness, asperity deformations, normal load, electrical load, surface topography were taken into consideration. The fretting mechanism proposed by him is the basis of the model. Both the filling of surface valleys with debris produced by fretting and contamination of surface asperities by the corrosion products were considered to be the causes of fretting corrosion. Based on the mechanism, the model calculated the amount of corrosive products generated on the exposed surfaces during cycles of fretting. Assumptions which correlate mixing to plastic flow and modern composite theory were used to estimate the conductivity in the contaminated asperity. The asperity resistance produced by the integration over the asperity volume and the total resistance were predicted by Greenwood's theory. The theory and model are able to explain the general fashion of the progression of electrical resistance, as shown in Figure 1-5 [51]. This figure reveals transients of the resistance of electrical connectors under the vibration test with single frequency and single amplitude. During cycles of relative motion of contacting surfaces, the electrical resistance increased slowly first, and then rose tremendously after a critical fretting cycle. Based on Bryant's model and mechanism of fretting corrosion, the phenomenon can be generally divided into three stages. At the first stage, the contact micro structures, asperities and valleys, only had the elastic deformation. Secondly, the fretting motion began and wear debris was generated. The escape of debris from the metal to metal contacts was facilitated by fretting
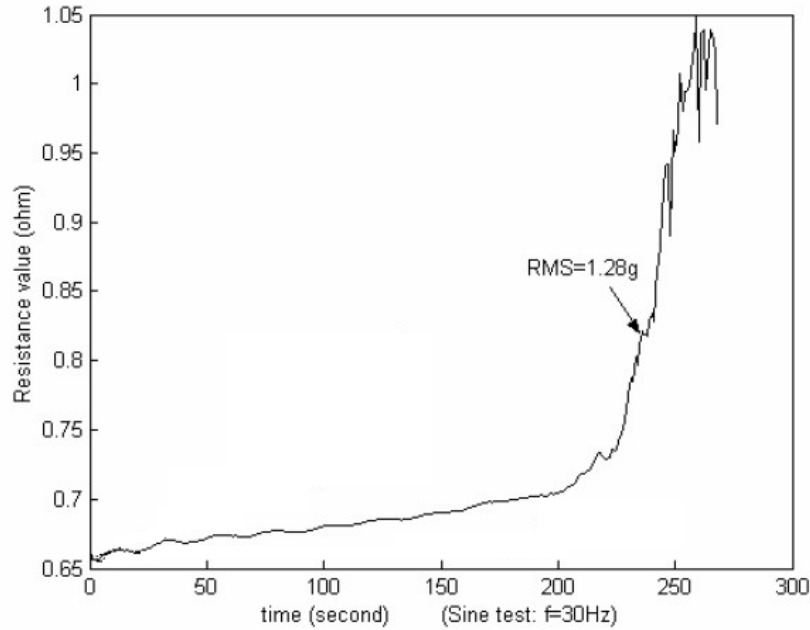
Figure 1-5: Typical Fretting Curve in Sine Vibration Test [51]

actions. So the low contact resistance was maintained. At the third stage, insulating layers

containing oxides and wear debris accumulated. Metallic contacts lost and contact resistance

fluctuated. Eventually, contact resistance became high and the connector fails. In recent years,

many new applications of the studies of fretting corrosion in electrical contacts were extended by

computer simulations. This technology has been being used to assist and guide the experiments

and analyses of many companies and researchers. In 1996, Villeneuve et al. [52] at Ford Motor

Company used finite element method to model the terminal crimping process of vehicle

connectors. In his model, the terminal grip cross section, the punch tooling and wire strands were

involved. For simulating the real application, the grip was forced into the punch as it sit on an

anvil. In terms of results, the friction between the grip surface and the punch surface was found

to be crucial to a "good" crimp. In 2005, Monnier et al. [53] applied FEM for simulating the

performance of a sphere-plane electrical contact as a high current flowed through it. In this

simulation, the mechanical, electrical and thermal coupling was involved. The validity of the

model was confirmed by the high consistency of the simulation and experimental results. The contact terminal voltage, the contact resistance of the system and the solid temperature, which were not able to be measured in experiments, were provided by the simulation.

As one of the most critical fields affected by fretting corrosion, vehicle electronics are in the environment combing mechanical vibration, harmful temperature and humidity. The complexity of fretting corrosion in vehicle environment was reported by Swingler et al. in 2000 [54]. In their study, the temperature of automotive connectors was being monitored during real operation to evaluate stress levels. According to real environmental data gained from tests, an empirical model of temperature behaviors of various electrical connectors was presented. In order to improve this study, some micro-sensors were embedded in a connector housing, which provided real information about phenomena taking place at the connector interface for the first time. Piet van Dijk performed an investigation of fretting corrosion in electrical connectors considering the dynamic characteristics. Not only the spring part in receptacle that applies a normal force to the blade, but the rigid part with comparatively higher stiffness was also taken into account. It was realized that the slip of contact area was shorter than the displacement applied to a connector due to the micro deformation of connector structure [55]. Fretting behavior of electrical connector systems considering periphery components was studied comprehensively by Flowers et al. [56]. Using a shaker system, fretting motion was induced in a connector with a single frequency vibration. The testing configuration is illustrated in Figure 1-6 and Figure 1-7. The frequency response and dynamic behavior of the system were detected using a non-contacting laser measurement system. By avoiding adding more weight on the light connector components, this approach was proved better than the methods applying accelerometers. During vibration, the connector pair and cables were excited and dynamics of

the entire system led to rocking mode vibration between pins and sockets. In this study, the direction of exciting vibration was perpendicular to cable and connector pair which brought about a transverse vibration The primary mode of connector interface motion (rocking- type motion), the relative motion at the contacting location, served as an indicator of the fretting rate. The rocking motion led one side of connector pin to be exposed to the air, and to isolate another side from the air. As shown in figure 1-8, the fretting corrosion mostly happened on the side of the pin that contacts the air. The threshold levels of excitation for fretting corrosion, above which the fretting corrosion occurs, were revealed in the study. As shown in figure 1-5, the behavior of resistance increase was found close to that found in previous research where the vibration of
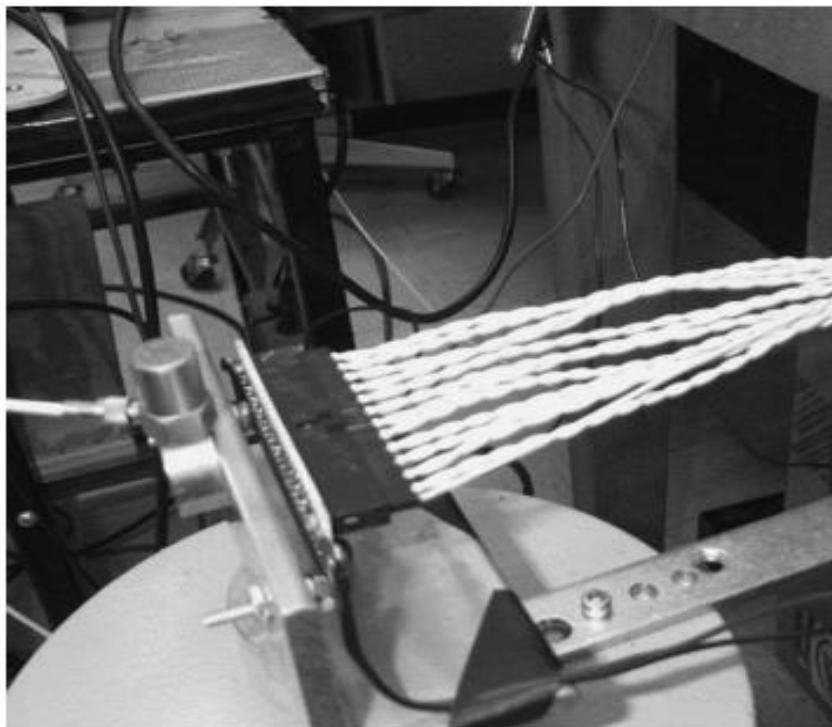
Figure 1-6: Experimental Setup Used by Flowers et al. [56]

connector system was not taken into consideration. This threshold was larger than that observed in previous researches on solid contact interface because the kinetic energy was dissipated by

motions of connectors and cable. With the vibration at a specific frequency, the increase of excitation levels above the threshold led fretting rates to rise monotonically at the early stage. The threshold excitation levels values at various frequencies were found influenced by the dynamic behavior of the connector system. It indicated that the moment applied as the result of the given excitation level and frequency was reasonably estimated by a transfer matrix model. An empirical fit of the data was in a good correlation with the model as the damping was considered. The analysis demonstrated that the bending moment caused by the excitation levels and tie-off configurations at the contact interface was significant to analyze and predict the threshold level. .
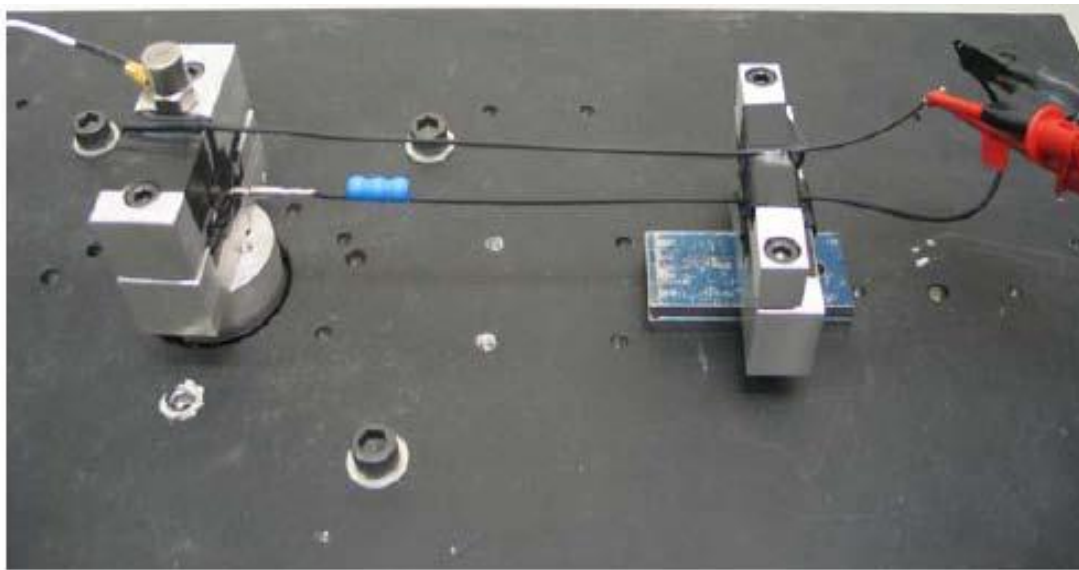
Figure 1-7: Experimental Setup Used by Xie et al. [51]
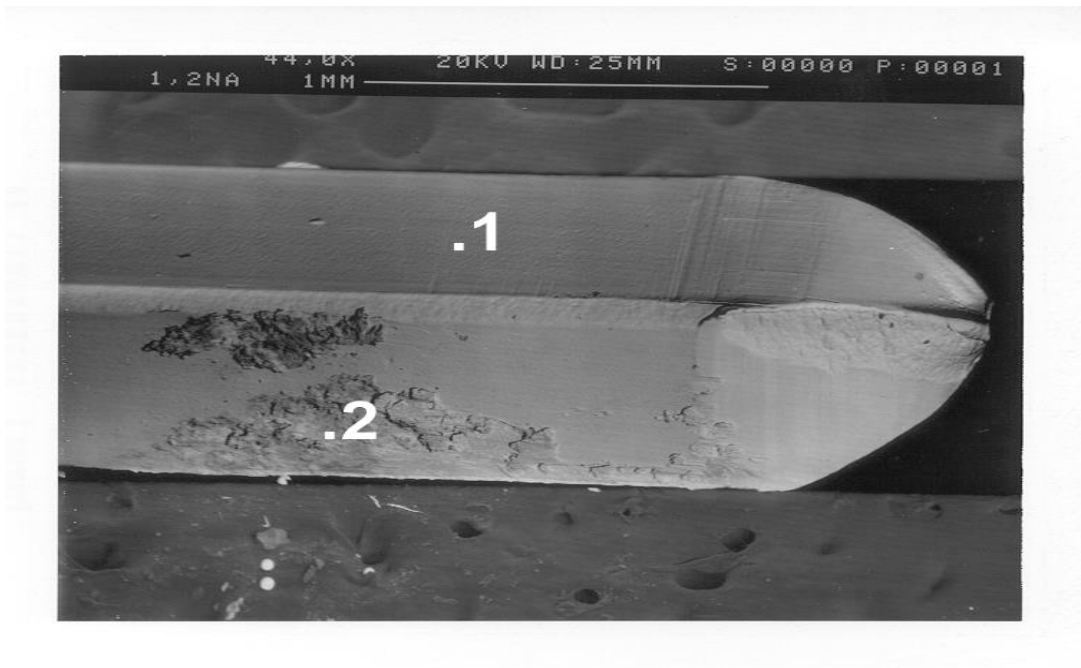
Figure 1-8: Corrosion Spots on Connector Pins Caused by Fretting [56]

Fretting behavior of connector systems under random vibration was studied by Flowers et al.. The measurement of frequency response including transfer function and relative motion were performed. With a higher excitation level, the resistance rate under random vibration rose monotonically, as illustrated by Figure 1-9. While the vibration excitation was smaller than 5

Grms, the electrical resistance did not grow. With excitation levels that are higher than 6 Grms, the rate of the resistance increase rises monotonically. The threshold g-level should be between 5 to 6 Grms, and the accuracy of the measurement was dependent of the period of the test run-in. The researchers also found that the threshold g-level varied as a function of the dynamic behavior of the connector, the tie-off configurations and the mass and stiffness properties. For PC and automotive connectors normally with a housing, frequency response cannot be measured directly on terminals using laser measurement system [57]. By measuring through a hole drilled on a plastic housing, there was slight variation on relative motion between blade and receptacle. Tie-off length was observed a sensitive variable affecting the frequency response of the rocking motion. A linear behavior of rate of resistance increase was detected with a rising excitation level.
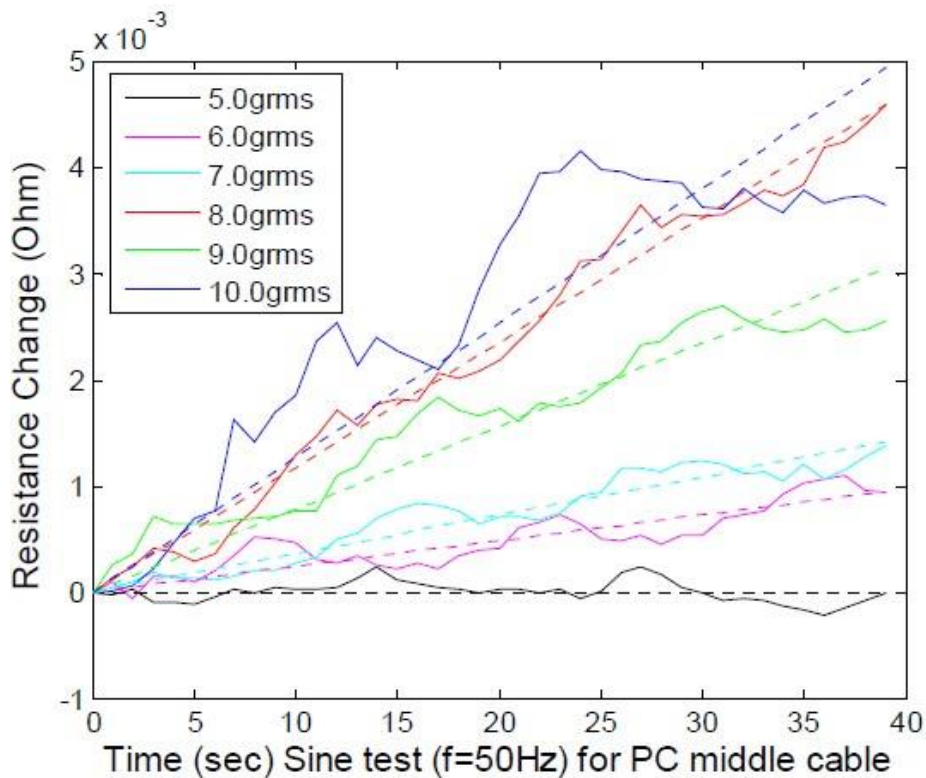
Figure 1-9: Electrical Resistance Transients under Excitation Levels [58]

A two dimensional FEA model was developed to simulate the dynamic fretting behaviors of the connector system. This model was correlated well with the experimental results on frequency response of motion between the blade and receptacle in the condition of multiple tie-off lengths. In addition, based on an assumption that the threshold relative motion amplitude between blade and receptacle was independent of excitation frequency, the thresholds of excitation energy at a frequency spectrum were in a good agreement with experimental results [57]. A three dimensional FEA model was developed to predict the vibration characteristics and thresholds for connector systems with two types of contact coefficients and three normal forces [59-60]. The different contact designs slightly changed the frequency response of the system. During fretting motion, oscillating relative slip at the contact area was observed to increase with a larger excitation level. The simulation results of relative motion indicated a good agreement with the experimental thresholds. Moreover, the linear rate of resistance increased with higher excitation levels which were also successfully simulated by the 3-D model. However the calculation cost of the three-dimensional model, with the comparative calculation accuracy, has been proven to be much worse than the 2-D model. A study of influence of thermal factor on the fretting behavior of the connector systems was performed. The static friction coefficient of the contact surface was measured at different temperatures. The surface profile was measured to develop a relationship between the surface physics and fretting behavior. Using the three-dimensional FEA model, a well correlation was found between fretting performance and dynamic characteristics of the connector system between experiments and simulation. The results did not exhibit a significant effect of temperature on the threshold and early stage performance. The effect of pollution to the contact areas was never investigated in previous research. Thus, a study on connector systems with sands in micrometer scale involved between blade and

receptacle was performed to mimic the scenario of severe air pollution [61]. The three-dimensional FEA model was applied to simulate the frequency response and fretting thresholds with contaminants in the contact interface. It was found that the failure of fretting degradation occurred much more easily with polluted surfaces.

Compared to the transverse vibration, a study was performed on fretting corrosion in connector systems subjected to axial vibration excitation [62]. Using random noise, a frequency response measurement was conducted and three vibration modes was observed. One was the rocking motion between the blade and receptacle; the other two corresponds to two axially induced transverse vibration of cable and connector pair that took place in two perpendicular planes. The threshold amplitude of input vibration was found related to the frequency response of the system that low threshold amplitudes were at the natural frequencies of two transverse modes. It was concluded that relative slip was a more significant failure mode than relative rocking motion. With various tie-off lengths, frequency response measurement was conducted and it was found the natural frequency of mode I decreased monotonically with a longer cable. The threshold of connector system with cable in 4 cm was the lowest due to the highest transmissibility. Except for this specific situation, threshold of Mode I generally increases with a longer tie-off setup. A dynamic model was developed based on the geometry of connector configuration, experimental data of system dynamics and a static friction force at contacts. The static friction force was measured using a tensile machine. In order to improve the alignment, fish lines were applied to fixed the connector pair to the head of tensile machine. A good agreement was found between the experimental and modeling results. A three-dimensional FEA model was proposed to predict the fretting behavior under axial vibration [63]. Incorporating the friction force and frequency response, connectors with three types of normal forces and two

kinds of friction coefficients were simulated. The threshold results were in a good agreement with that of experiments.

Another approach to measure the relative motion inducing fretting corrosion was reported by Lam et al. in 2005 [64]. In the study, a novel thick film sensor measuring the displacement at the connector interface was used to test for environmental effects on fretting corrosion in electrical contacts. This sensor was assembled into a connector sample to replace the male component. While the relative motion occurred at the interface, the relative displacement of the contact point resulted in a corresponding electrical resistance change, which was measured by the connection of male and female parts. After the validation by a series of experiments, the sensors were subsequently used in a field test to research on the relationships between the fretting influences and temperature, humidity and differential pressure. The researchers found that the differential pressure dominates the relative movement behavior at the interface of connector samples in condition that the influences of temperature and humidity on measured relative motion are negligible.

Fu et al. investigated the fretting mechanisms of silver-plated high power connectors induced by vibrations [65]. His results indicated that the variation of electrical contact resistance (ECR) of connectors subjected to vibration is primarily due to periodic changes of contact area caused by relative motion between the contact pairs, rather than other fretting corrosions. This finding was reinforced by observing a good correlation between relative motion and the variance of ECR under vibration. When a vibration stopped, the ECR decreased to a value that was slightly higher than the original value. A surface analysis showed no apparent degradation until the coating was worn away. An FEA model to predict the instant electrical resistance change during vibration was developed in his research.

Angadi et al. [66] proposed a multi-physics coupled simulation with the mechanical, thermal and electrical interactions predicting contact forces, electrical contact resistance (ECR) and thermal contact resistance (TCR) in the rough surface contact regions. This model was developed in terms of multi-scale sinusoidal rough surface (MSRS) contact model using a MATLAB code that communicates with ANSYS. In the bulk connector material, it provided predictions of the stresses, strains, Joule heat effects, current flow, electric potential and the temperature distributions between the spring and pin parts of the connector. Finally the results illustrated the significant proportional rise in voltage drop and temperature across the bulk regions of connector parts.

Electrical connectors were widely applied in various areas including power and signal transmission. In the study of conventional contacts, contact resistance was the most important quantity in fretting corrosion in electrical contacts. As the speed of data transmission increases, contact impedance is supposed to be considered significant to affect signal integrity. When two metallic surfaces are compressed, the real contact area much smaller than the apparent contact area is constituted by the touch of asperities on two sides of contact surfaces. Therefore, there are non-contacting spaces in the surrounding of the cluster of micro scale contact spots. The distributed non-contacting gap areas can be assumed as many micro capacitors. Dervos et al. firstly proposed a RC parallel circuit to simulate the contact impedance behavior, where constriction resistance of real contact area and capacitive effect of non-contact area. [67] In this study, current with high density passed through a silver contact of which the phase shift between current and voltage was detected to produce a closed loop in a single period of powering. The area of the loop determined the electrical energy stored at the contacting interface. Testing results showed energy stored at a given metallic contact increases with a higher ampacity values,

lower operation temperatures and higher contact forces. Using two previously developed models, a statistical model based on random variations of surface features was proposed to estimate the contact resistance and capacitance [68]. This model calculated capacitance and resistance values for clean and degraded contacts that resistance rose and capacitance initially increased and then dropped as oxidation film grew up. Through an impedance measurement of a coaxial fixture and adapter, the skin effect on series resistance were analyzed. The results showed the effect of degraded contact to high frequency data transmission. Further study using the statistical model revealed that the high frequency signal will be affected by the short-tem discontinuities. It was noted that compared to high frequency components, low frequency components were vulnerable as a result of capacitive coupling [69]. A three dimensional FEA model was developed to simulate the impact of contact interfaces to coaxial transmission line [70]. The transmission behavior of the transmission line with clean spherical, flat and single asperity contacts were compared with regard to the insertion loss and return loss results. For dielectric films with various thicknesses at the contacting interface, the degraded electrical interface was evaluated. It was found that the low frequency signal was significantly impacted and the distortion level was closely related to the contact geometries and film thicknesses. Based on results of time domain analysis, the deleterious influence of dielectric film build-up to the signal integrity was significant. It was believed that if only one metallic contact existing at the contact area, AC signals can be passed and no obvious distortion would be observed. Using the same FEA coaxial model, the influence of various oxides were compared in regard to insertion and return loss. It was found the degraded contact with different oxide films performed worse than the clean contact at the low frequency. However the high frequency behavior was close to the clean contact [71]. Another model incorporating resistance, capacitance and inductance was proposed

27

to take account for the high frequency behavior of metallic contacts. The detrimental effect of degradation to GHz signal transmission was also found [72].

1.4 Overview of Current Work

This dissertation is focused on the impact of degradation in electrical contacts on high frequency data transmission. It discusses three research projects on the topic of performance of contacts subjected to vibration induced fretting corrosion. Each project is introduced in a single chapter. In total there are five chapters in this dissertation. The content of each chapter are as follows:

Chapter one is the introduction and literature review. It introduces the concept of fretting degradation, the mechanism of fretting corrosion and the progress of research concerned with fretting corrosion of contacts.

Chapter two describes the first research project that is focused on tin plated copper contact pair. This is a study of physical characteristics of degraded contact due to vibration induced fretting corrosion. This chapter opens with a discussion of the purpose of this work, and the experimental details including experimental samples, test approach and setup are followed. The experimental results are given along with the data analysis. At last, a statistical model describes the development of contact capacitance with higher levels of oxidation regarding the experimental results and analysis.

Chapter three depicts the second project which examines the impact of degraded contact interface to high frequency data transmission. An experimental setup that mimics the coaxial transmission system is proposed and a network model is developed with the objective of evaluating the degradation effects. This chapter discusses the purpose of this projects, and

provides a description of the experimental and modeling results. Finally the results from the simulation are compared with the results from the experimental part of this work.

Chapter four presents the third project: effects of fretting motion on signal transmission through electrical contacts. There are two parts of this project, namely the experimental and a modeling part. Then experimental work and mathematical models are developed to reveal the phenomenon that harmonics and inter-modulation effects between the transferred signal and mechanical vibration would be produced during fretting motion.

Chapter five concludes the study presented in this dissertation. It also provides some recommendations for further directions of study on this topic of fretting degradation in electrical contacts.

CHAPTER 2   IMPEDANCE BEHAVIOR OF ELECTRICAL CONTACTS SUBJECTED TO VIBRATION INDUCED FRETTING CORROSION

2.1 Introduction

Fretting corrosion is generally recognized a major cause for failures in electrical connectors where non-precious metallic contacts are subjected to mechanical stress and chemical reactions[5][9]. As fretting degradation proceeds, the buildup of a insulating oxide layer between the blade and receptacle results in a significant resistance increase that is considered a fundamental quantity in the conventional electrical contacts.
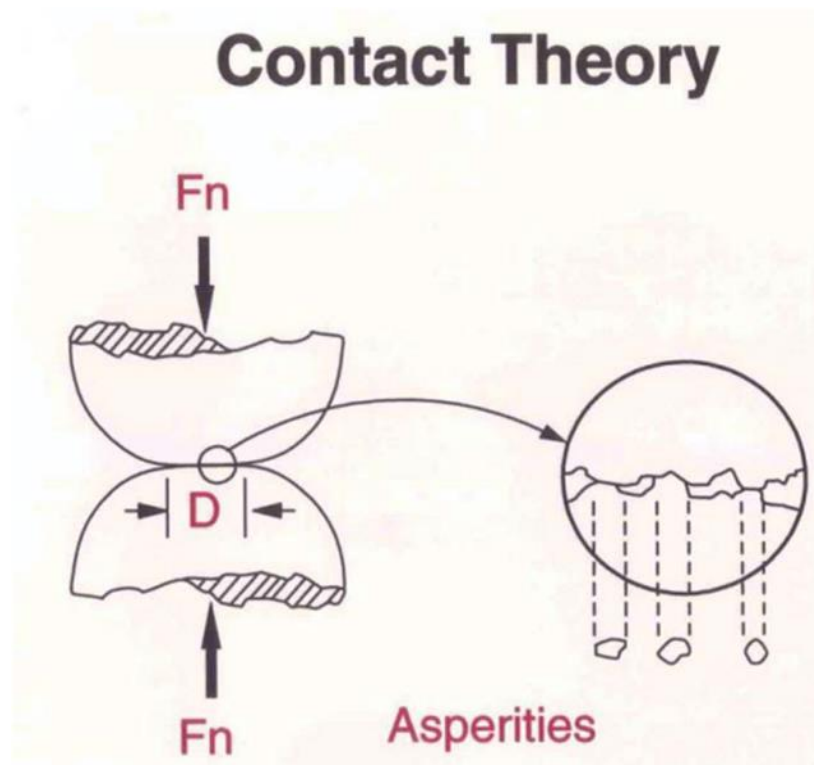
Figure 2-1: Contact between Two Sufaces [71]

While two metallic surfaces come to contact, as shown in Figure 2-1. Asperities on each side of the contacting interface contribute to a real contact area that is smaller than apparent contact area. Because of the presence of non contacting gaps among distributed contact points, an effective capacitor exist between two contact surfaces. As the speed of data transmission increases, rather than DC resistance, contact impedance of widely used electrical contacts should be considered as an important factor for a sufficient bandwidth of a transmission line. Especially in the case of contact damage, it is necessary to understand whether and how the change of contact impedance potentially induces signal losses and distortion.
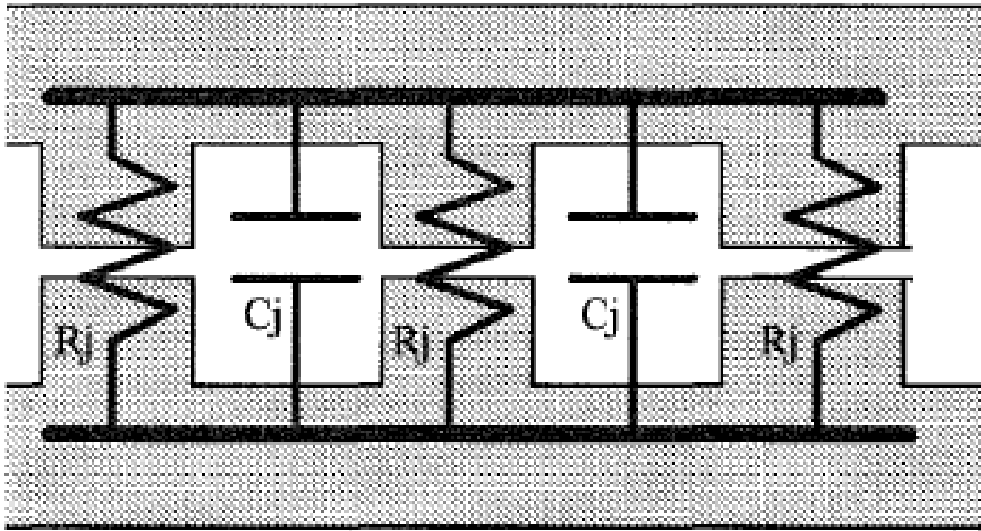
Figure 2-2: An Equivalent Circuit for Impedance of an Electrical Contact [67]

An equivalent circuit, as shown in Figure 2-2, was firstly proposed by Dervos et al. based on the presence of contact asperities [67]. Accordingly a simple model was developed as described in the following equation

$$R_{eff}^{-1} = \sum R_j^{-1} \qquad (1)$$

$$C_{eff} = \sum C_j \qquad (2)$$

where R_{eff} denotes contact resistance and Rj denotes the constriction resistance of a single micro contact. C_{eff} denotes the effective capacitance consisting of micro capacitors denoted by Cj. Using a typical multi-point model of contacting interface, Malucci et al. evaluated the impact of degraded contact to integrity of high frequency transmission [68][70]. It was demonstrated that even if it was fully degraded, contact would provide an acceptable integrity of the high frequency signal transmission. The low frequency signal transmission, however, tends to be influenced.

In the previous research on conventional electrical contacts, analysis of fretting corrosion was focused on contact resistance and DC principles [70]. The influence of fretting on contact oxidation film build-up of various metal coating such as gold, silver, tin, nickel-phosphorous, nickel-boron, lead-free solder alloys, etc., has been well studied [17][65][73-75]. Considering the dynamic system of connector and wire, the threshold behavior of fretting amplitude for the onset of fretting degradation was observed and investigated [56][76].

Recently, multiple techniques have been introduced for faulty detection of connectors [77-79]. As the corrosion takes place at the contact interface, the contact is considered damaged once signal losses and distortion are observed. Due to the high complexity of electronic, it is possible for a corrosion fault to be wrongly detected and located, especially in lack of well understanding of impedance behavior of degraded contacts. In the present work, therefore, an experimental measurement of the impedance was conducted on electrical contacts subjected to multiple levels of fretting corrosion. According to the existing model, RC parallel circuit, the contact capacitance was extracted from the testing results. A series of SEM and EDS tests were involved to validate the phenomenon. A tribology model developed by Malucci [68] was applied to explain the capacitance variance due to levels of fretting corrosion.

2.2 Experimental Configuration

2.2.1 Experimental Samples
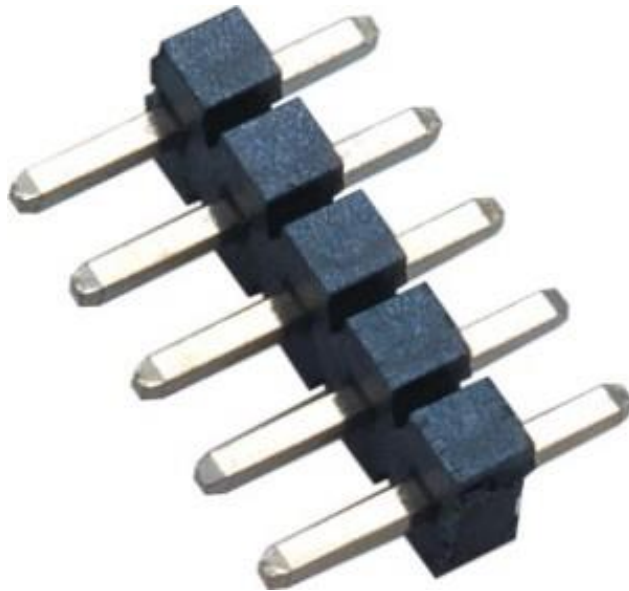
Figure 2-3: Photograph of the Tin Plated Header Connectors

A typical type of tin plated header connectors were applied in this study, as shown in Figure 2-3. Pin headers were widely used to transmit signals, or as low power connectors on various PC boards. They usually work as male connectors in board-to-board or board-to-wire connector pairs. Ji et al. performed a research on contact impedance and the high frequency effect due to atmospheric corrosion [80]. In that study, a contact of coaxial connector adaptor was applied as the testing article, regarding to its commonly usage in the field of high frequency data transmission. The transmission line components were subjected to gas corrosion, but a fresh contact between the ground layer was guaranteed by a gas isolator. There are 3 small contact areas between the gold plated pin and socket. During the test, measurement calibration was done using fresh connector pair. For different levels of degradation, separated connector pairs were exposed in corrosive air environments for various time lengths. And then impedance measurement would be performed on reassembled degraded pairs. Experimental results showed a

large distribution which was attributed to the multiple-contact setup and reassembling procedures. The resistances of three contact areas between the pin and socket could be non-uniform, even not close, which led to a inaccurate understanding between resistance and resistance development. In addition, repeated reassembling tended to wipe and remove the oxide film built up at the connector surface. This phenomenon was also common on fretting degraded contacts that a small movement may significantly change the contact resistance by the variation of the oxidation film structure. In consideration of these experiences, a simple contact pair was set up, as illustrated in Figure 2-4. Two pins were removed from the original structure, and contacted at the tip of each one. The pins were respectively soldered on two PC boards which were specially designed for the sake of mechanical and electrical setup. Under a specific contact force, the contact would be mechanically affected by nothing but the fretting motion, which reduces the unexpected impacts. The single contact configuration also aimed to avoid the potentially external impedance influence from connector pair and to constitute a structure suitable for high frequency signal transmission.
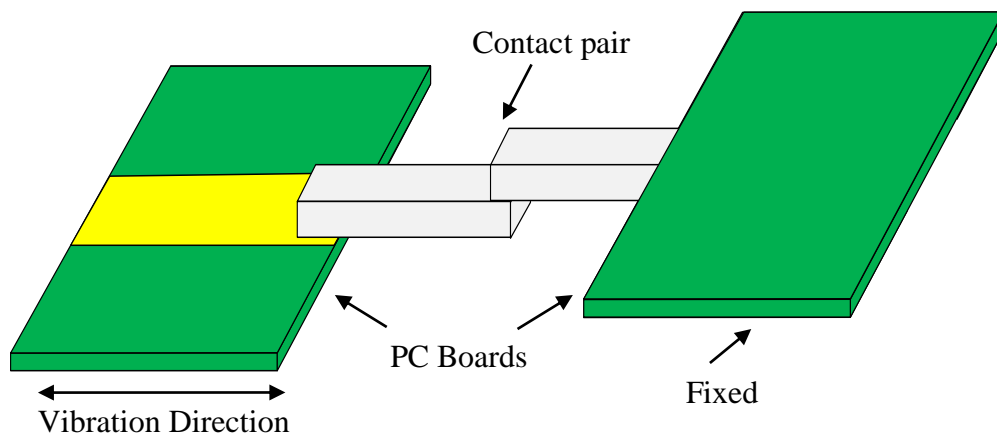
Figure 2-4: Schematic Diagram of Contact Setup

2.2.2 Experimental Equipment

34

The experimental equipments used in this study include an Agilent 4294A precision impedance analyzer, which is used for the measurement of contact impedance values; Polytec laser vibrometers systems measuring the displacements of the selected locations on connector samples; an HP 35665A dynamic signal analyzer, which generates different types of excitation signals (such as sine wave, random noise, etc) for the shaker and analyzes the frequency response; a vibration system that consists of a Dactron vibration control system, a PA500L Amplifier and a V408 Shaker. The details of these major components are mentioned below.

Figure 2-5: Photograph of the Agilent 4294A Precision Impedance Analyzer

2.2.2.1 Agilent 4294A Precision Impedance Analyzer

As shown in Figure 2-5, the Agilent 4291A precision impedance analyzer is applied in the experiment for contact impedance measurement [81]. As an integrated solution for efficient impedance measurement and analysis of components and circuits, the 4294A precision impedance analyzer covers a wide test-frequency spectrum from 40 Hz to 110 MHz with basic

measurement accuracy:+/-0.08 %. Excellent High Q/Low D accuracy allows the possibility of analyzing low-loss components. The measurement signal level ranges from 5m V to 1 Vrms or 200 uA to 20m Arms, and the DC bias could vary between -40 V and +40 V or from -100m A to +100m A. The broad signal-level ranges enable to evaluate device behaviors during operating. Advanced calibration and error compensation functions avoids measurement errors when measuring in-fixture devices.

Figure 2-6: Photograph of the Polytec Laser Vibrometer System

2.2.2.2 Polytec Laser Vibrometer System

As shown in Figure 2-6, the Polytec laser vibrometer system is used in the experiment for the non-contact displacement measurements [82]. The system consists of two Polytec OFV 353 sensor heads (lasers), and two Manfrotto tripods to hold the lasers and two Polytec OFV 2610 controllers. The system provides the methods for a displacement measurement based on the fringe counter principle. An analog voltage signal is available at its output that is proportional to the vibration amplitude of the measurement object. This signal can be visualized with an oscilloscope or can be entered into a data acquisition and processing system, such as the HP 35665A dynamic signal analyzer. Table 2-1 shows its displacement decoder specifications.

Table 2-1: Displacement Decoder Specification of the Laser Vibrometer System

Measurement Range	Full Scale Output(Peak to Peak)	Resolution	Max Vibration Frequency	Max. Velocity	Max. Acceleration
μm/V	Mm	Mm	kHz	m/s	G
20	0.32	0.08	20	1.6	20,000
80	1.3	0.32	20	1.6	20,000
320	5.2	1.3	20	1.6	20,000
1280	20.5	5	20	1.6	20,000
5120	82	20	20	1.6	20,000

2.2.2.3 HP 35665A Dynamic Signal Analyzer

As shown in Figure 2-7, HP 35665A dynamic signal analyzer is a two-channel fast Fourier transform (FFT) spectrum/network analyzer with a frequency range that extends from 0.19531 Hz to 102.4 kHz in the single channel mode and from 0.097656 to 51.2 kHz in the two channel mode [83]. The analyzer has a built-in signal source providing random noise, burst random noise, periodic chirp, pink noise, and fixed sine. Measurements can be saved to an internal 3.5-inch flexible disk drive, or an external HP SS-80 disk drive, or can be directly printed out. The main characters of this analyzer applied in this study are listed as below:

· Input Noise Level: < -140 db

· Full Span FFT Noise Floor: < -76 db (-85 db typical)

· FFT Cross-Channel Gain Accuracy: ± 0.04 db (0.46%)

· FFT Cross-Channel Phase Accuracy: ± 0.5 degree

· Minimum Frequency Resolution: 122 μHz (Two Channel Mode)

Figure 2-7: Photograph of HP 35665A Dynamic Signal Analyzer

2.2.2.4 Vibration System

The vibration system utilized in this research is comprised of a PA500L Amplifier and a V408 Shaker, as shown in Figure 2-8 and Figure 2-9 respectively. The shaker provides the vertical vibration and a set of fixtures are designed and attached on the shaker for the experimental setup.

The configuration of the vibration control system is shown in Figure 2-10. The vibration system generates time-domain signals containing the required frequency domain characteristics and sends them to the amplifier. Then the amplified signal drives the shaker to vibrate with a larger current and voltage. The accelerometer installed on the payload senses the vibration on the shaker and converts it into an electrical signal that is then sent back to the vibration control system. The time-domain signal is processed by the vibration control system and is transferred into the frequency domain by FFT. And then the frequency-domain characteristics of this signal are compared with the original setting by this control system. If differences exist, the output

signal will be revised by the vibration control system accordingly. This process repeats until the frequency-domain characteristics of the signal on the shaker match the required characteristics specified by the original setting.

Figure 2-8: PA 500L Amplifier
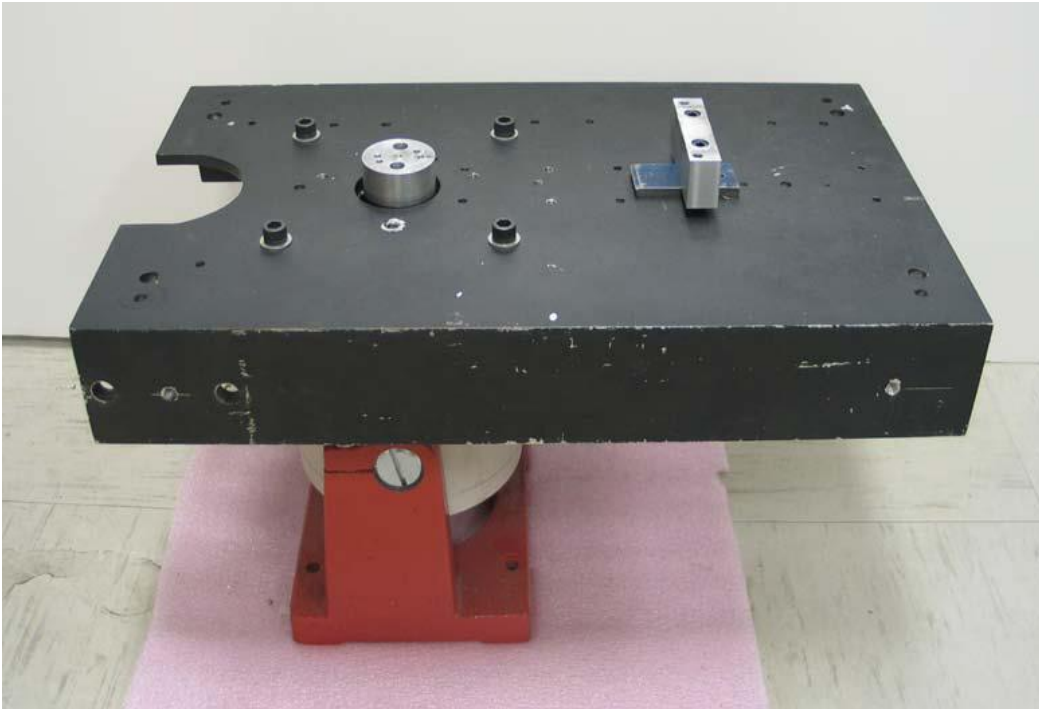
Figure 2-9: V408 Shaker and Fixture Table
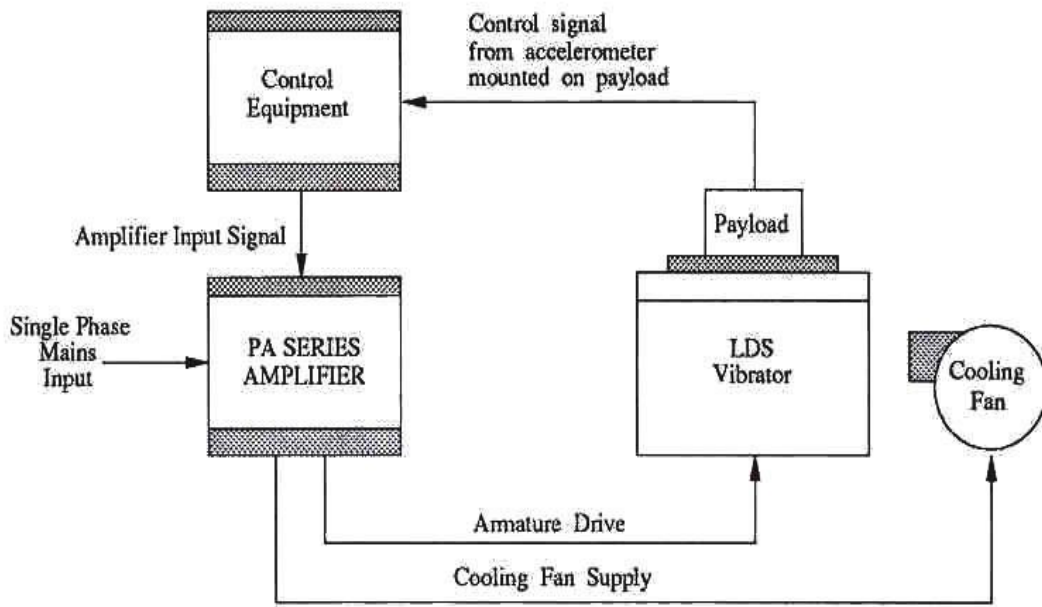
Figure 2-10: Typical Vibration System

2.2.3 Experimental Setup

Figures 2-11 and 2-12 illustrate the basic impedance measurement for the contact specimen. Through the power amplifier, the signal generator drove the shaker to keep the testing article vibrating with a specific profile which produced fretting motion at the contact interface. One of the PC boards where pins were soldered was fixed on a shaker head, and the other one was attached on a stationary fixture. The shaker table and the fixture were placed with a specific displacement which contributes to a constant overlapping area between the pins. The overlapping area was fixed with the length of the axial side in 1 mm. This mechanical configuration allowed fretting to proceed with specific parameters including normal force, frequency and amplitude. The part of the fixture near the article was made of Teflon in order to reduce the potential interference of metallic environment to the test. The contacting pair was connected with another testing fixture attached on an Agilent 4294A impedance analyzer through straight copper trace

on the PC boards and two extensional copper wires. From another prospective, the pins, boards and wires work as the extension of original fixture between the contact interface and the impedance analyzer. Due to the fixture extension, testing spectrum's upper limit decreased from 110MHz down to the actual 40MHz.
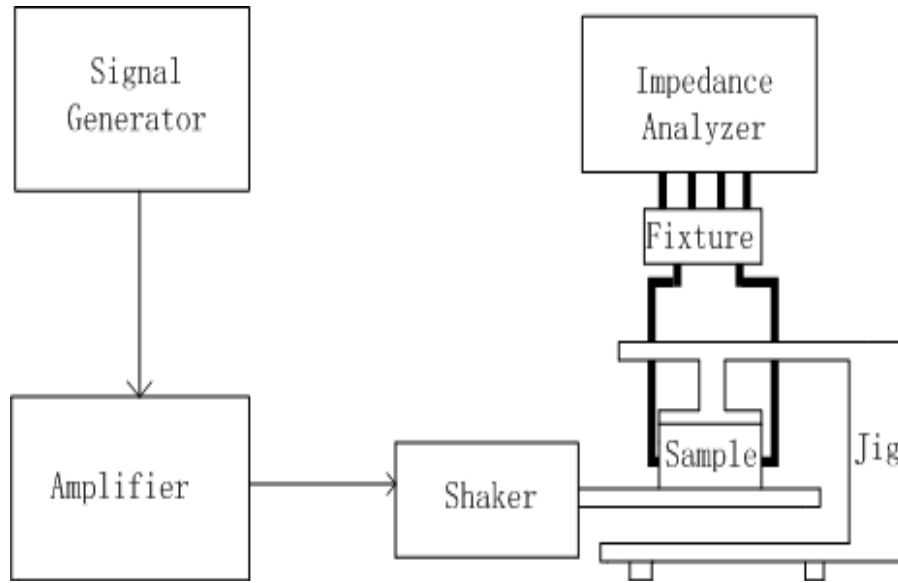
Figure 2-11: Schematic of the Experimental Configuration

Before the impedance measurement, circuit calibration was attempted through an open/short/load procedure. Through this step, all reactive effects of the copper wires, traces and pins were eliminated, and the measured results equaled the corroded contact impedance. Because the impedance was measured based on a frequency sweep taking more than 10 seconds, unlike resistance measurement, it is impossible for the impedance to be recorded inline during fretting motion. Thus, once an impedance variance was observed, the shaker was paused and a stable impedance value of the degraded contact was recorded. Contact impedances were measured at various degradation levels in regard to resistance values and fretting cycles. Dimensional deformation of the measurement circuit was not allowable before or after the calibration since it
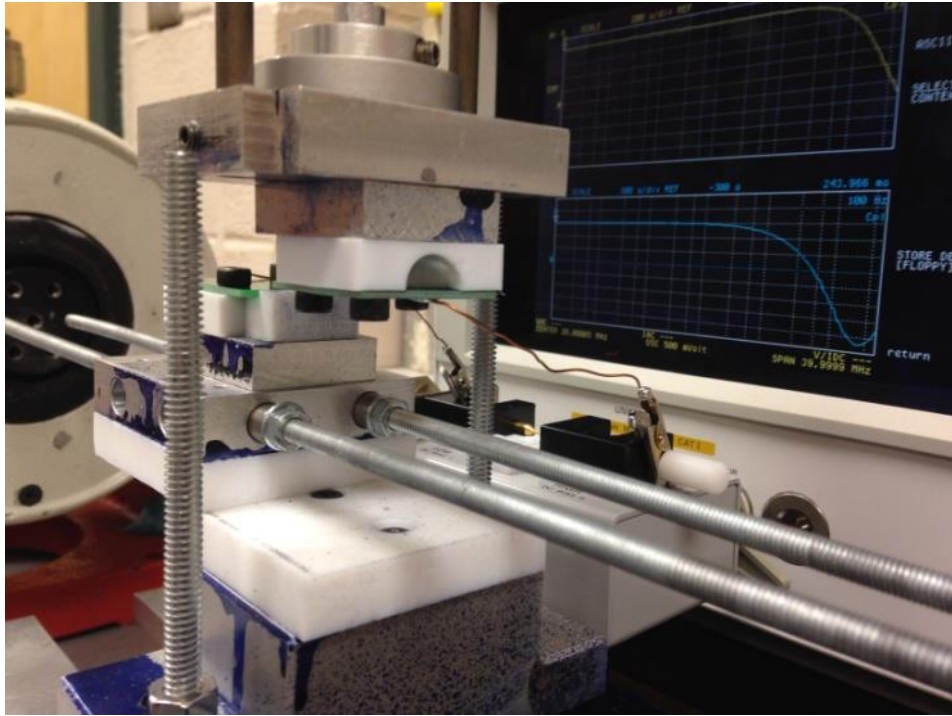
Figure 2-12a: Photograph of the Experimental Configuration
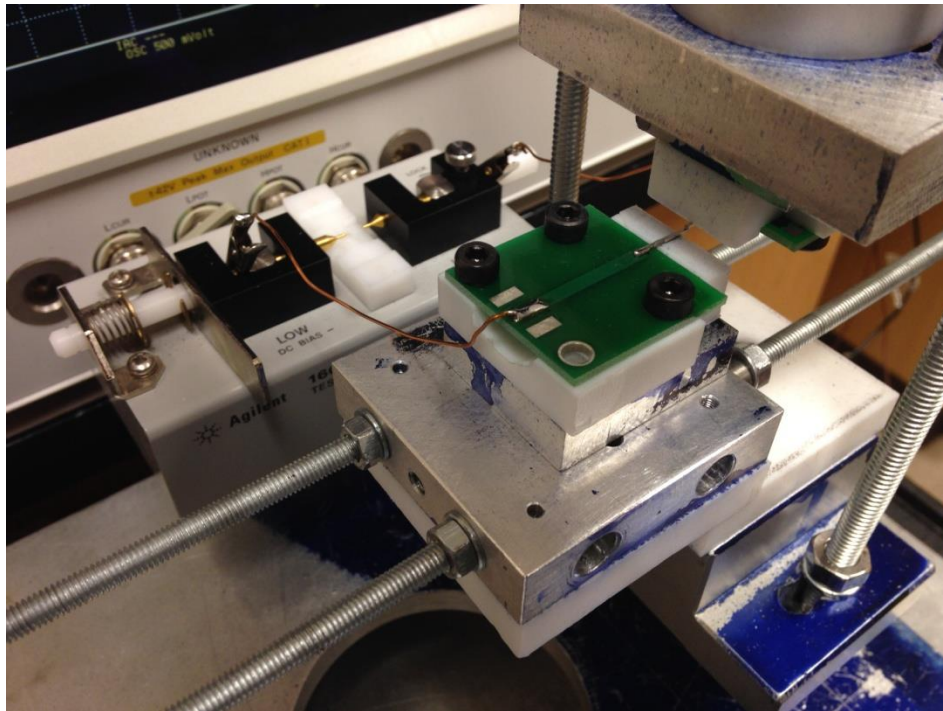
Figure 2-12b: Photograph of the Contact Setup

resulted in unexpected impedance variances. A series of baseline tests were performed using a level of vibration power that was slightly lower than the fretting threshold to validate that the testing circuit was not affected by input vibration and the impedance variance was solely caused by fretting corrosion. Fretting parameters, including vibration amplitude in 30 um peak-to-peak, vibration frequency in 200 Hz and normal force in 1.0 N, were determined in initial trials,.

2.3 Results and Discussion

2.3.1 Impedance Measurement
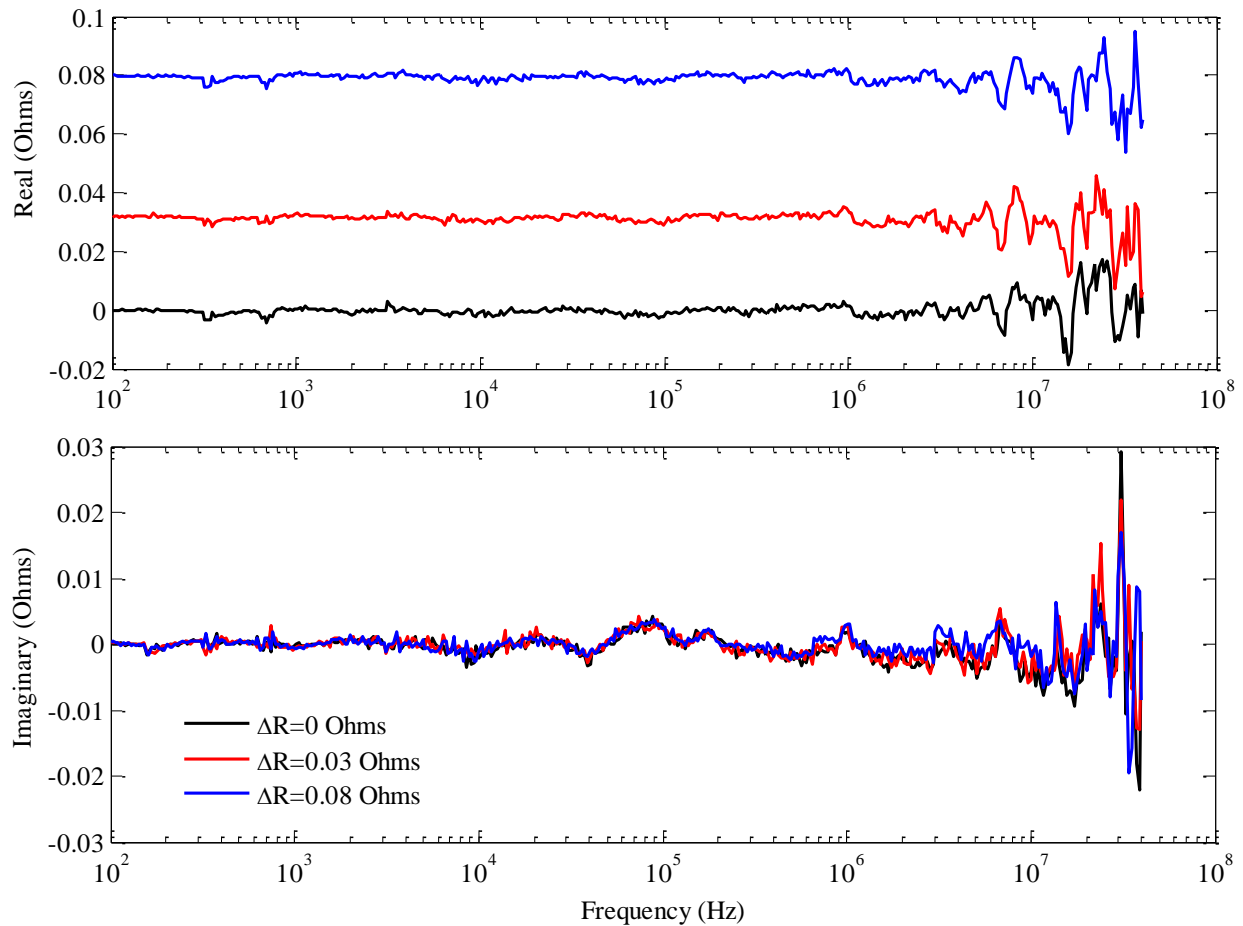
Figure 2-13a: Impedances of Fretted Electrical Contacts while Contact Resistances Increase by 0, 0.03 and 0.08 Ohms
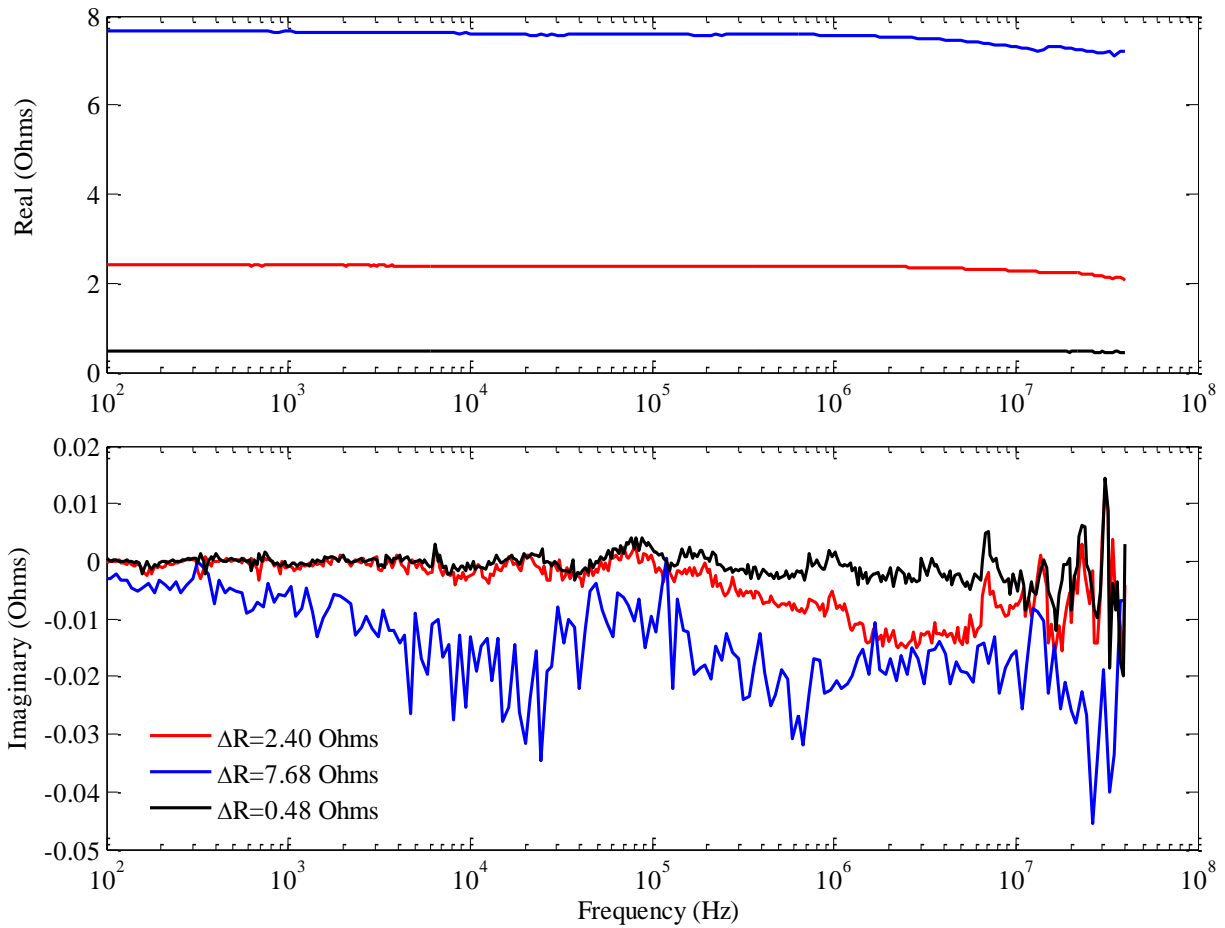
Figure 2-13b: Impedances of Fretted Electrical Contacts while Contact Resistances Increase by 0.48, 2.40 and 7.68 Ohms

Due to the accuracy limitation of the impedance analyzer, the impedance of the lightly degraded electrical contact was hardly measurable. The measurement between 5MHz to 9 MHz suffered from a level of distortion because of imperfection of transmission traces of the impedance analyzer. Figure 2-13a illustrates the impedance of the electrical contact at the early stage of fretting degradation. DC resistance is considered close to the impedance magnitude at 40 Hz. Real and imaginary parts of the fresh contact are both approximately zero. As a normal phenomenon after calibration, the power of noise of the frequency response measurement rises with a higher frequency. As the fretting corrosion proceeds, the resistance increases gradually.

The real parts of the contact impedances are primarily the resistance values; the imaginary parts are small and vary about zero.

The impedances of the degraded contact with higher resistances, including 0.48, 2.40 and 7.68 Ohms, are demonstrated in Figure 2-13b. The real parts of them are approximately constant at the low frequency range, but roll off at high frequencies. For the case of ΔR in 7.68 Ohms, the real part rolls off to 7.095 Ohms at 40 MHz, and the other two respectively descend to 2.053 Ohms and 0.4356 Ohms. Compared to the curves with lower resistances, the imaginary part doesn't change obviously while the resistance is 0.48 Ohms. As resistance increases, however, the imaginary part is observed to roll off from zero to negative values with a larger scale at a lower frequency. While contact resistance is extremely high, this characteristic is more apparent as demonstrated in Figure 2-14. The real part is constant at low frequencies, but rolls off at the high frequency range. Imaginary part gradually decreases to negative values from zero, and then after a cut-off frequency, goes up back to zero. The magnitude remains constant at a low frequency range and declines at a high frequency spectrum; the phase angles shift from 0° to about -90°. The cut-off frequency of the high-pass filter descends with a higher resistance. The capacitive behavior is identical to the model proposed by Malucci and Dervos [67][71], as illustrated in Figure 2-2. At the fresh electrical contact with a thin film of tin oxide at the surface, free electrons are the main charge carriers. As fretting proceeds, oxide layer builds up which results a increasing number of metallic bonds to become covalent bonds and ionic bonds at the contacting interface. Dielectric characteristics turn dominant, as less free electrons serve as the charge carrier. This model is also an equivalent model of the lossy dielectric where energy is stored in the capacitor and the effect of the resistor represents the loss.
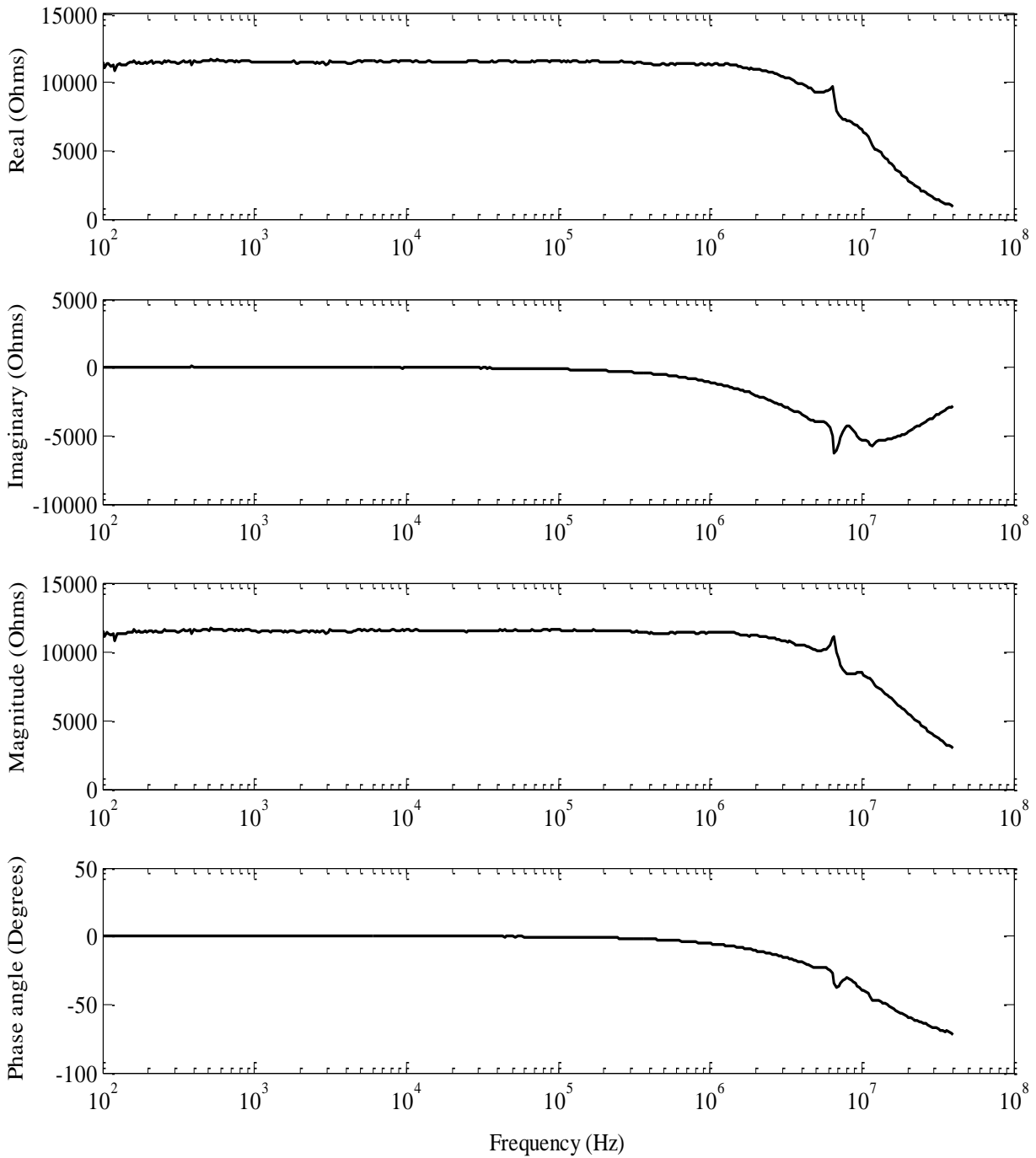
Figure 2-14a: Impedance of Highly Fretted Electrical Contact while Contact Resistance Increases by 1.153×10^4 Ohms
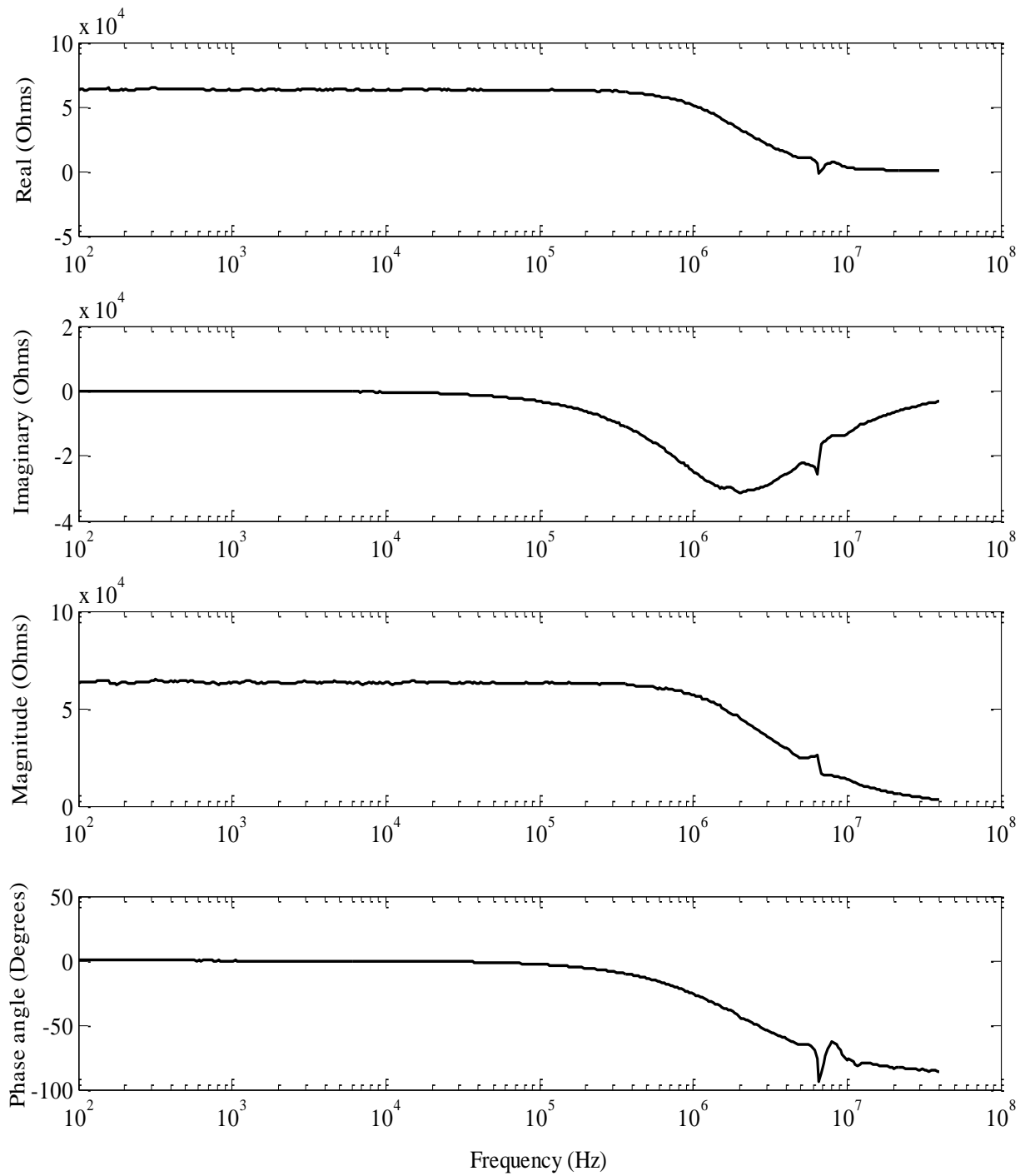
Figure. 2-14b: Impedance of Highly Fretted Electrical Contact while Contact Resistance Increases by 6.309×10^4 Ohms
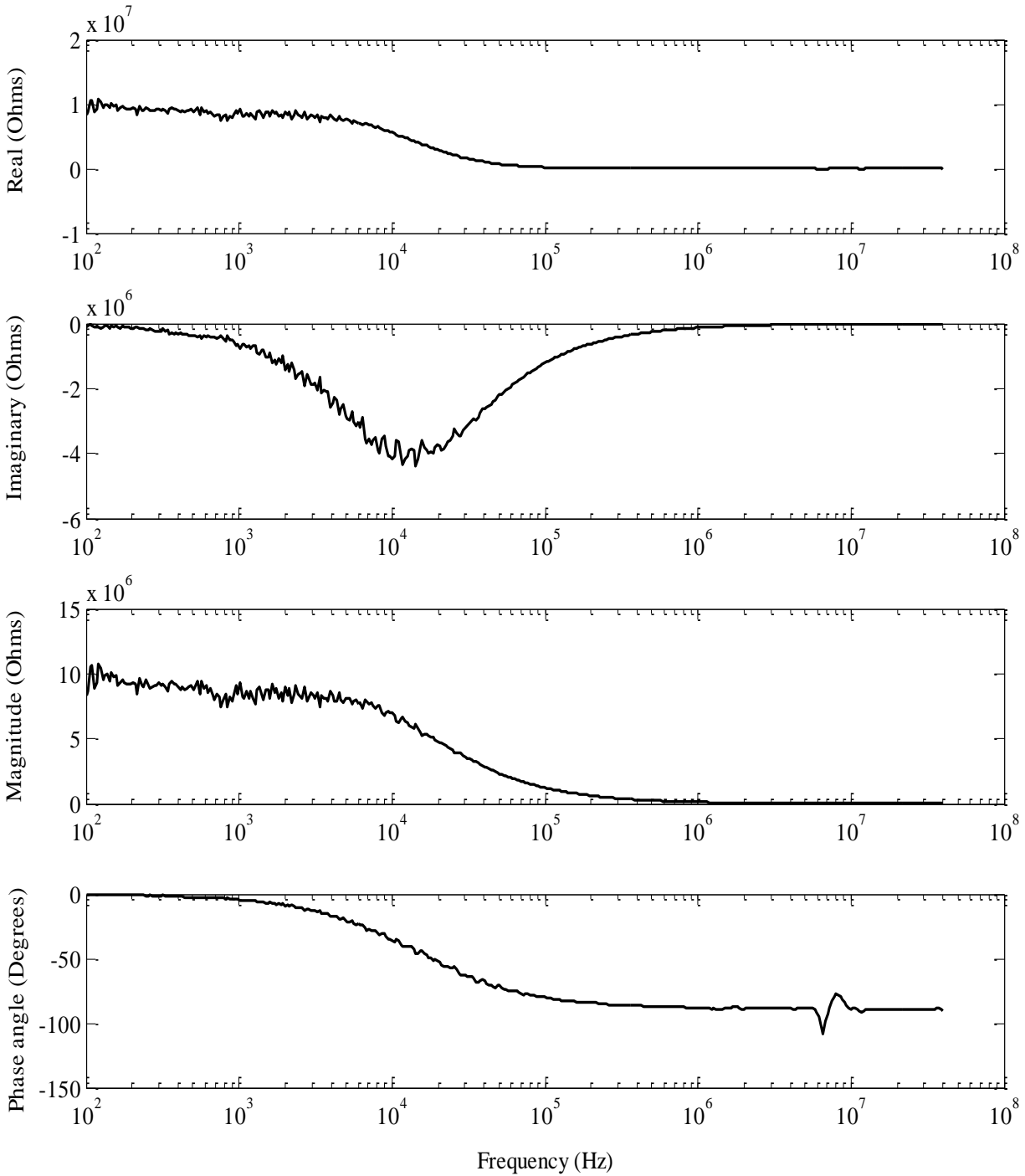
Figure. 2-14c: Impedance of Highly Fretted Electrical Contact while Contact Resistance
Increases by 8.329×10^6 Ohms

2.3.2 Capacitance Extraction
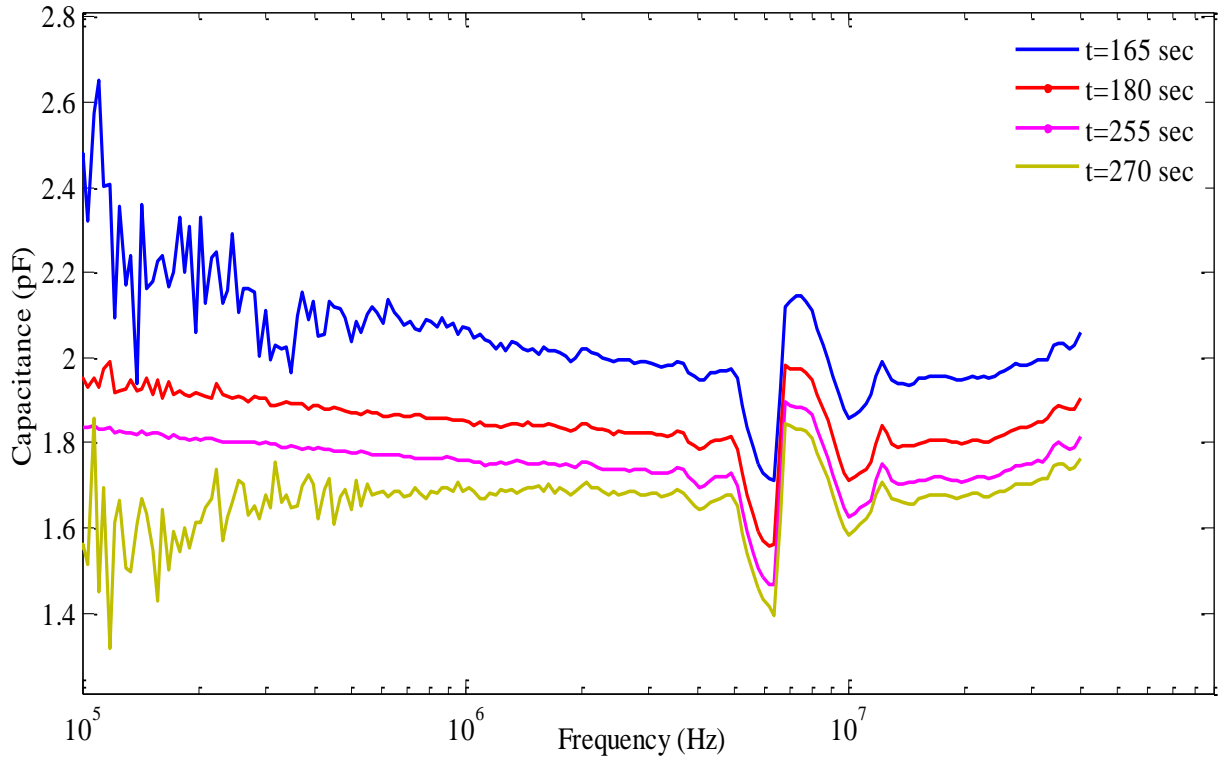
Figure. 2-15: Contact Capacitance of Fretted Contact Subjected to Different Fretting Levels

The contact capacitance value is extracted from the impedance results based on the RC parallel circuit proposed to describe the contact impedance [67][71]. The contact impedance is expressed as

$$\frac{R_{eff}}{1 + j\omega R_{eff}C_{eff}} = R_C + jX_c \ , \tag{3}$$

from which it is found that

$$C_{eff} = -\frac{X_C}{\omega\left(R_C{}^2 + X_C{}^2\right)} \ , \tag{4}$$

where R_c and X_c denote the real and imaginary parts of the contact imepdance, and ω denotes the angular frequency. For lightly fretted contacts, capacitive characteristics are not found in the impedance measurement results, thus extraction is only applied on high resistance cases to study

the capacitance development as fretting occurs.

As shown in Figure 2-15, frequency dependent contact capacitance varies at different resistance levels and after various fretting periods. Because typical capacitive property appears at the high frequency range, the interference of noise is most observable at the low end of the spectrum. The bumps between 5MHz to 9 MHz result from the imperfection of transmission traces of the impedance analyzer. According to all measurement results, the extracted capacitances are between 0.80 pF and 5.09 pF at the testing spectrum. From the results, it is observed that capacitance develops in a close correlation with fretting periods, rather than resistance values. It's believed that the capacitance value generally decreases with a longer fretting period.
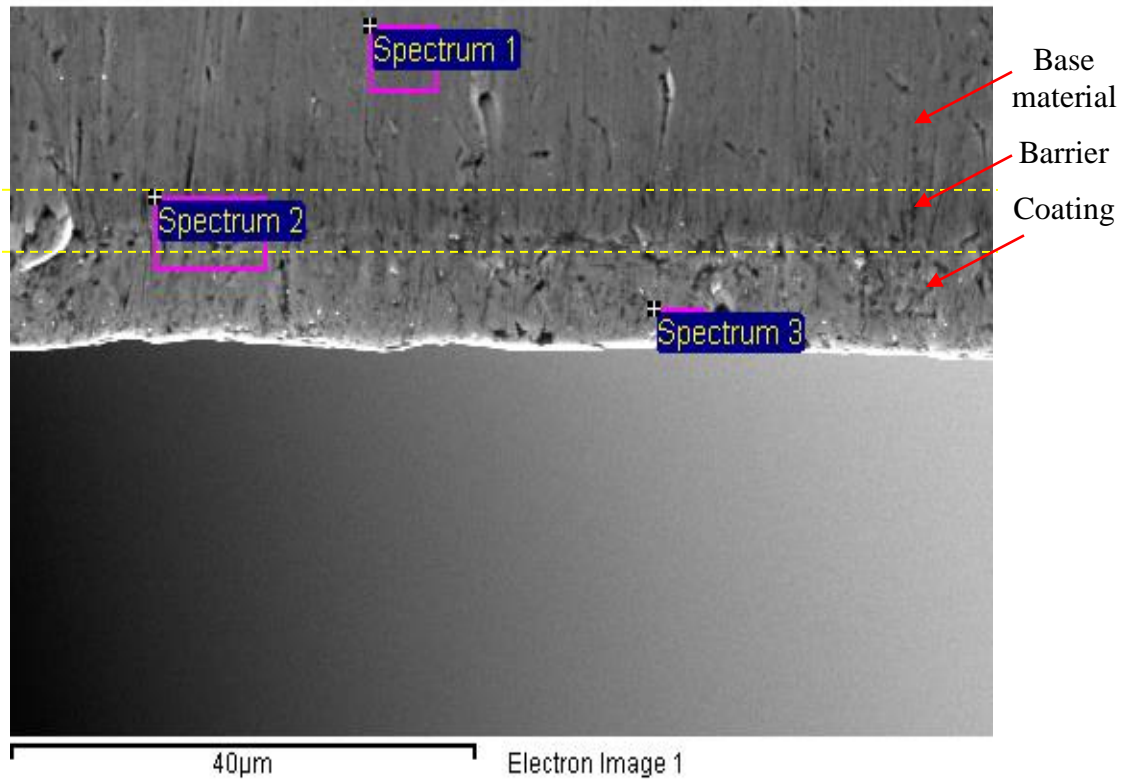
Figure 2-16: SEM Photo of Cross Section of Fresh Sample

2.3.3 Observation Using SEM and EDS

Table 2-2: Composition of Fresh Sample

Measurement Location	Cu (%)	Sn (%)	Ni (%)
Spectrum 1	91.99	8.11	0
Spectrum 2	6.6	54.85	38.55
Spectrum 3	2.03	97.97	0

Figure 2-16 illustrates the photograph of the cross section of the fresh sample. At different measurement locations, the significant variance is observed on compositions as demonstrated in Table 2-2. At Spectrum 1, copper and tin occupied 91.99% and 6.11%. The area of Spectrum 2 consisted of nickel in 38.55%, and tin in 54.85%. At Spectrum 3, tin was observed as the most element occupying 86.02%. These locations correspond to the tin coating, nickel barrier and phosphor bronze base material.
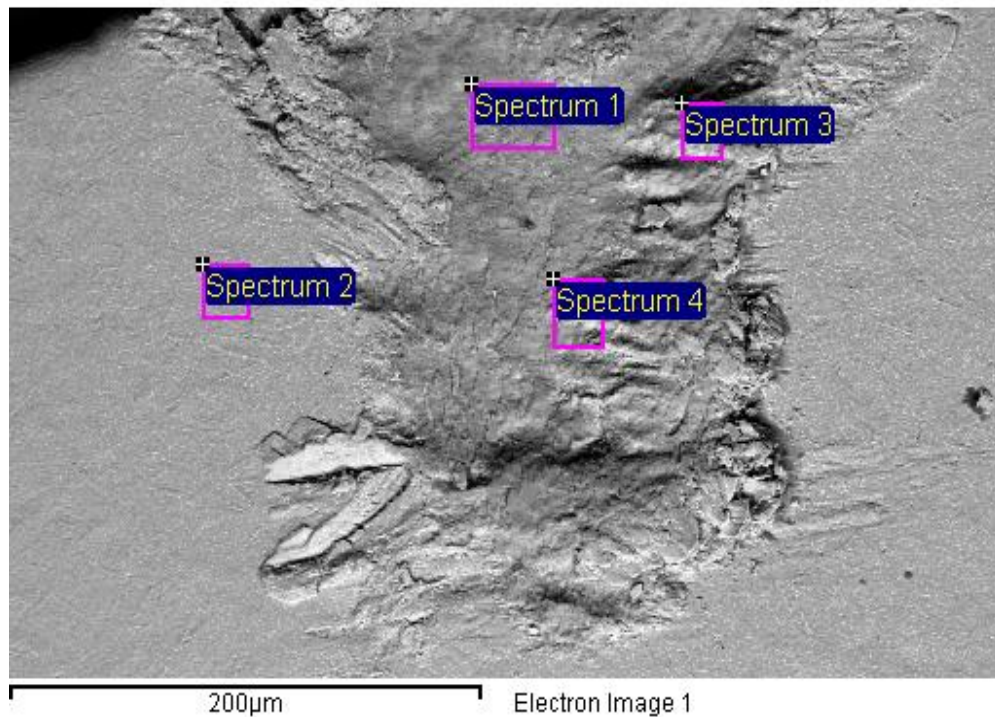
Figure 2-17: SEM Photo of Lightly Fretted Contact

Table 2-3: Composition of Lightly Fretted Contact

Measurement Location	Cu (%)	Sn (%)	Ni (%)	O (%)
Spectrum 1	1.22	64.27	4.92	29.59
Spectrum 2	0	99.8	0	0
Spectrum 3	1.58	76.46	2.55	19.41
Spectrum 4	0	68.58	7.59	23.83
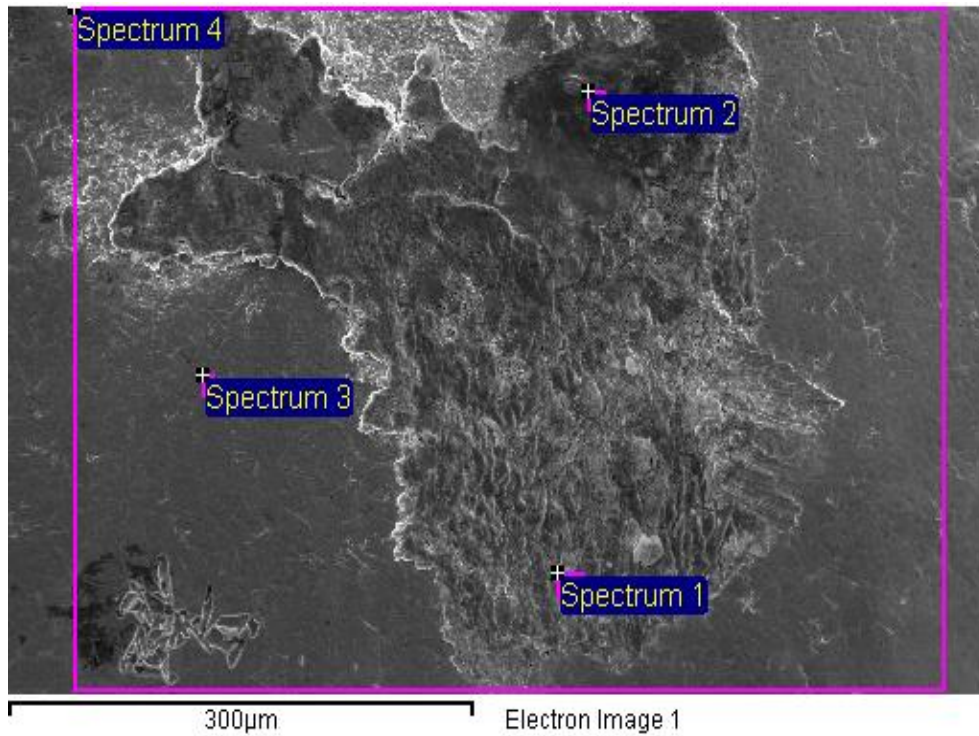
Figure 2-18: SEM Photo of Heavily Fretted Contact

Table 2-4: Composition of Heavily Fretted Contact

Measurement Location	Cu (%)	Sn (%)	Ni (%)	O (%)
Spectrum 1	0	62.96	2.68	34.37
Spectrum 2	0	30.61	28.42	40.97
Spectrum 3	0	96.83	3.17	0
Spectrum 4	0	74.01	3.71	22.31

In Figure 2-17, the sample was degraded for 10 seconds, and the contact resistance of it

was 0.135 Ohms. At Spectrum 2, the weight percentage of tin of the unfretted area was found as 92.05%, and no oxygen or copper was observed. In fretting areas of Spectrum 1, 3 and 4, oxygen occupied at least 20.67%, and the percentages of tin were between 56.92% to 68.74%. Copper was only observed at Spectrum 1, which occupies 1.08%. In this sample, base material layer was not exposed at the fretted area. In Figure 2-18, a sample fretted for 180 sec with about 8×10^4 **ohms** is shown. At Spectrum 1 and 2, the elements are oxygen, tin and a very amount of nickel. There was no copper found from Spectrum 4 that covers the whole contact area. Therefore the dielectric layer at the contact interface consists of tin oxide and nickel oxide for the heavily fretted specimen.
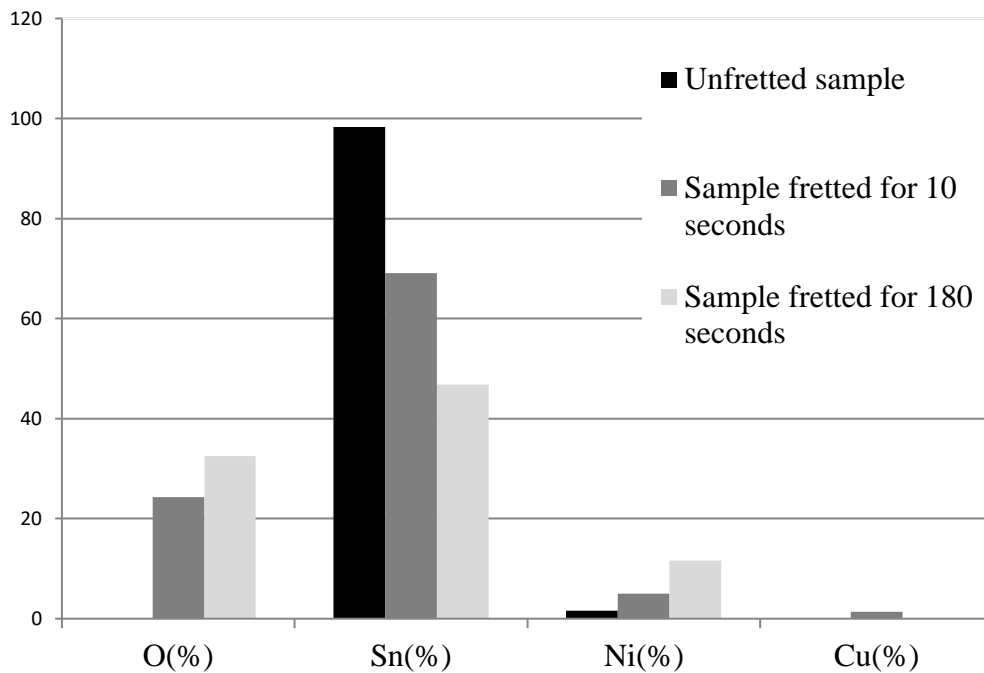
Figure 2-19: Comparison of Compositions at Contact Areas under Light and Heavy Fretting

The comparison of compositions at the entire contact areas with different levels of fretting is illustrated in Figure 2-19. On the surface of the fresh sample, tin and nickel were observed to respectively occupy 98.32% and 1.58%, and no oxygen or copper was found. With

a longer fretting period, more oxides were generated and accumulated at the fretted area which led to a rise of the ratio of oxygen. As the nickel barrier layer was gradually exposed, the ratio of nickel increased which consequently resulted in a reduction of the ratio of tin.

As an important fretting wear parameter, fretting depths at the contact surfaces with various fretting time lengths were measured with respect to SEM photographs on cross sections in Figure 2-20. The experimental result and a fitted curve of depth of fretting scar are illustrated in Figure 2-21. At the early stage, the depth increased faster than that of the latter stage. This can be attributed to the difference of micro-hardness between tin, tin oxide and nickel. A higher hardness of tin oxide and nickel compared to tin led to a less weight loss at the latter stage. This behavior is in the close fashion with the estimated metallic weight loss in a study on film development of tin plated contacts. [80]
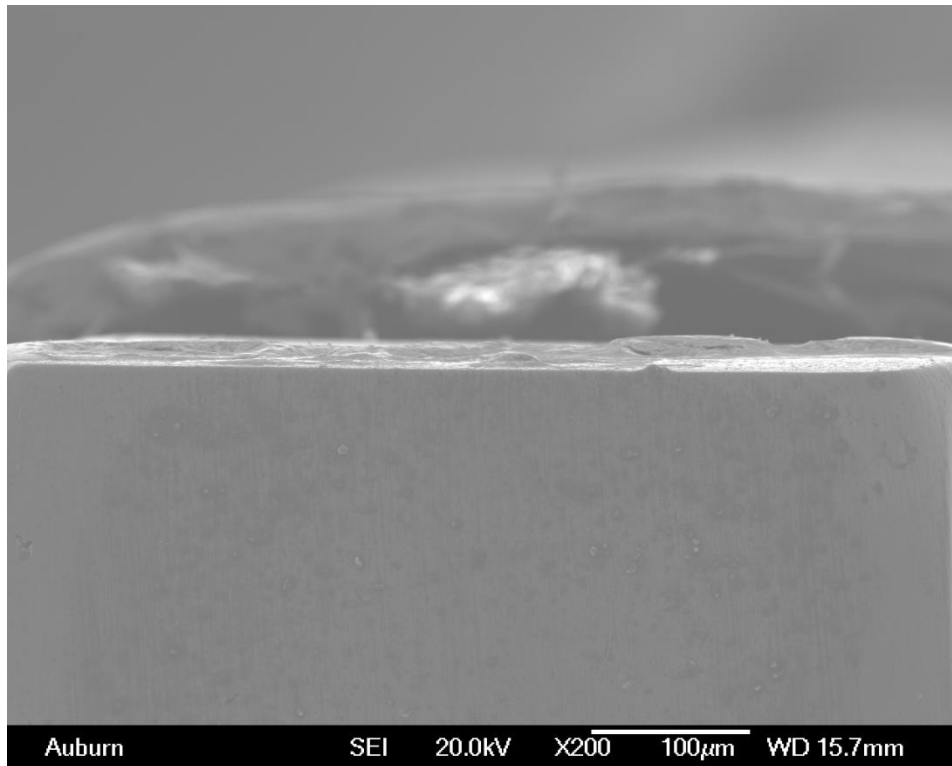
Figure 2-20a: SEM Photo of Cross Section after 30-Sec Fretting

54
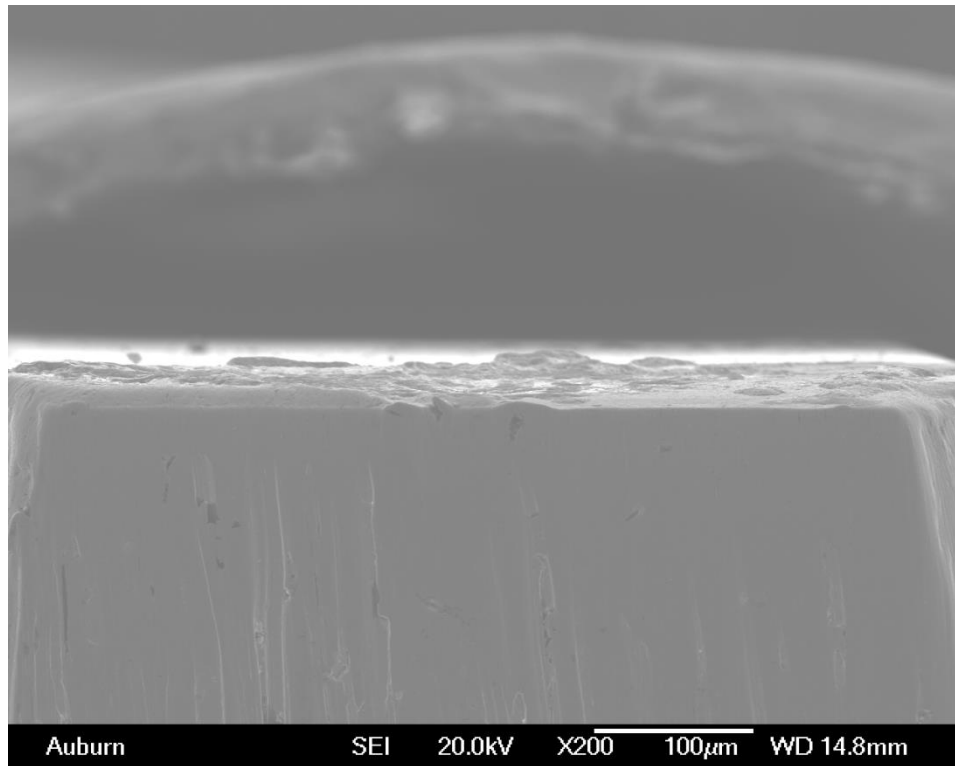
Figure 2-20b: SEM Photo of Cross Section after 60-Sec Fretting
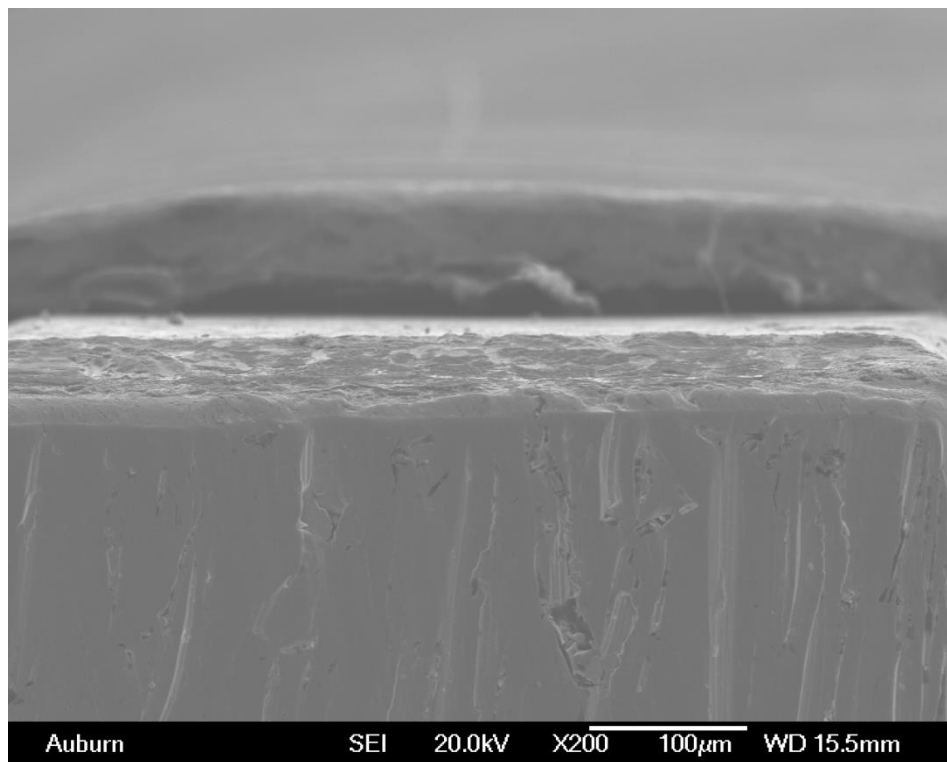
Figure 2-20c: SEM Photo of Cross Section after 120-Sec Fretting
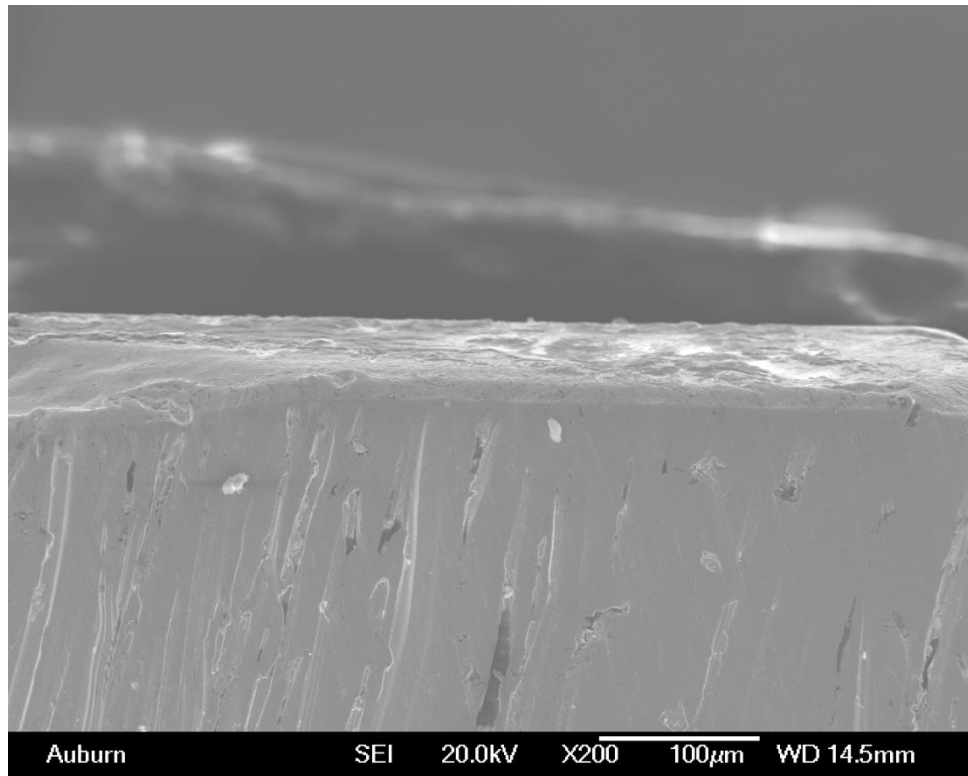
Figure 2-20d: SEM Photo of Cross Section after 240-Sec Fretting
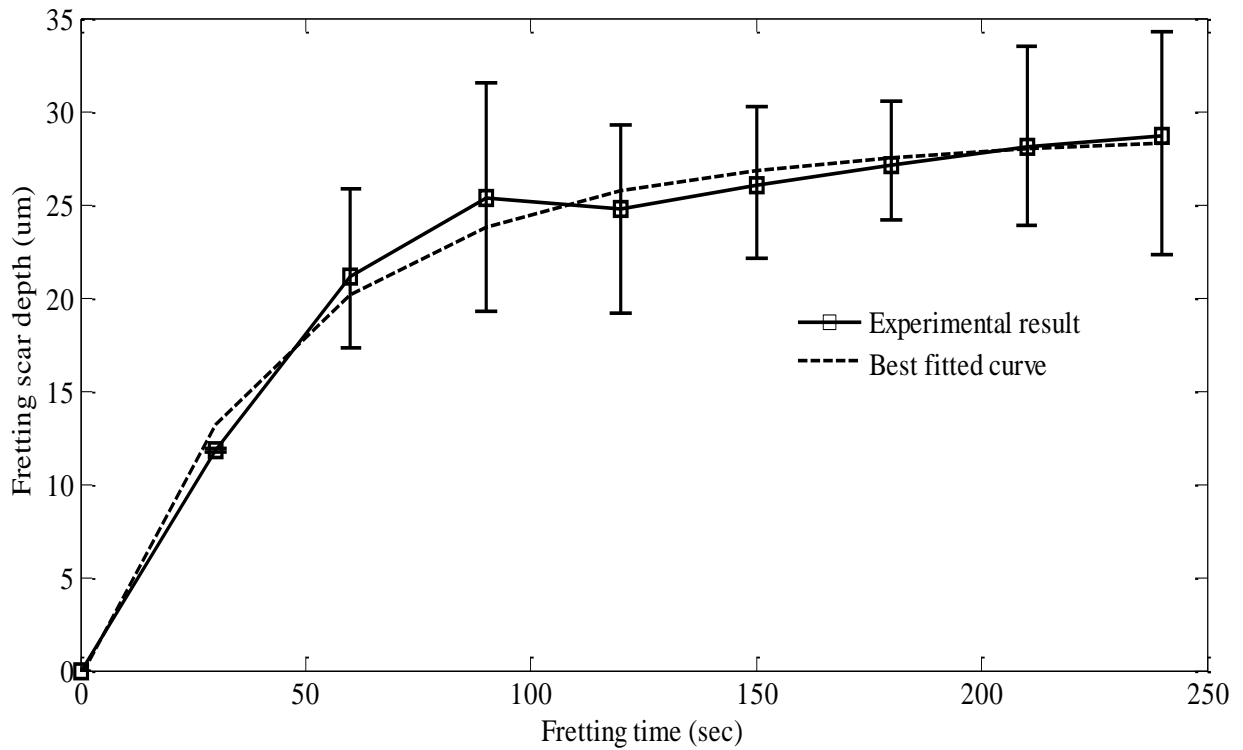
Figure 2-21: Depths of Fretting Scars after Various Fretting Periods

2.4 Model Development

Based on the existing statistical model [47], a tribological modeling work was proposed by Malucci to estimate the value of contact capacitance at different degradation levels [68]. As shown in Figure 2-22, h and h' are heights of asperities on two sides; e denotes the distance of the two contact surfaces; Z denotes the sum of h and h'. If two contact surfaces are considered uniform, they have the same largest height of asperities, h_0, before contacting. In the condition that two surfaces contact with a zero normal force,

$$\max(Z) = 2h_0 = e \tag{5}$$
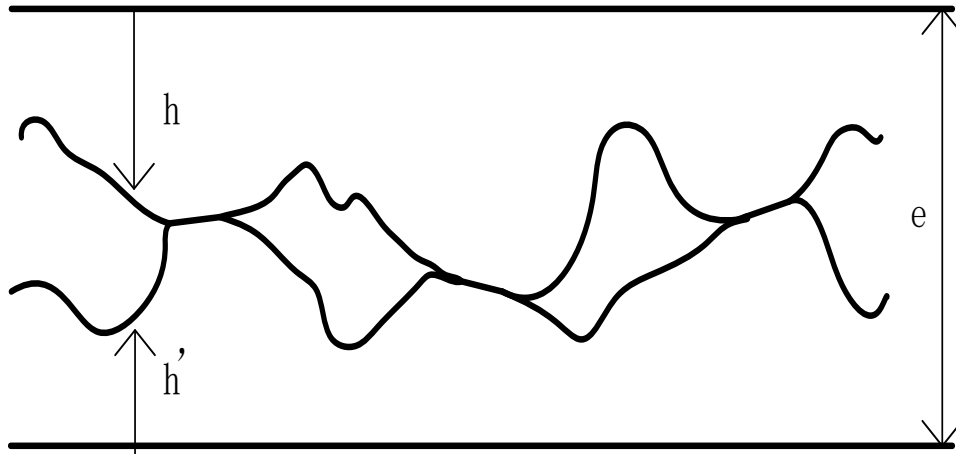
Figure 2-22: Schematic of Real Contact Area at Contacting Interface

With a larger contact normal force, Z turns larger than e. The micro capacitance values caused by the non-contacting areas are approximated using an parallel plate capacitor model where the fringe fields are neglected. The density of h is assumed to vary in a random fashion. The density function of h is expressed as [47]

$$W(h) = \frac{\pi}{2h_0} \cdot \sin\left(\pi \cdot \frac{h}{h_0}\right).$$

(6)

This equation depicts only one surface. The density of sum of h and h' was accounted for using a procedure outlined by Kimura [84] described in the following equation

$$W(Z) = \left(\frac{d}{dZ}\right) \iint\limits_{h+h'\leq Z} W(h) \cdot W(h') \cdot dh \cdot dh'$$

(7)

where Z is in the range $0 < Z < 2h_0$. Using Equation (6) and (7), on the assumption that the roughness of the two surfaces is uniform, the density function for Z is obtained as

$$W(Z) = \frac{\pi}{8h_0}\left[\sin\left(\frac{\pi Z}{h_0}\right) - \frac{\pi Z}{h_0}\cos\left(\frac{\pi Z}{h_0}\right)\right].$$

(8)

Equation (8) describes W(Z) in the case that $0 < Z < h_0$. When $Z > h_0$, W(Z) is expressed as
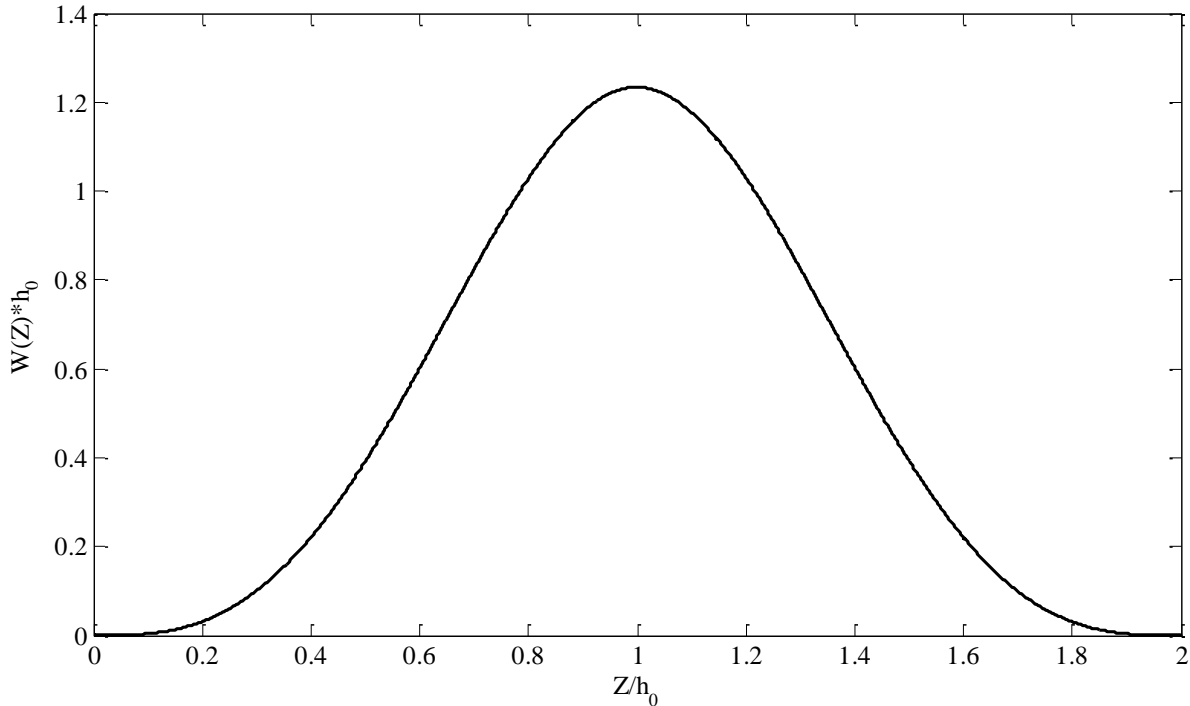
Figure 2-23: Probability Density Function for the Sum of h and h'

$$W(Z) \cdot h_0 = \frac{\pi}{8} \left[\sin \left(\pi(2 - \frac{Z}{h_0}) \right) - \pi(2 - \frac{Z}{h_0}) \cos \left(\pi(2 - \frac{Z}{h_0}) \right) \right]. \tag{9}$$

A plot of density function of W(Z) represented by Equation (8) and (9) is illustrated in Figure 2-23.
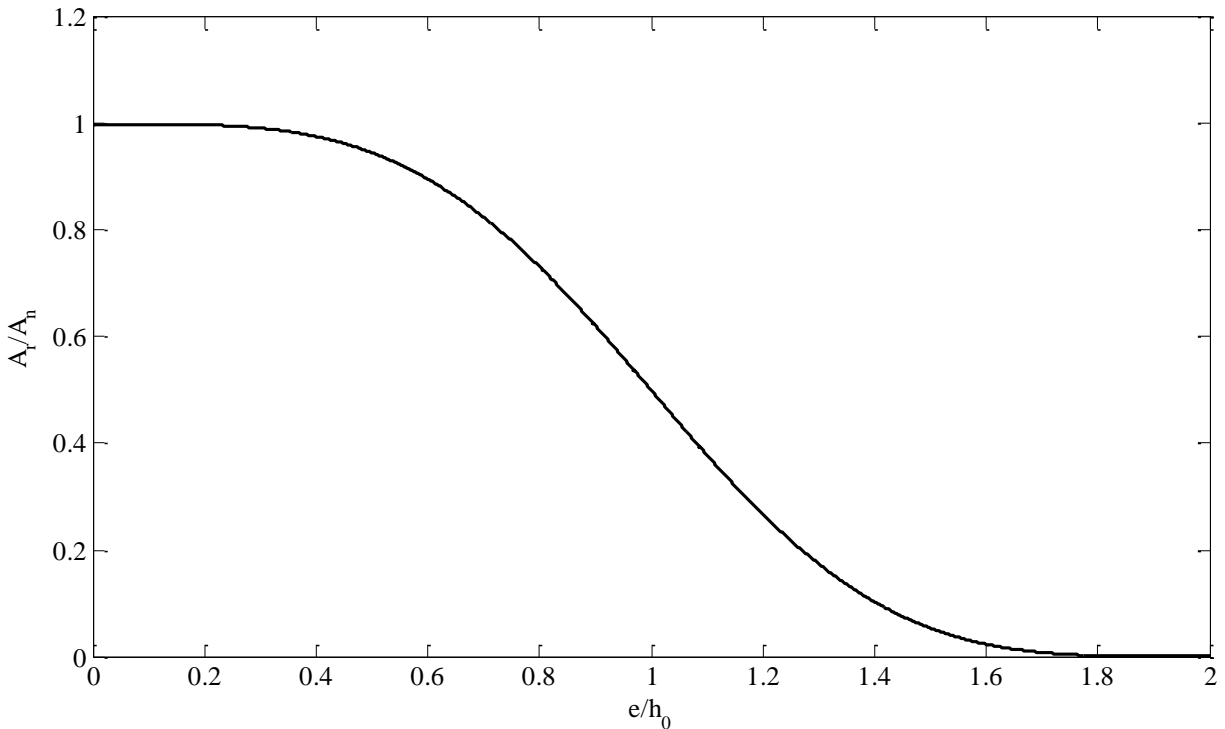
Figure 2-24: Fraction of Contact Area versus Clearance between Two Surfaces

Matching like components in the preceding relation results in

$$\frac{A_r}{A_n} = \int_e^{2h_0} w(Z) dZ \tag{10}$$

where A_r and A_n respectively denote real and nominal contact areas. Using Equation (10), Figure 2-24 shows A_r/A_n versus e/h_0. This figure demonstrates the variation of percent of contact area with the separation of the surface. In the condition that e equals $2h_0$ where two surfaces just

touch with no asperity deformation, the normal force is zero and A_r is zero. As two surfaces are gradually compressed, the A_r increases and eventually equals A_n and there is no gap spaces between two surfaces.
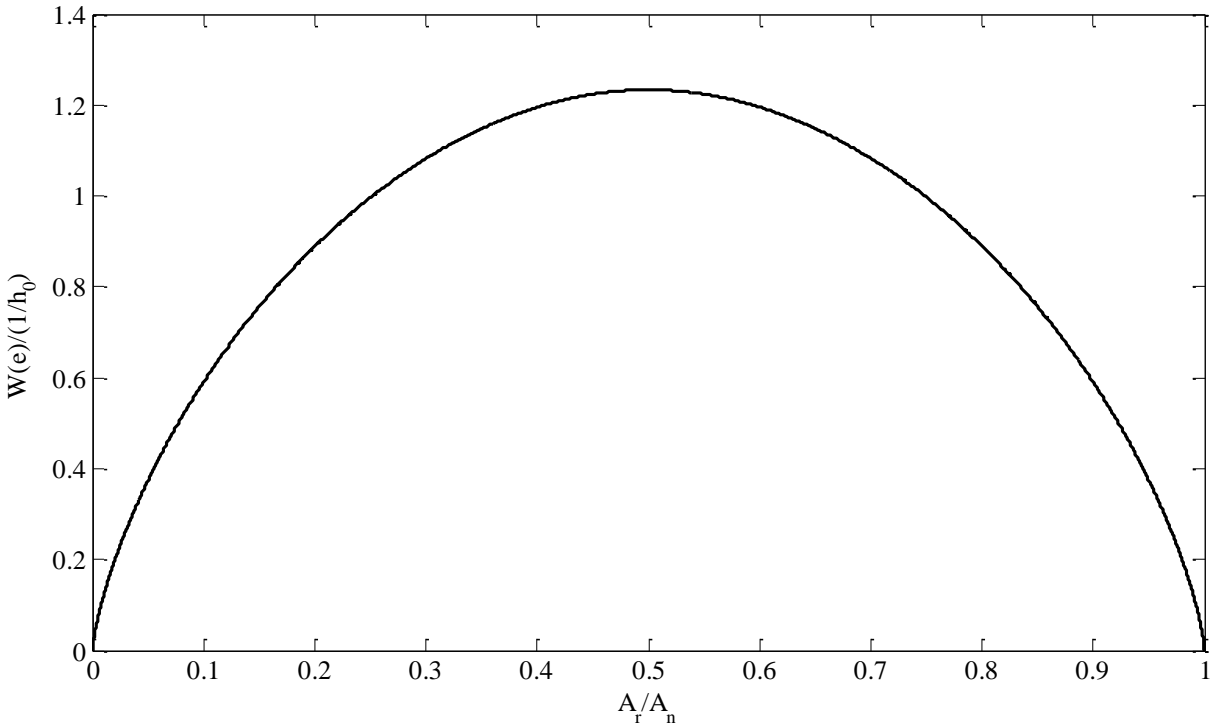
Figure 2-25: Density Function at e versus Fraction of Contact Area

Using Figure 2-23 and 2-24, the density function at e versus the fraction between real and nominal contact is shown in Figure 2-25. In the condition of contact degradation, the original contacting asperities are separated by a layer of dielectric film. In addition, dielectric debris are also removed from the asperities and stay at the gap space. The equation describing the contact capacitance of fretted contact area is

$$C_T = C_R + C_O \tag{11}$$

where C_T denotes the total contact capacitance; C_R denotes contacting area capacitance; and C_O denotes gap area capacitance. The distributed micro capacitors are assumed parallel plate elements with the fringe fields neglected. Therefore C_R and C_O are respectively the sums of micro capacitors at contacting and non-contacting areas. The calculation is done using the following expressions

$$C_R = \epsilon \epsilon_0 \frac{A_r}{2n} \tag{12}$$

$$C_O = \epsilon \epsilon_0 \, A_n \left\{ \int_0^{e-2n} \frac{W(Z)}{[2n + \epsilon \, (e - 2n - Z)]} dZ + \int_{e-2n}^{e} \frac{W(Z)}{2n} dZ \right\} \tag{13}$$

where ϵ_0 is vacuum permittivity and ϵ denotes relative permittivity of dielectric layer at the contacting area. The equivalent thickness of dielectric film on each side of contact, n, is assumed uniform over the contact area, between the contact asperities and in the gap. The result of simulation showed that the contact capacitance increases as the contact load increases and decreases with a thicker film [68].

To incorporate experimental data in the model, A_r/A_n is to be obtained according to a relation between micro-hardness of surface layer and nominal pressure [85]. There are several potential expressions of the relation for different scenarios. Based on the experimental data of the samples and testing setup, the A_r is expressed as

$$A_r / A_n = P / H \tag{14}$$

where H is the micro-hardness of contact surface; P denotes the contact normal pressure. In the present case, H, micro-hardness of tin plating is 58.8399 MPA [86]. A_n is averaged as 0.144 mm² according to the SEM observation of contact areas as shown in Figure 2-26. Using a profilometer, the h_0 of the fresh contact is averaged at 0.266 um.
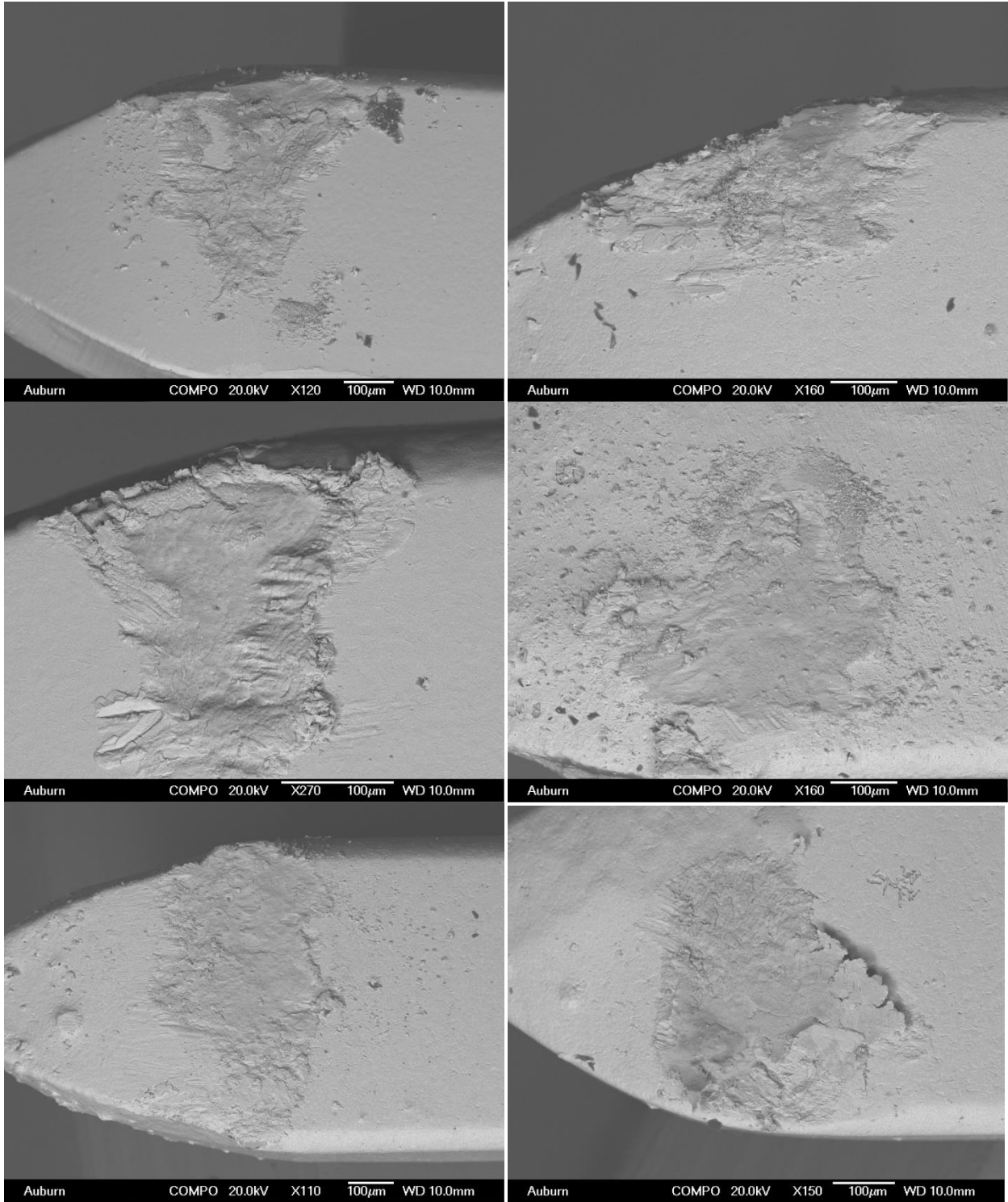
Figure 2-26: Example SEM Photographs of Fretted Surfaces
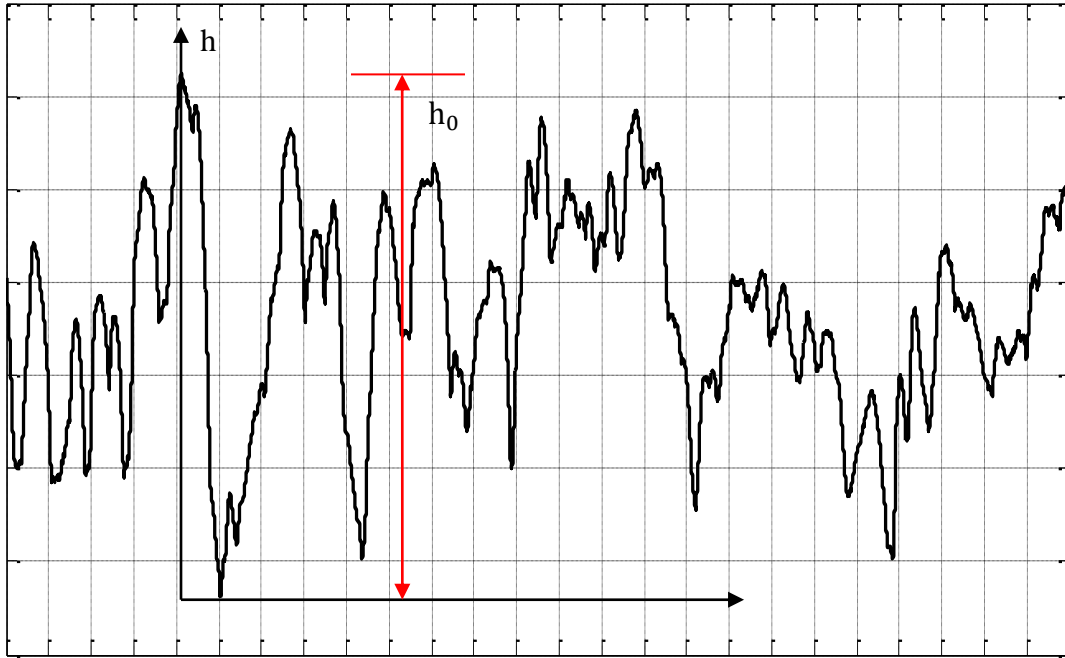
Figure 2-27: A Profilometer Trace of the Surface Profile

In the existing model, e and h_0 are considered constant which indicates that the corrosion is assumed limited at the asperities. However, with respect to the experimental results, fretting leads to weight loss and a scar with a depth larger than the scales of asperities. The average h_0 of the fresh specimen which is much smaller than the depth of fretting scar after 2-second fretting in Figure 2-21. Thus in this work, e and h_0 are considered increasing during the fretting motion, and h_0 of fretted contact is expressed as

$$h_0(t) = h_0(0) + d(t) - l(t) \tag{15}$$

where $h_0(0)$ denotes h_0 of fresh contact; $d(t)$ denotes the increase of depth of fretting scar; $l(t)$ represents effects of the decrease of size of dielectric particles and removal of them from the contact area which decline the gap distance [87]. $d(t)$ is obtained experimentally as shown in Figure 2-21, and $l(t)$ is assumed a linear function of time with a coefficient k_1. As h_0 varies, e

also changes as a function of time with the correlation as shown in Equation (9).

The corrosion products of tin and nickel have been study using XPS analysis, which are identified as SnO and NiO [88-89]. Due to the close relative permittivities of SnO and NiO, weakly approximate to 10 and 11, and the large portion of SnO corrosion, $\in$ is simplified as 10 in this model [90-91]. Because the rate of oxidation of SnO at early stage can be recognized as a linear function of time [92], the thickness of dielectric film, n, is assumed a linear function of $d(t)$ with a coefficient k_2. Matching like components in the preceding relation leads to a revised C_R and C_O expression as

$$C_R = \in \in_0 \frac{A_r}{2 \cdot k_2 \cdot d(t)} \tag{16}$$

$$C_O = \in \in_0 A_n \left\{ \int_0^{e(t)-2 \cdot k_2 \cdot d(t)} \frac{W(Z)}{[2 \cdot k_2 \cdot d(t) + \in (e(t) - 2 \cdot k_2 \cdot d(t) - Z)]} dZ \right.$$

$$\left. + \int_{e(t)-2 \cdot k_2 \cdot d(t)}^{e(t)} \frac{W(Z)}{2k_2 d(t)} dZ \right\} \tag{17}$$

Figure 2-28 summarizes the experimental and modeling capacitance developments versus fretting periods. In the comparison, there was no experimental results obtained before 50 seconds, because of the low resistances at the early stage. With a low resistance, the imaginary part of impedance is close to zero without obvious trend which results in the difficulty of the extraction of contact capacitance. For the experimental results, a generally decreasing fashion of capacitance is observed for each testing sample. The modeling capacitance also decreases once fretting proceeds which matches the trend of the experimental results. The simulated capacitance of the fresh contact is about 86 pF, which is in the same scale of results in Malucci's estimation [68]. According to the comparison, though oxidation products with a relatively large dielectric constant are introduced, the increased thickness of the oxidation layer and the depth of fretting

scar separate the micro capacitor which dominantly contribute to a declining fashion of contact capacitance.
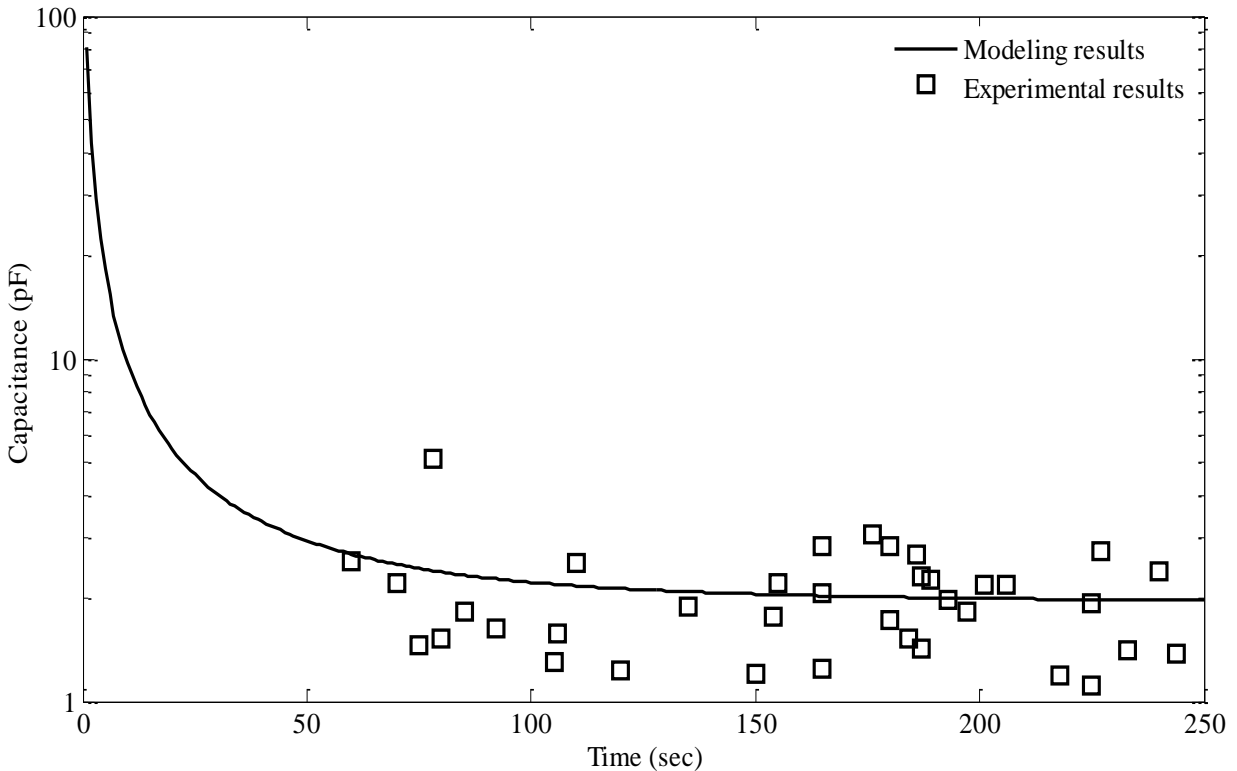
Figure 2-28: Experimental and Modeling Results of Capacitance at Various Fretting Periods

2.5 Summary and Conclusions

A study of vibration induced fretting corrosion in electrical contact was presented. To develop an understanding of impedance behavior and corresponding mechanism of contact subjected to fretting degradation was the current major aim. Towards this end, this investigation examined the correlation between impedance and fretting levels, based on an experimental study and a statistical model on a simple contact configuration. According to the experimental analysis, capacitive characteristics were obviously observed on highly degraded contacts. As a result, the major impact of fretting to signal transmission is at the low end of the frequency spectrum. It was also observed that no significant reactive influence was caused by lightly fretted contact over the

testing frequency range. The experimental and modeling results were well correlated to indicate a decreasing trend of capacitance as fretting corrosion proceeds.

This insight naturally lends itself to a faulty detection strategy of electrical connectors and interconnections in high frequency data transmission application. If an additional dielectric properties was found with a performance like a high pass filter in an application where electrical contacts were involved, the occurrence of fretting corrosion would be reasonably suspected.

CHAPTER 3   EFFECTS OF FRETTED ELECTRICAL CONTACTS TO HIGH FREQUENCY DATA TRANSMISSION

3.1 Introduction

Fretting degradation has been considered one of the most common failures in electrical connector in various applications [2]. The significance, necessity and considerable research efforts on this continuing topic have been demonstrated in previous chapters. With the procession of fretting corrosion in electrical connectors, the buildup of an insulating oxide layer between the blade and receptacle results in an increased resistance which leads the current passing through the contact interface to be distorted and thus is deleterious on signal and power transmission.

Nowadays, high frequency data transmission has been widely applied and various types of RF connectors, such as BNC, SMA, AMC, etc., are adopted in multiple industries. Contact impedance, rather than contact resistance, of electrical contacts in RF connectors is supposed to be taken into account as a significant factor, especially when damage occurs. Thus, it is necessary to understand whether and how the contact damages potentially induces signal losses and distortion. The author's previous investigation on the topic of vibration-induced fretting corrosion has already revealed some interesting behaviors. Based on an experimental impedance measurement, capacitive characteristics were observed at the contact interface subjected to vibration induced fretting corrosion. The increasingly significant capacitive properties are prone to impact low frequency signal integrity. The model considering the resistance and capacitance

of a typical contact interface has been employed and modified to explain the development of contact capacitance with different degradation periods.

Using FEA modeling, Malucci et al have implemented transmission line parameters and field effects to study the impact of contact geometry and degradation on wave propagation. Time domain and frequency domain signal integrity analyses were both performed [70]. In the further study, the critical parameters of a capacitive coupled contact interface were taken into account. The correlation between the physics of the contact interface and contacts relying on capacitive coupling was built. This study helped to define the contact parameters such as real contact area, dielectric film and properties for high frequency signal propagation [71].

The present investigation further extends the response of the electrical contacts to higher frequencies. An experiment was performed on a simplified wired communication scenario with a pair of tin plated contact. Due to vibration induced fretting degradation, the contrast between high frequency signal transfer through fretted contact versus traditional metallic contact was conducted. A network model incorporating the transmission line and capacitive coupling parameters was developed to explain the high frequency performance. Before the description of the details of the work, a brief introduction of wired communication and corresponding techniques is introduced below.

3.1.1 Introduction of Transmission Line

In wired communication, physical wires are applied for data transfer between transmitter and receivers. Compared to wireless communication, the wired technology has multiple advantages including reliability, high speed, low cost, quality of service and high life expectancy. The internet connection through fiber optic cables and signal transmission through metal

conductor on a printed circuit board (PCB) have been widely applied. The demands for high speed of data transfer has increased continuously due to a growing number of devices and users.

Transmission lines refer to metal conductors through which electrical signals are transmitted from transmitter to receiver at a high speed. They are traditionally recognized as telecom based cables operating over long distances. Short traces transmitting digital signals can also be considered transmission lines [93].

Microstrip is a type of electrical transmission line fabricated using printed circuit board (PCB) technology to convey microwave frequency signals. As shown in Figure 3-1, it is comprised of a conducting metallic strip, a ground plane and a dielectric layer between them known as the substrate. Various microwave components can be formed from microstrip. For example, the entire device of antennas, couplers, filters, power dividers etc. often exist as the pattern of metallization on the substrate. Compared to the traditional waveguide technology, microstrip is much less expensive and far lighter and more compact. With the capability to route signals with minimal distortion, and avoiding high cross-talk and radiation, microstrip lines can also be used as high-speed digital PCB designs.
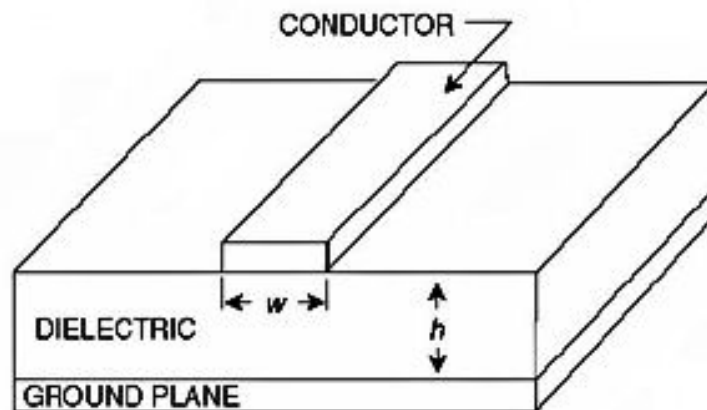
Figure 3-1: Microstrip Transmission Line [94]

A stripline circuit refers to a transmission line with a flat strip of metal sandwiched between two parallel ground planes as shown in Figure 3-2. The dielectric material substrate works to separate the strip and ground planes. Stripline is much harder to fabricate than microstrip. Due to the second ground plane, the conductor width of a stripline is much narrower than that of the microstrip for a given impedance and board thickness. The width of the strip, the thickness and relative permittivity of the substrate determine the characteristic impedance of the transmission line.
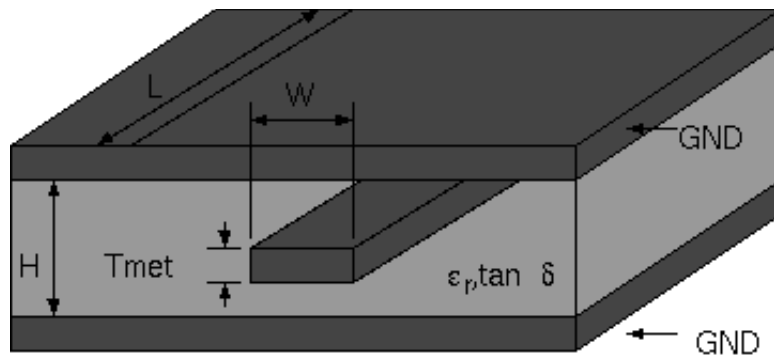
Figure 3-2: Stripline Transmission Line [95]

Coplanar waveguide (CPW) uses a ground conductor coplanar with the signal conductor. The characteristic impedance is determined by the signal line width and the ground gap. The commonly used configurations are coplanar waveguide and coplanar waveguide with ground as shown in Figure 3-3. Coplanar waveguide has the best ability to taper in to a pin since it concentrates the field in the gap. If transitioning from a microstrip line into a CPW, special attention is required. For this case, coplanar waveguide with ground (CPWG) is easier to deal with because the wide gap of a microstrip or a stripline can gradually transit to the coplanar

waveguide with ground connection.

(a) CPW   (b) CPWG
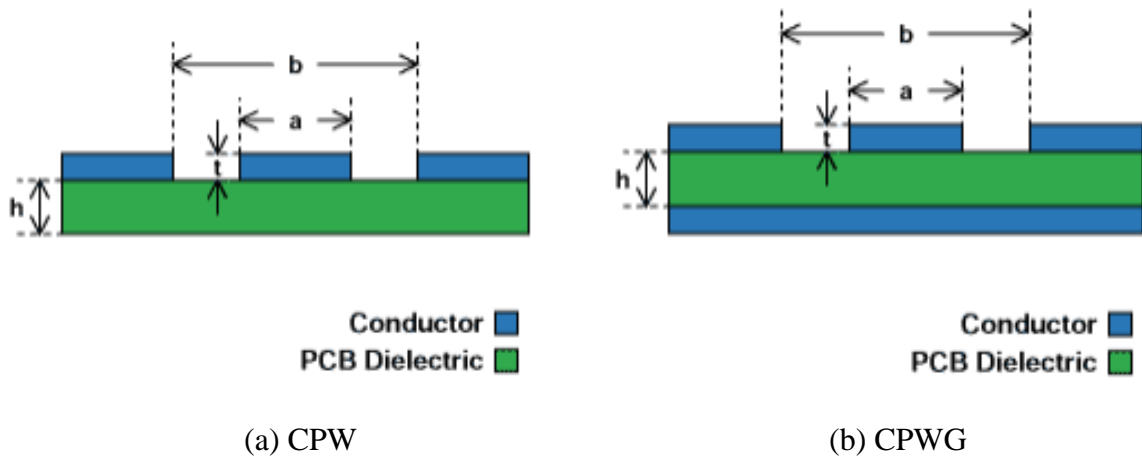
Figure 3-3: Configurations (a) Coplanar Waveguide (b) Coplanar Waveguide with Ground [96]
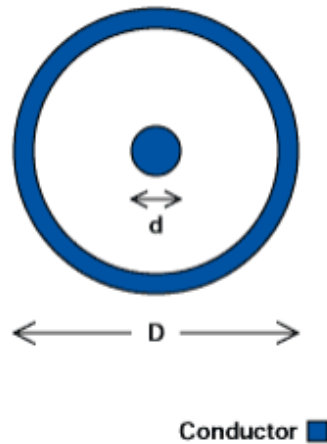
Figure 3-4: Configuration of Coaxial Line [96]

Coaxial line is the simplest transmission line configuration with inner and outer conductor as shown in Figure 3-4. There is an exact solution for its characteristic impedance and propagation velocity based on physical parameters Therefore, coaxial line equations are used to match these transmission lines to the surrounding circuitry and thus minimize the discontinuity. Coaxial lines are used in some scenarios on printed circuit boards. When routing a signal from

one layer of the printed circuit board to another, round pads on each layer and holes plated with metal to connect these pads are always applied. The pad for the via and a ground plane cut-out surrounding it constitute a short section of coaxial transmission line. In low volume production, as rework, and for prototyping, coaxial lines can also provide a fully shielded path for signals on printed- circuit boards.

One of significant parameters of the transmission line is characteristic impedance (Z_0). It is determined by line parameters including the width and thickness of the conductor, height of the PCB core on either side of the trace, configuration of the lines and dielectric constant of the core. In order to maximize the signal transfer, it is necessary to optimize the transmission line to reach a characteristic impedance matched with impedance of transmitter and receiver. The mismatch of the line with the terminal impedance leads the signal to get reflected. Then it is possible for multiple reflections to occur within the system which deteriorates the performance of the system. In practice, traces have to be designed with controlled impedance for digital speeds greater than 1 Gbps. In the case of mismatch, signals are reflected back and forth within the system, and the reflection would continue until all the energy of the signal is dissipated. At high data rates this process may produce errors in signaling by inducing detrimental effects such as overshoot, undershoot, ringing and stair step waveform.

3.1.2 Definitions

S-parameters (or scattering parameters) depict the electrical behavior of electrical networks that undergo steady state changes by electrical signals [97]. Electrical properties of components such as resistance, capacitance and inductance can be acquired using S-parameters like gain, return loss, insertion loss, and voltage standing wave ratio and reflection coefficient. Generally S-parameters are expressed as complex numbers either in rectangular form or polar

form. An electrical network may have multiple ports which are the points where the signal enters or exits the network. For example, a two-port network is an electrical network with two ports, two pairs of terminals constituting the interface to connect the input network and other networks. Signal enters through input port and exit through output port. Figure 3-5 illustrates a schematic of a two-port network with port 1 as the input port and port 2 as the output port. V_1, I_1, V_2 and I_2 respectively denote voltages and currents for two ports.
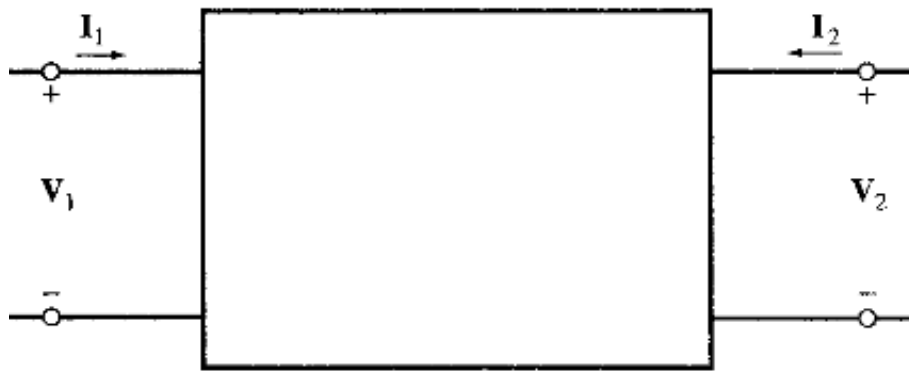
Figure 3-5: A Typical Two-Port Network
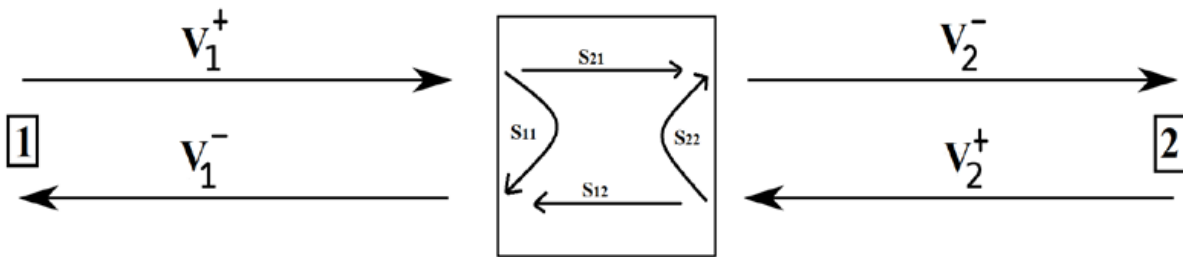
Figure 3-6: Two-Port S-parameter Network Model [98]

For two-port network four S-parameter elements constitute a 2×2 square matrix. Figure 3-6 shows a two-port network with reflected and incident power waves. For a matched load, S-parameters for a two-port network is expressed as

73

$$S_{11} = \frac{V_1^-}{V_1^+} \qquad S_{12} = \frac{V_1^-}{V_2^+} \qquad S_{21} = \frac{V_2^-}{V_1^+} \qquad S_{22} = \frac{V_2^-}{V_2^+} \tag{1}$$

where S_{11} denotes input port voltage reflection coefficient; S_{12} denotes reverse transmission coefficient; S_{21} denotes forward transmission coefficient; S_{22} denotes output port voltage reflection coefficient.

Insertion loss is the extra loss of the network present between the ports. Insertion loss is a measurement of forward transmission coefficient expressed in terms of decibels

$$\text{IL} = -20 \cdot \log(S_{21}) \ (\text{dB}) \,. \tag{2}$$

For maximum signal transfer, forward transmission coefficient is supposed to be high and insertion loss should be close to 0 dB. If the system impedance mismatch with terminal impedance then signal is reflected at the input and output ports. Return loss (RL) is a measure of input port reflection coefficient.

$$\text{RL} = -20 \cdot \log(S_{11}) \ (\text{dB}) \,. \tag{3}$$

For maximum transfer of signal, reflections at the input port should be low and, as a rule of thumb, and return loss with a expression in decibels should be below -30 dB.

3.2 Experimental Configuration

3.2.1 Experimental Sample and Equipment

As shown in Figure 2-3, the tin-plated pin header samples were the testing vehicle in this study. There have been numerous research efforts on understanding the process of tin coating subjected to fretting corrosion. In this study, the knowledge from previous research was involved to explain the high frequency characteristics of degraded contact interfaces.

Fretting degradation on the tin-plated contact was produced by a shaker system and a specially designed testing fixture which were introduced in last chapter. A signal generator

produced signals in respect of different vibration profiles. With the function of a power amplifier, the signals were amplified to drive the shaker to vibrate at an expected pattern. The stationary fixture was designed to be able to apply specific normal force on the contact area.

3.2.1.1 E5061B Vector Network Analyzer
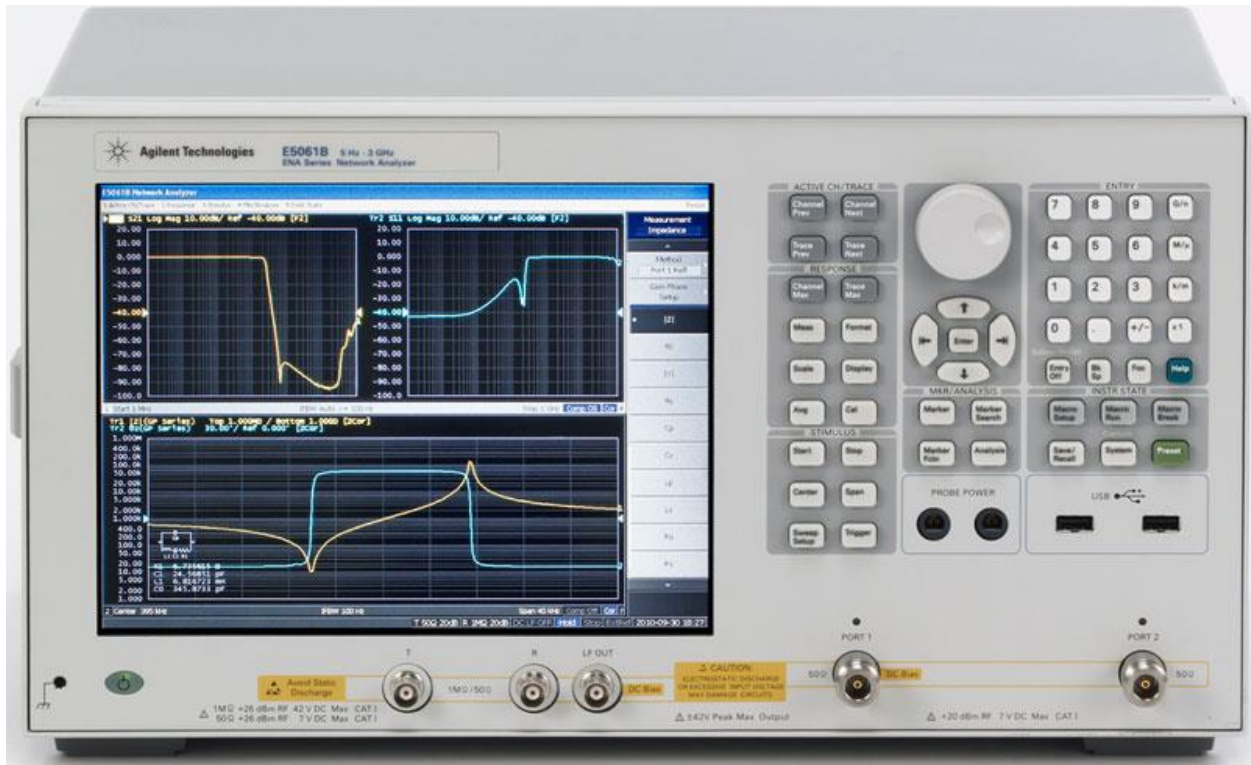
Figure 3-7: Photograph of the Agilent E5061B Network Analyzer

A vector network Analyzer (VNA) is an instrument measuring the network parameters of electrical networks, and is widely used in radio frequency design applications [99]. As shown in Figure 3-7, this two-port VNA is often used to characterize two-port networks like amplifiers and filters. Since reflection and transmission of electrical networks are easy to measure at the high frequency spectrum, E5061B VNA measures S-parameters. It has been applied for multiple measurement objectives such as distance-to-fault, return loss, insertion loss/gain, LF Circuits, etc.

The operating frequency of it ranges from 5 Hz to 3GHz. Compared to scalar network analyzer (SNA), VNA can explore both amplitude and phase properties of various networks. The dynamic ranges up to 120dB; the output power can be as large as 10 dBm. In this study, it was used to measure the network parameters of a transmission line where a degraded contact was involved, in order to evaluate the effect of fretting degradation on high frequency transfer.

3.2.2 Experimental Setup

The testing article was as the same as the study described in last chapter. A pair of tin-plated pin were widely used in printed circuit boards as board-to-board level and board-to-wire level male connectors. The reason they were chosen as the contact interface, instead of pin-to-socket pair, was that the simplest contact structure was favorable to avoid any external effect from dimensions of receptacles.

Figures 3-8 and 3-9 show the setup of the contact pair. This configuration consists of two same printed circuit boards, a pair of pins and two copper wires. Each board was with the same microstrip design of which the signal conductor forms a straight signal trace. They were sized to achieve a 50 Ohm characteristic impedance based on the board material properties and dimensions of the board design. A connector pin was soldered on a pad which was connected to the signal trace. An SMA connector was soldered on the opposite side of the board and the signal pin of it connects the signal trace on the board. With a flipped arrangement, the two tin coated pins touched at a small contact area at tips. The shaker head and fixture were mounted at specific locations for a constant contact area for different samples. And then, the pins, signal traces and SMA were placed in the same direction. The ground layer of two boards were connected using two flexible copper wires soldered on pads that were on the opposed side of pins. The wires were

symmetrically placed on two sides of the pins. All of the arrangement built up a high frequency

structure. Through two coaxial cables and adapters, the SMA connectors were connected to the
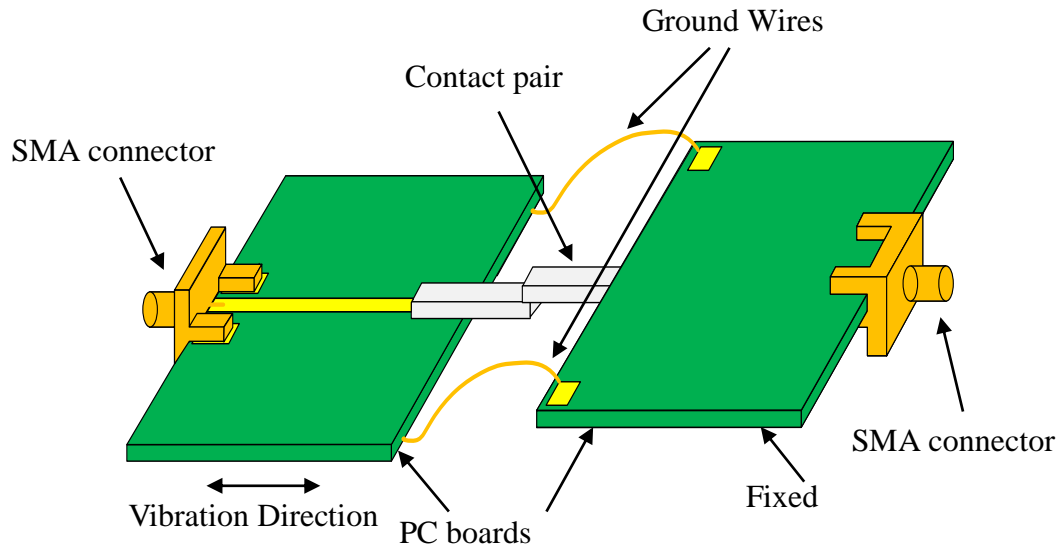
Figure 3-8: Schematic of Setup of Contact Pair
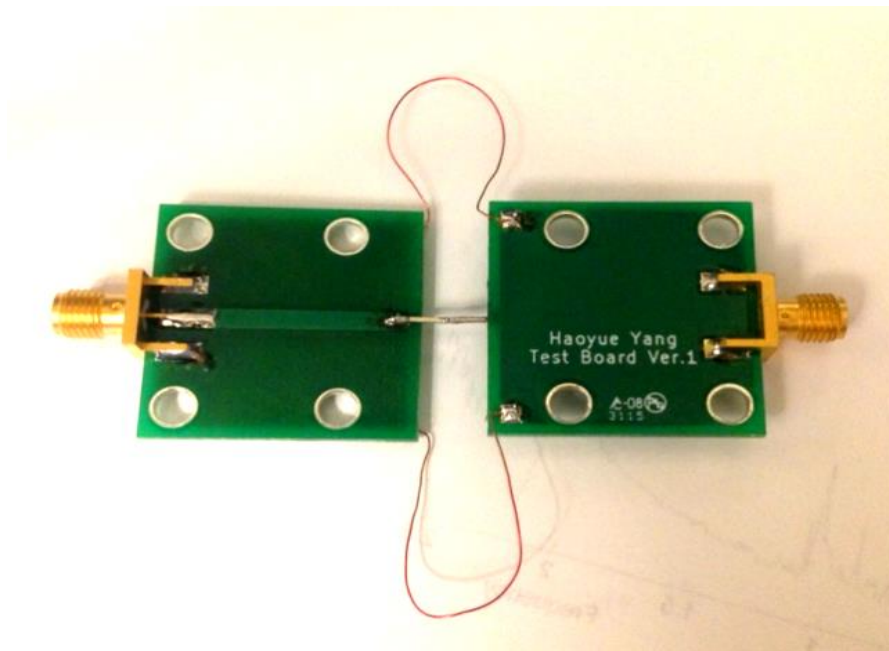
Figure 3-9: A Photo of Setup of Contact Pair

the vector network analyzer for the measurement of parameters of the high frequency

transmission line. In order to allow the relative motion between the pins, the wires were slightly longer than shortest distance between two boards. During the fretting process, the board on the left moved axially back and forth, and the one on the right kept stationary.
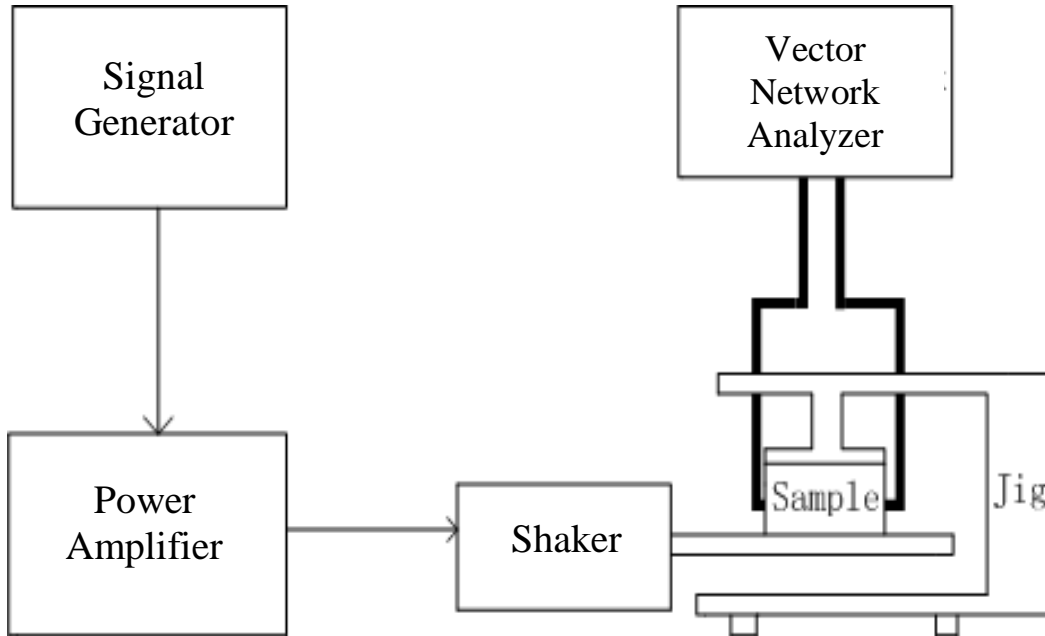
Figure 3-10: Schematic of Experimental Configuration

As shown in Figure 3-10, the same dynamic system as last study was used to produce the relative fretting motion at the contact pair. One of the PC board was fixed on the shaker table, and the other one was attached on the fixture. Two ports of the VNA were respectively connected to the testing transmission line through two SMA connectors. The testing specification was mentioned in Table 3-1. The shaker vibrated at 200Hz with an amplitude to produce a 30 um peak to peak relative motion between the connector pins. The jig applied 1.0 N as the normal force at the contact interface. All parameters were as the same as that of the study in last chapter in order to incorporate the behavior of contact impedance to understand the influence of fretting degradation to the transmission line's characteristics. VNA measured reflection and transmission coefficients in the range from 5 Hz to 3 GHz which extends the measurement spectrum of last

study.

<div align="center">Table 3-1: Testing Specification</div>

Vibration Frequency	200 Hz
Relative Displacement	300 um (peak to peak)
Normal Force	1.0 N
Measurement Frequency Range	5 Hz to 3 GHz

Before the measurement, the VNA was calibrated using a CalKit through an open/short/load procedure. Through this step, all reactive effects from measurement cables to internal components of the VNA were eliminated, and thus the measured results only revealed the behavior of the testing network which was considered DUT, device under test, of this study. The frequency domain network parameters were measured by VNA based on a frequency sweep through the testing spectrum. Compared to resistance measurement, it was impossible to make an inline record at the duration of fretting motion, which was like the impedance measurement. The Z-parameters, network impedances, were also inspected during the testing. The magnitude of impedance at 5 Hz was assumed fairly close to the resistance of the signal line. That means once if the contact resistance increases due to fretting, the low frequency impedance also increases, which was considered an indicator of fretting occurrence at the contact interface. However, it was possible that, at the very early stage of the fretting corrosion, resistance increased slowly, but the high frequency impedance changed significantly as a result of variation of micro structure at the contact area. Thus the network parameters of the entire spectrum would be inspected as fretting proceeds. The network parameters of the stationary testing article with the fresh and degraded contacts were measured. Besides, S-parameters were measured at various degradation levels in regard to resistance values.

After the calibration, external mechanical disturbance to the setup was not allowed because dimensional deformation of measurement circuit tends to cause unexpected impedance variances. Even it was susceptible that the vibration induced dynamic movement of the PC boards or copper wires would lead to oscillatory impedance variation. This was unacceptable that the measured network parameters interfered by any other factors than fretting corrosion at the contact interface. Therefore a series of baseline tests were necessary to perform using the vibration power slightly lower than the fretting threshold to validate the reliability of the experiments from mechanical vibration disturbances.

3.3 Experimental Results
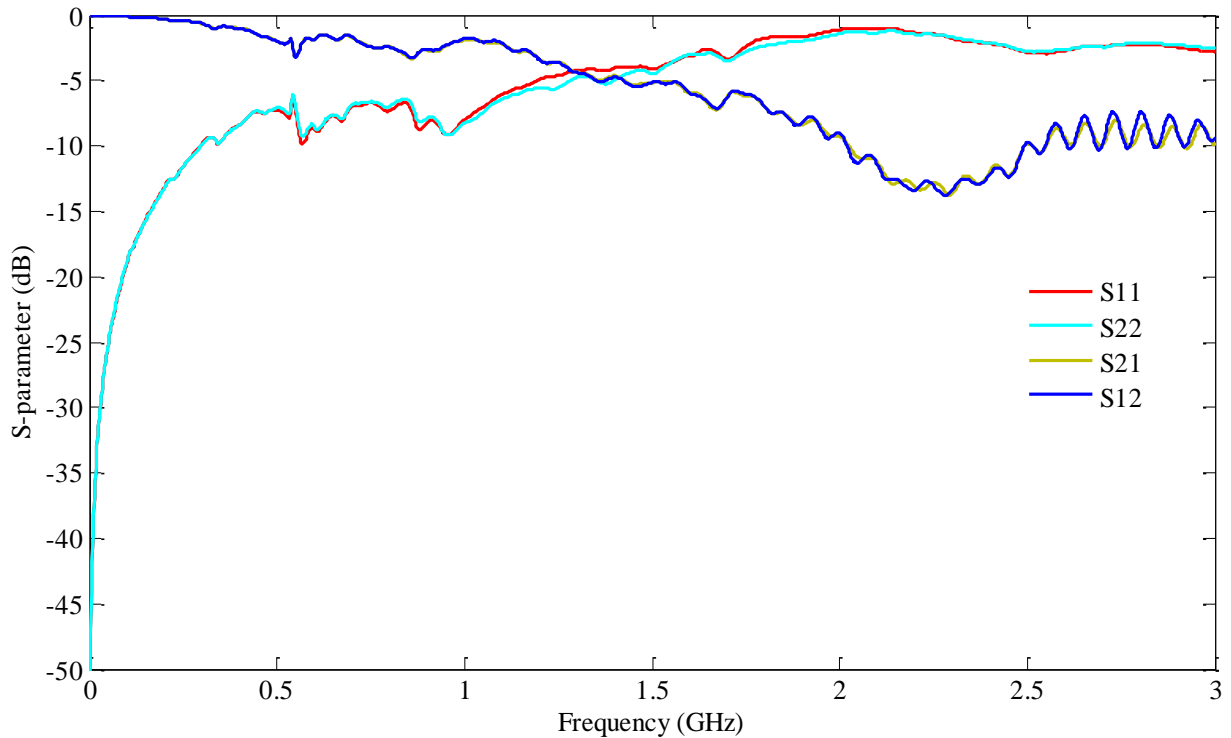
Figure 3-11: Experimentally Measured S-parameters of Fresh Contact

Figure 3-11 shows S-parameters of the testing network with a fresh contact. A good

match is achieved below 30MHz. The mismatch at the higher frequency spectrum is attributed to components not sized to 50 Ohms including the tin-plated pins as a part of the signal line and the copper ground wires. The symmetrical structure of the testing line leads to the fact that the S11 is close to S22, and S12 generally equals S21 over the measurement frequency range, as also shown in Figure 3-11.

The input impedance of the DUT at the 5 Hz, the lowest frequency of the measurement, is considered to be with the magnitude approximately as the same as the resistance of the signal line. Thus, the input impedance was monitored during fretting as a indicator of the corrosion.
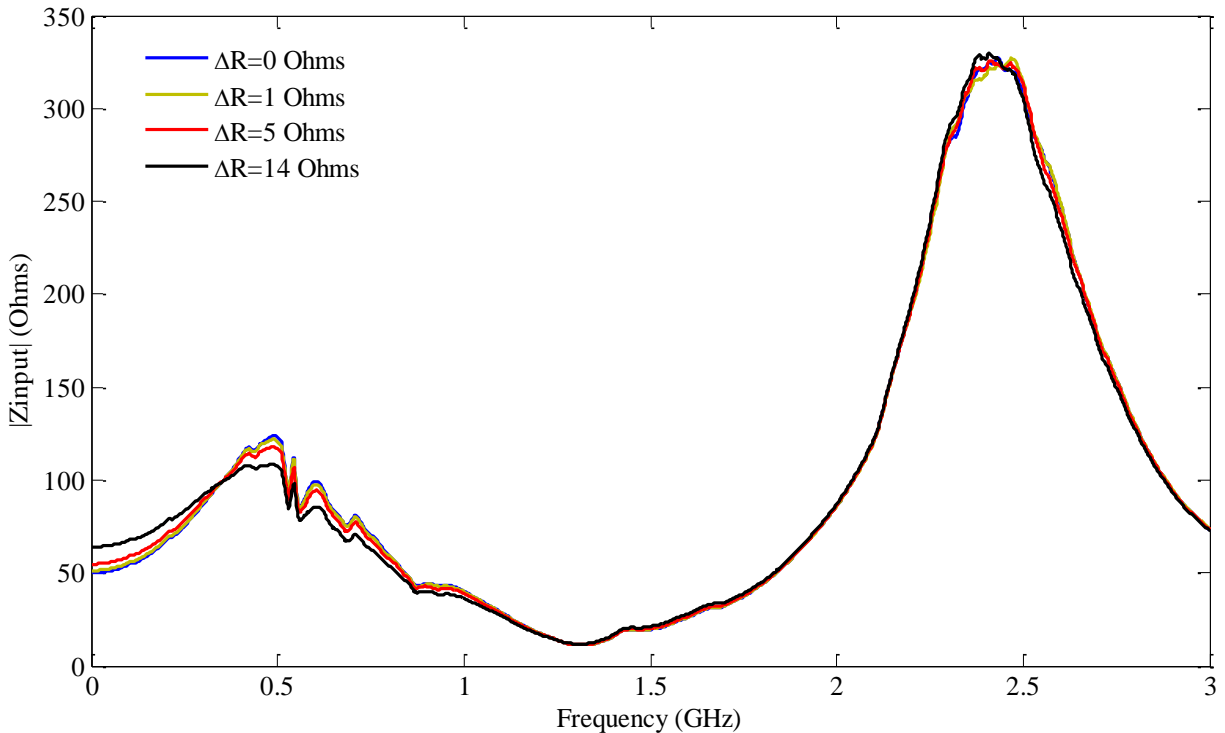
Figure 3-12: Input Impedance for Different Contact Resistances

In the condition that the contact resistance increases in a fairly small scale less than 50 mOhms, there is no obvious change found on S-parameters over the spectrum other than the magnitude values at the very low frequencies. However, as fretting proceeds and causes a larger
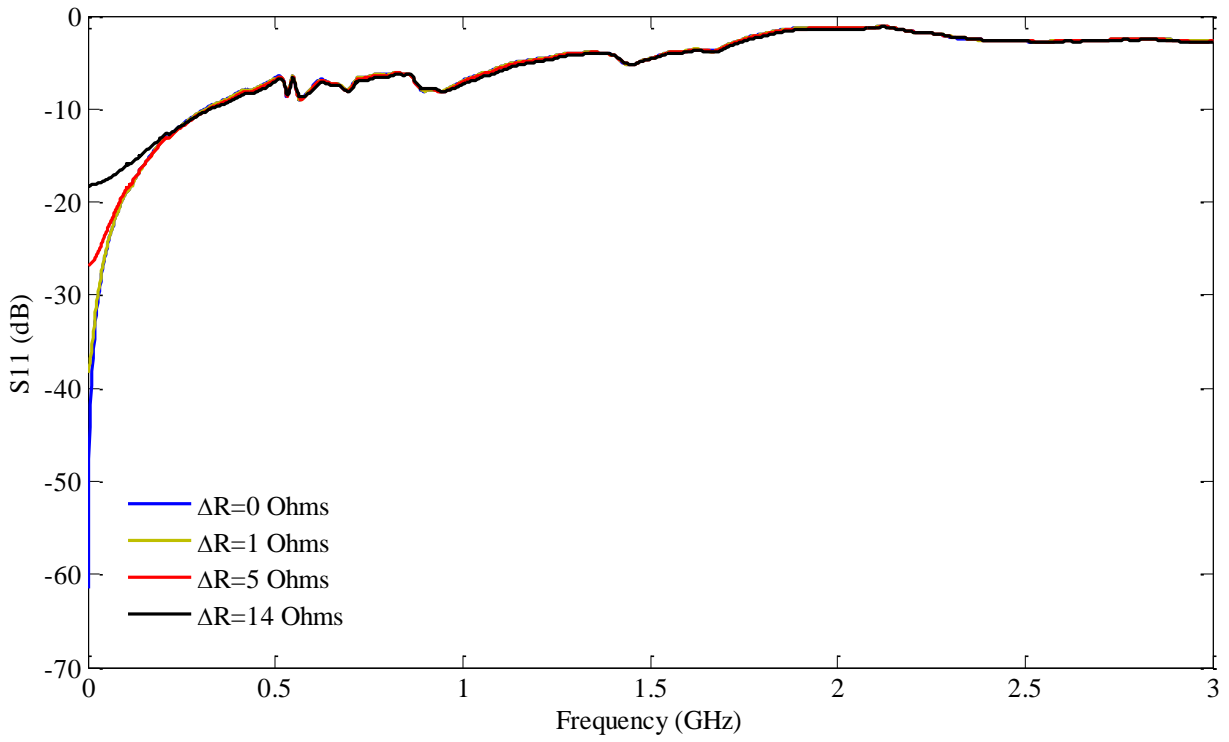
Figure 3-13a: S11 with Different Contact Resistances
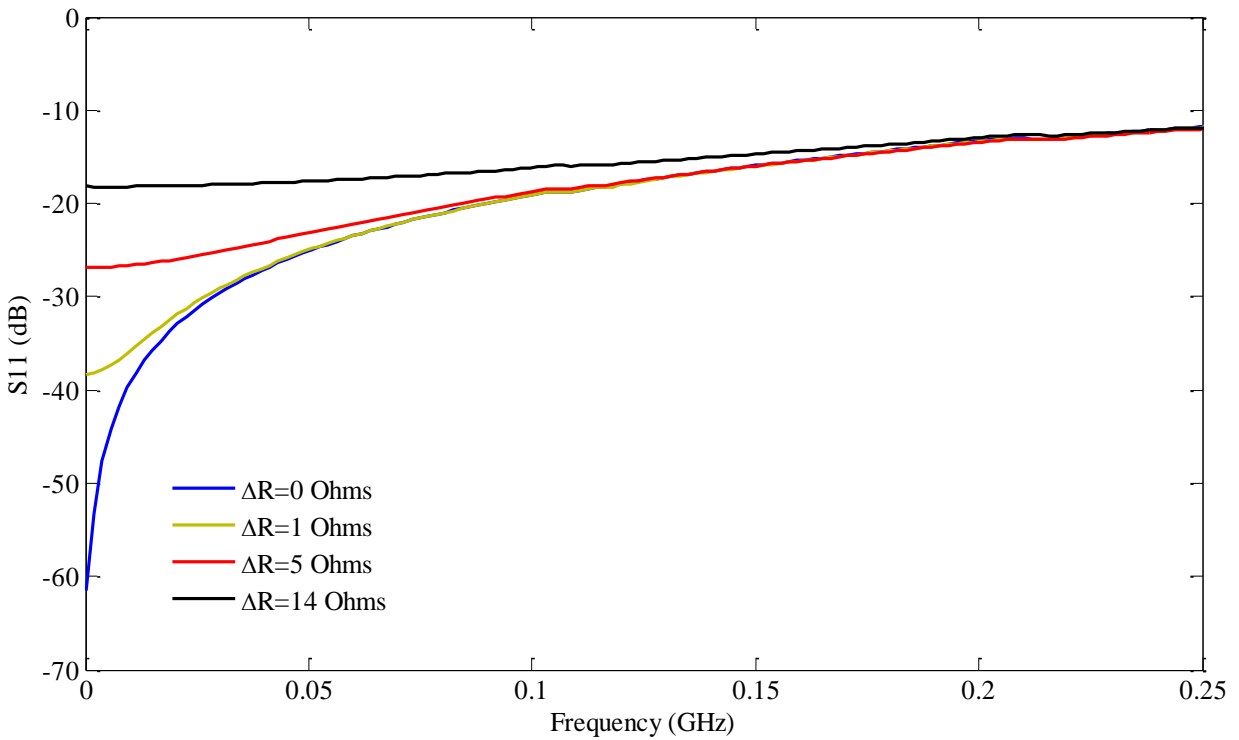
Figure 3-13b: S11 with Different Contact Resistances at Low Frequency Range

82
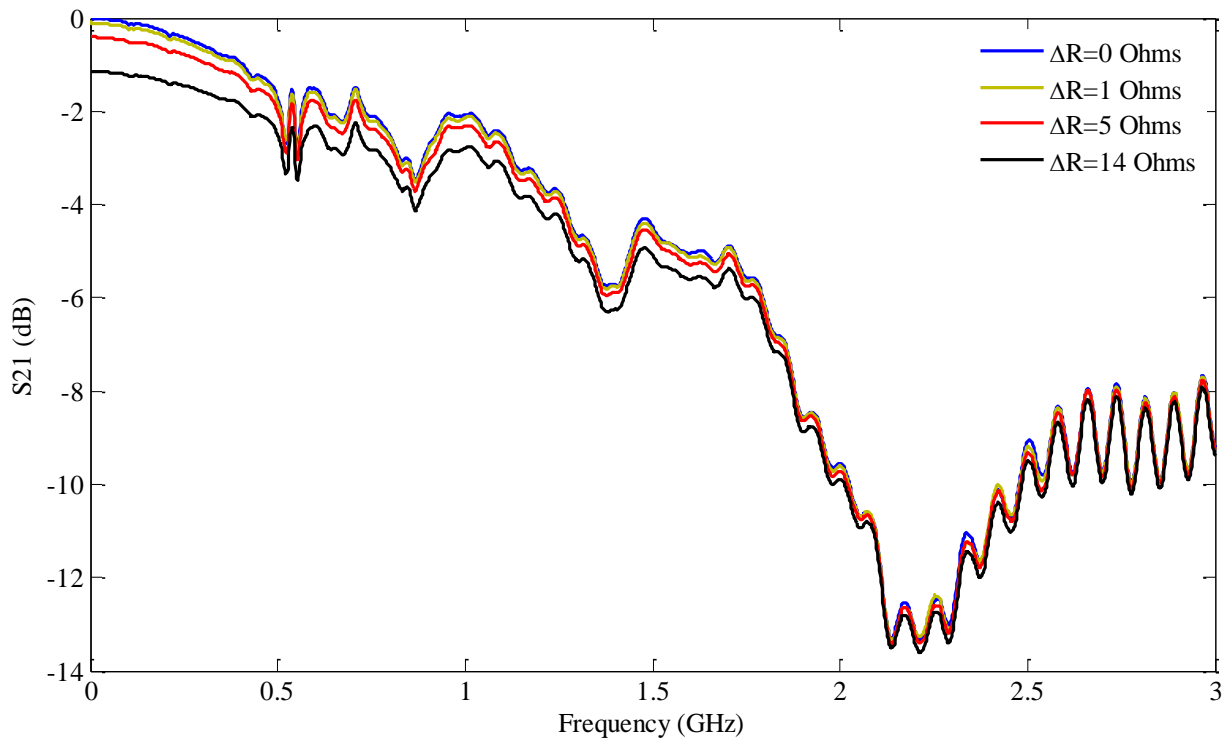
Figure 3-14a: S21 for Different Contact Resistances
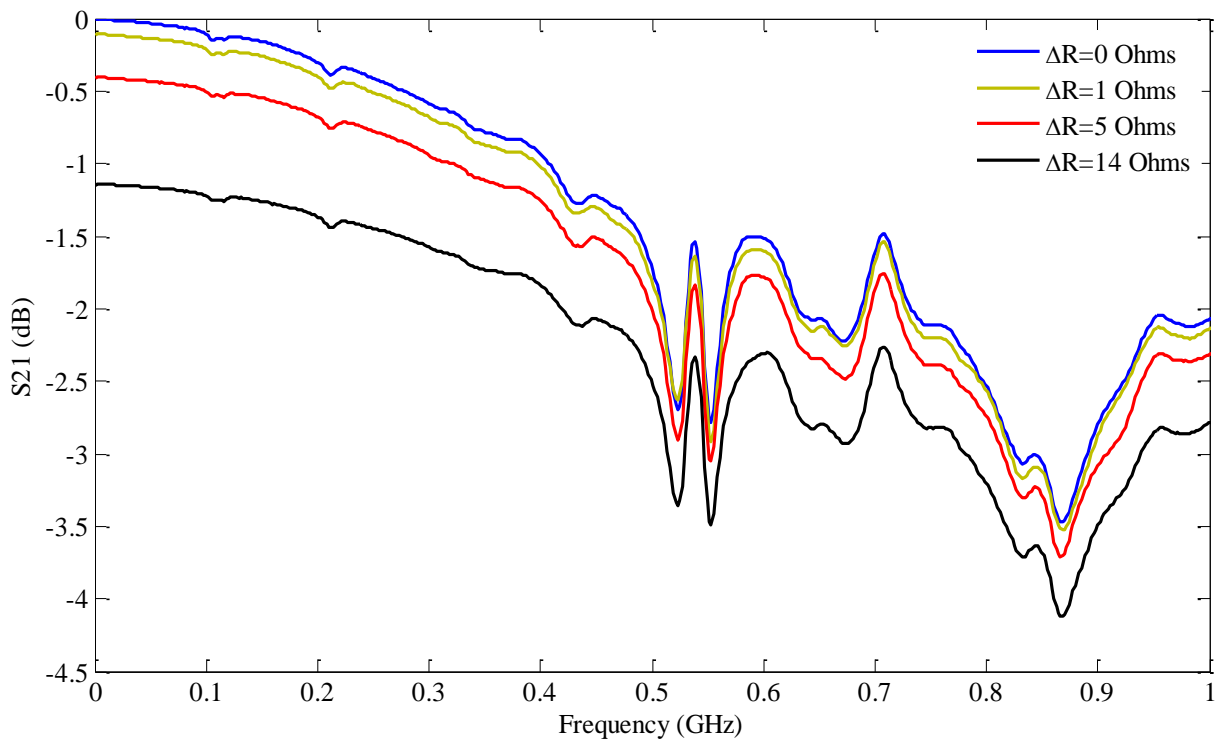
Figure 3-14b: S21 for Different Contact Resistances at Low Frequency Range
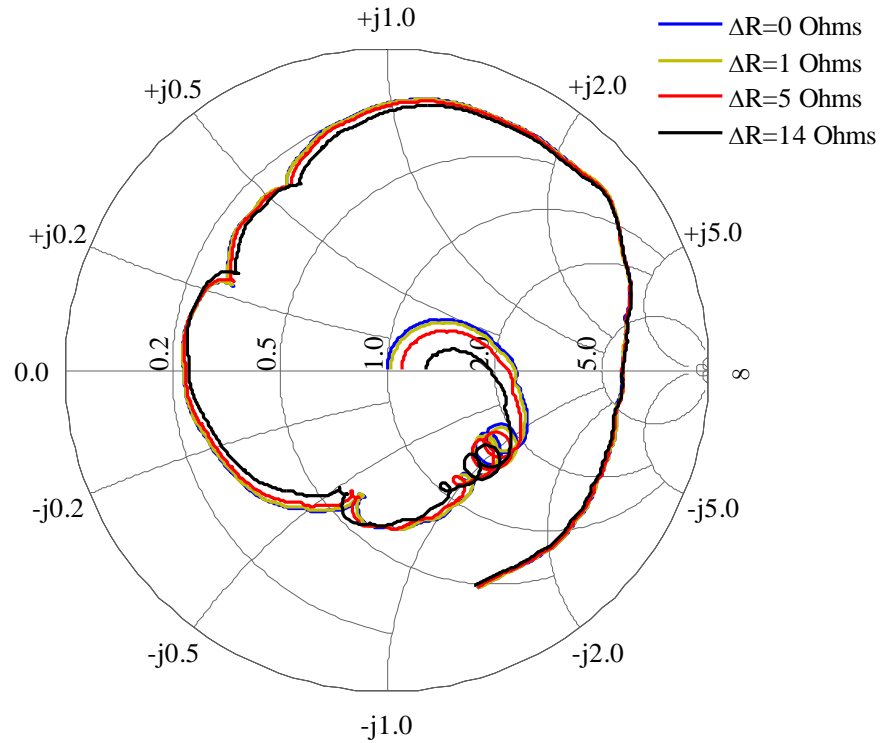
Figure 3-15: Smith Chart of S11 for Different Contact Resistances

scale of increase of contact resistance, significant variations are gradually observed on the network parameters. A shown in Figure 3-12, for the fresh contact without fretting induced resistance increase, the impedance magnitude at very low frequency equals 50 Ohms. As frequency increases, the good match corrupts and two peaks appear with magnitude higher than 100 Ohms. In addition, there is a valley between them, which is lower than 50 Ohms. The length and geometry of copper ground wire can significantly influence the peak values and frequencies,. Thus, all of these behaviors come from the dynamic and resonance performances of the mismatched testing network. With a higher contact resistance, the impedance magnitudes at very low frequencies monotonically rise and the values of two peaks decrease. As shown in Figures 3-13 to 3-15, with a higher contact resistance, a worse match is found in S11 below 250 MHz and in S21 almost throughout the spectrum. Some interference induced by the network layout is

observed on S21 beyond about 1.8 GHz, which is not eliminated by electromagnetic shielding. In addition, S11 and S21 are respectively close to S22 and S12, which indicates that the symmetrical and reciprocal properties of the testing network remains while degradation occurs at the contact area. This is an evidence that the variation observed is only caused by the fretting corrosion because the contact area is at the center of the symmetric testing network.

3.4 Model Development

A lumped circuit model of a trace with transmission line effect is assumed a combination of resistance, inductance, capacitance and conductance as shown in Figure 3-16 [100]. At low frequencies, transmission lines are considered lossless and wires are recognized ideal without resistance (R) and conductance (G). At a high frequency range, transmission line effects would become prominent in the network, as AC signals turns dominant. In this chapter, a circuit model is presented to simulate the effects of contact degradation to signal integrity.
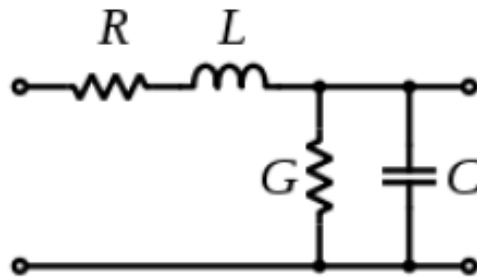
Figure 3-16: Lumped Circuit Model of a Transmission Line

For the sake of high quality simulation, Advanced Design System, ADS, was applied to perform the circuit modeling. ADS is an electronic design automation software system providing an integrated design environment for RF, microwave and signal integrity applications. It supports frequency domain, time domain circuit simulation and electromagnetic field simulation which allows to characterize and optimize designs using the single tool.
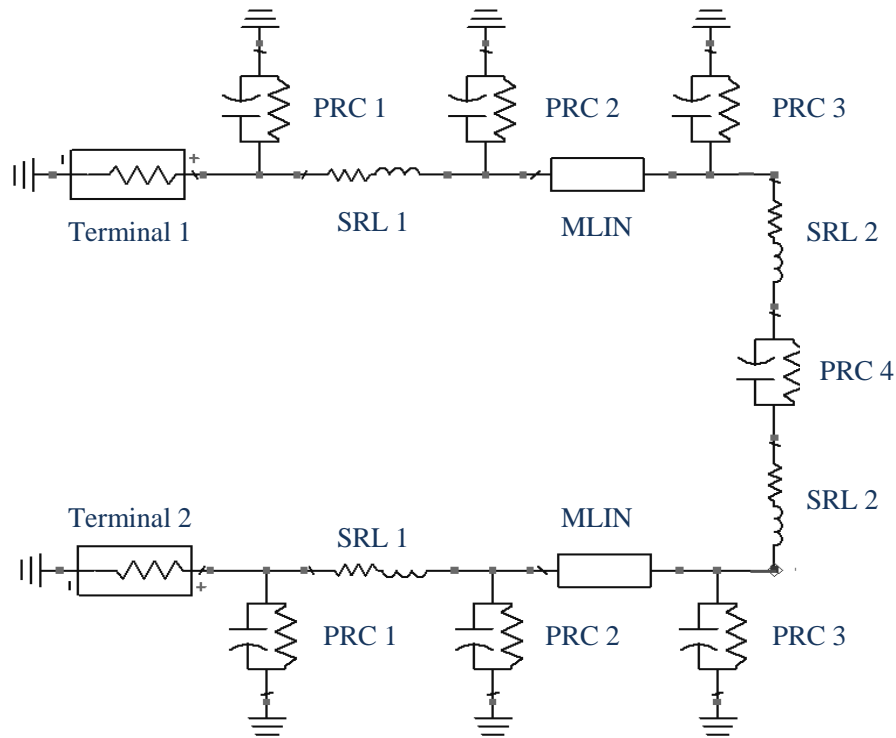
Figure 3-17: Circuit Model of the Testing Network in Frequency Domain Test

Based on models of the transmission line and electrical contact, a lumped circuit model was proposed to describe the configuration of frequency domain test on the testing network using network analyzer, as shown in Figure 3-17. In the model, two terminals of the network analyzer with impedances in 50 Ohms are located at the two ends of the network. A Parallel Resistor-Capacitor component, PRC 4, describes the contact of two tin plated copper pins. The Series Resistor-Inductor component, SRL 2 depicts the conductive copper pins to perform inductive at the high frequency range. According to the network layout and the experimental results of network parameters with and without the contact degradation, the system is symmetrical regarding the contact area. Thus, the circuits between each terminal and connector pins are with the same structure and component values. PRC1, SRL1 and PRC2 simulate the SMA connectors soldered on the boards. The linear microstrip component, MLIN, represents the effect of the

printed circuit board. PRC3 is used to simulate the effect between the connector pins and ground wires. Some values of the components are measured such as SRL1, SRL2. MLIN's behavior solely depends on the PC boards with respect to the dimensions and material parameters. The values of PRC 4 are determined by the statistical model developed in last study. The value of PRC 1, PRC 2 and PRC 3 are tuned to fit the modeling network parameters to the experimental results.
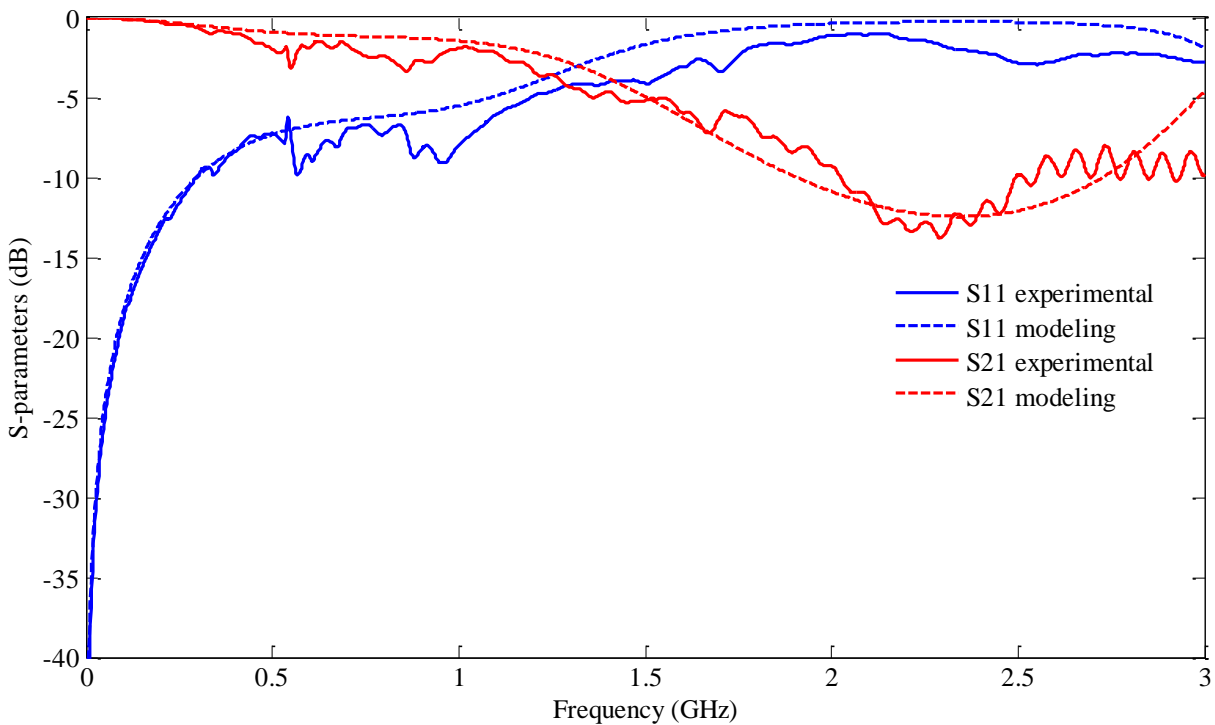
Figure 3-18: Comparison of S11 and S21 of Experimental and Modeling Results for Non Degradation Case

Due to the symmetrical and reciprocal properties of the sample line, S11 and S21 to be respectively close to S22 and S12. Through comparisons of S11 and S21 of the network model to that of the testing results, PRC 1, PRC 2 and PRC 3 were tuned to calibrate the network with fresh contact. Figure 3-18 shows the S11 and S21 curves from experimental and modeling results. Figure 3-19 illustrates a smith chart of S11 obtained from testing and simulation. The lumped

circuit model yields good agreements of the return loss and insertion loss with the testing network while fretting corrosion does not occur, especially at the low frequency range.
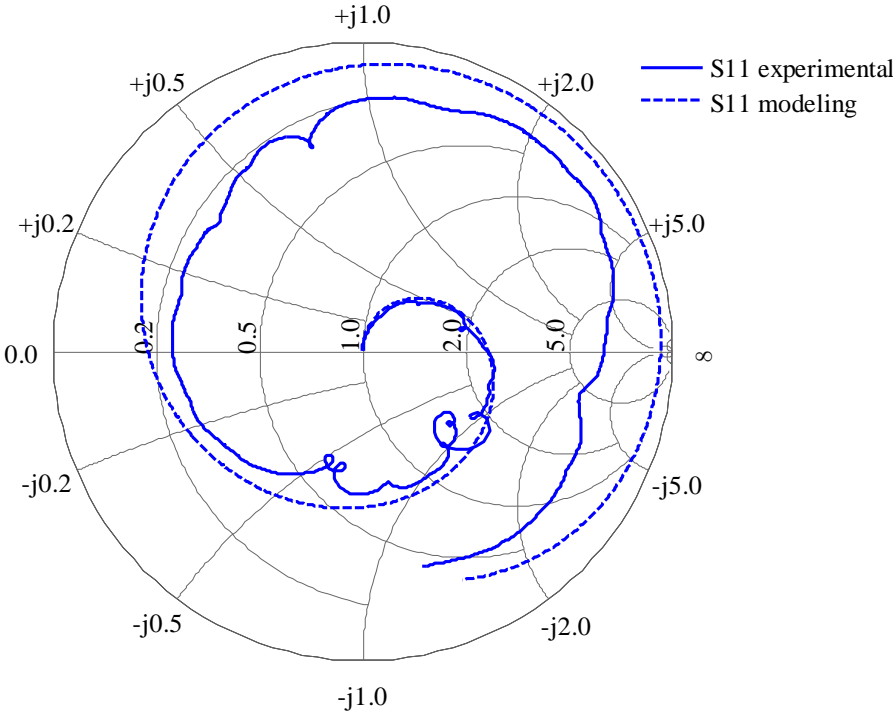
Figure 3-19: Smith Chart of S11 of Experimental and Modeling Results for Non-Degradation Case
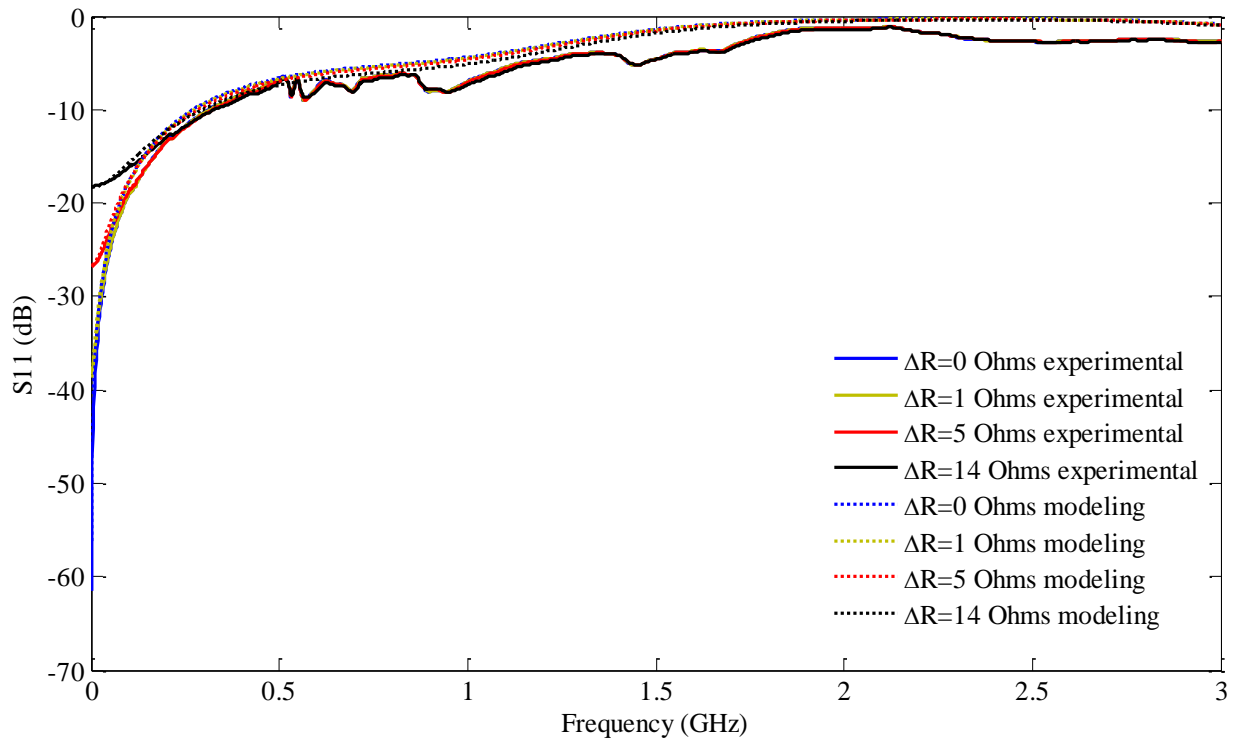
Figure 3-20a: S11 of Modeling Results of Degraded Contacts
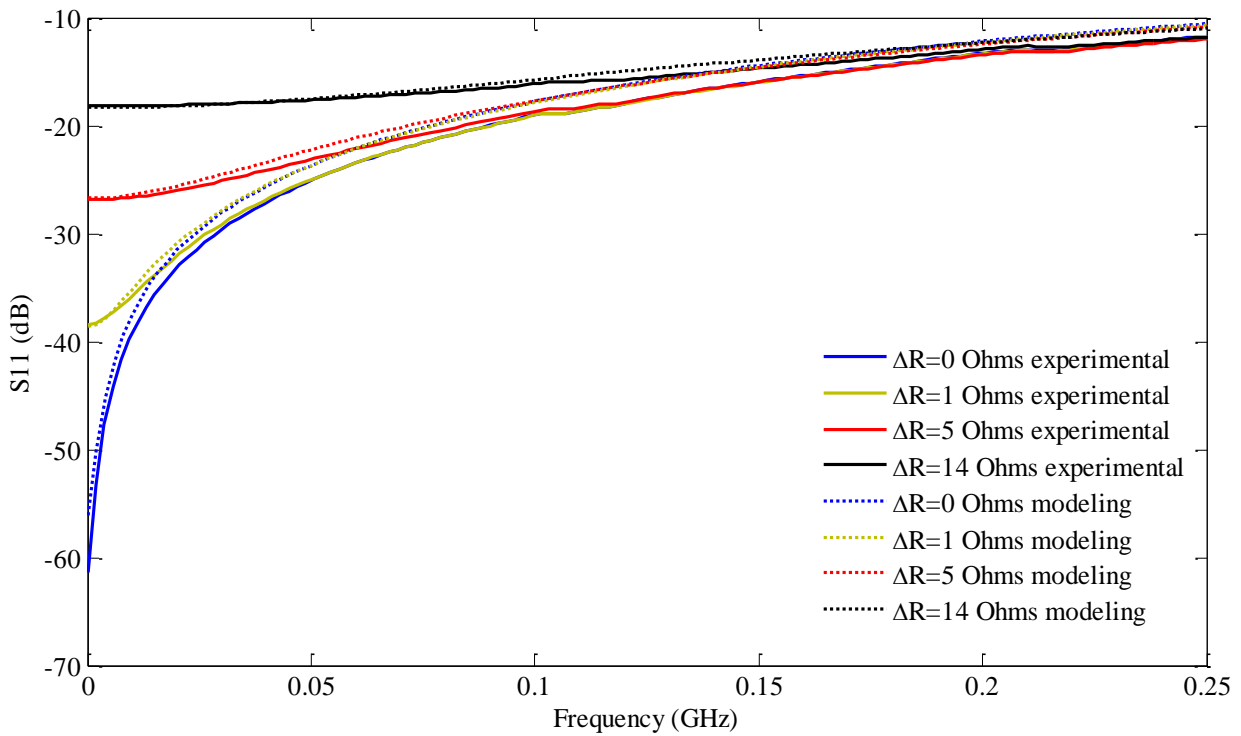
Figure 3-20b: S11 of Modeling Results of Degraded Contacts at Low Frequency Range
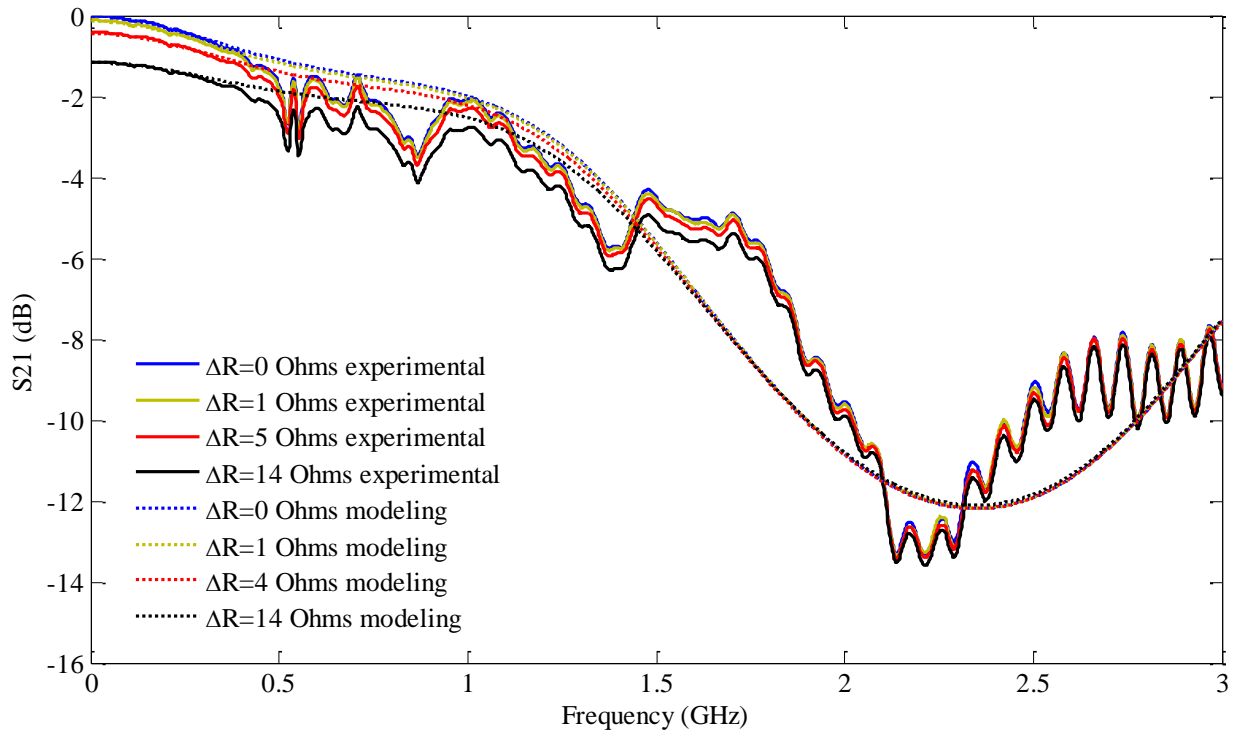
Figure 3-21a: S21 of Modeling Results of Degraded Contacts
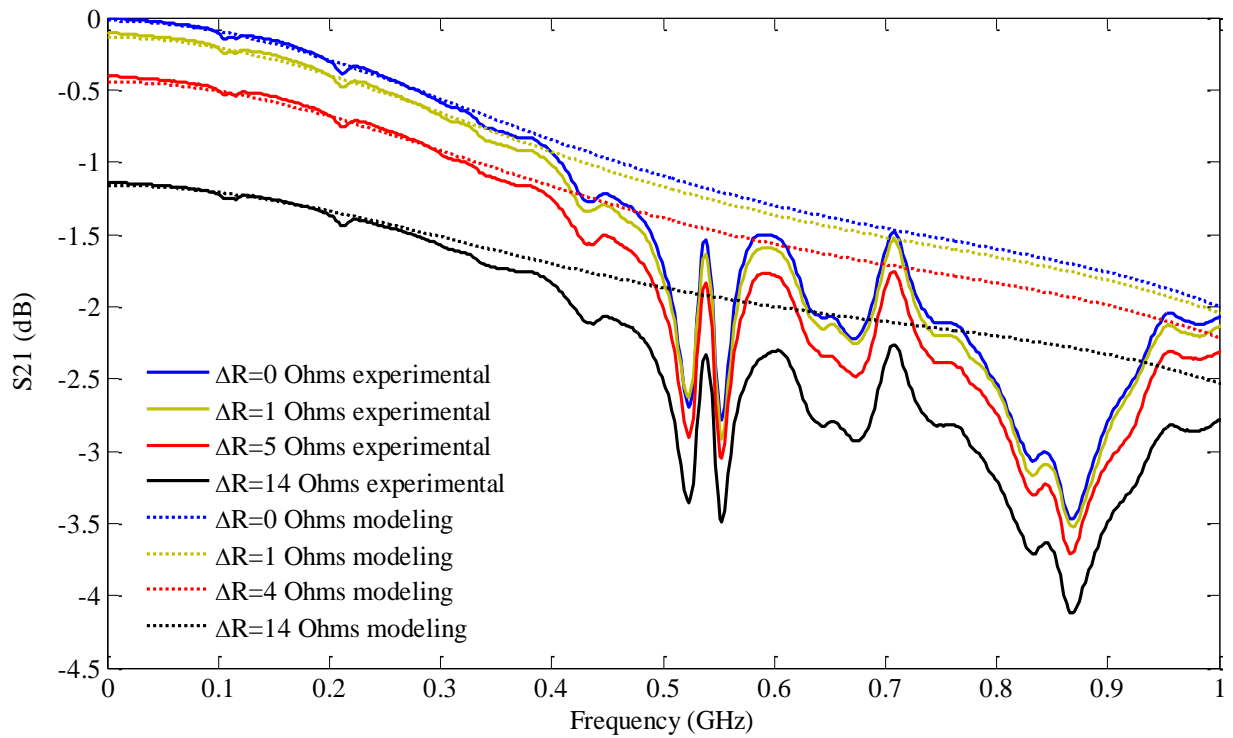
Figure 3-21b: S21 of Modeling Results of Degraded Contacts at Low Frequency Range
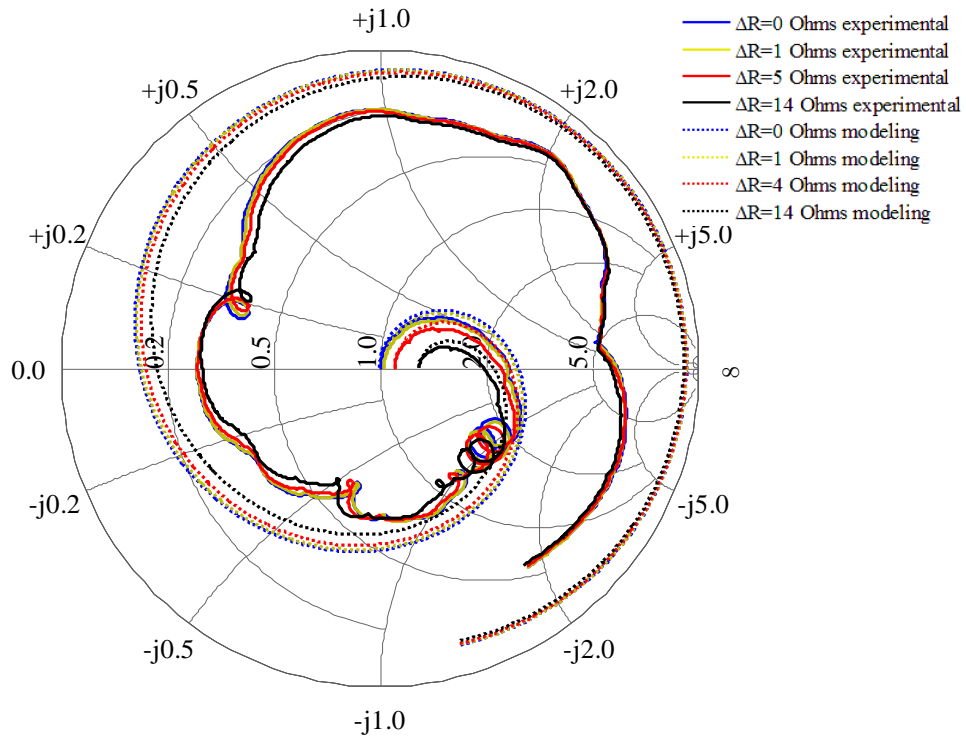
Figure 3-22: Smith Chart of S11 of Modeling Results of Degraded Contacts

As fretting corrosion proceeds, contact capacitance monotonically decreases due to the accumulation of oxides at the contact interface which separates the two sides of the contact. The contact capacitance values used in simulation are found in Figure 2-28. Figure 3-20 to 3-22 show the comparison between experimental and modeling results on the S11 and S21 with degraded contacts having different contact resistances over the frequency range from 5Hz to 3GHz. It is revealed that the degradation with an increased contact resistance results in a worse match at the low frequencies. A good agreement between testing and modeling results is achieved, especially at the low frequency range. In this modeling work, no transmission parameters were adjusted after calibration. The change is the corresponding contact impedance at checkpoints of the process of fretting corrosion as observed in the last study.

3.5 Summary and Conclusions

An investigation of the impact of degraded electrical contacts to high frequency signal transmission was presented. In order to develop an understanding of the behavior of transmission line subjected to vibration induced corrosion, this study examined the correlation between fretting levels and network parameters including S-parameters and Z-parameters, based on an experimental study and a circuit model on a simple contact configuration. With respect to the experimental analysis, degradation was significant in the low frequency range. This phenomenon matches the impedance of degraded contacts which shows capacitive properties and works as a high pass filter. While the contact resistance was low, there was no apparent network degradation because reactive impact of the lightly fretted contact was negligible which was found in the first study. Incorporating the impedance characteristics from the first study, the experimental and modeling results were well correlated.

Based on this understanding, a fault detection strategy of high frequency signal transmission applications with involved electrical contacts can be developed. Once the degradation significantly appears at the low frequency spectrum, it would be reasonably suspected that the fretting corrosion takes place at one or more contacts subjected to fretting corrosion.

CHAPTER 4   EFFECTS OF FRETTING MOTION TO ELECTRICAL CONTACTS

4.1 Introduction

In conventional electrical contacts, contact resistance is the main quantity to evaluate the process of degradation [68]. During fretting motion, the rate of resistance increase is dependent of parameters such as frequencies, amplitudes and normal forces. In recent years, the influence of the degraded contacts to AC signals, especially high frequency data transmission, has also drawn attention of many researchers. Dynamics of fretting motion brings about complicated effects to AC signals passing through the contact interface. An experimental study was performed on copper to copper interface under the condition of AC and DC voltages. During the process of fretting, AC signals that pass through the degraded contact were distorted [45]. Another experiment was proposed to study the effect of vibration induced fretting motion to microwave connectors. With the evolution of DC contact resistance, transmission loss and phase noise were investigated [101]. A direct correlation between the increase of the electrical contact resistance and degradation of phase noise was revealed. During the fretting process, the fretting displacement induced a phase noise that was independent of contact degradation, but depended on the amplitude and frequency of the relative motion at the contact interface. With respect to the precedent research and author's finding, a better understanding of the influence of dynamics of the fretting motion to the signal transfer is expected. Thus, in this study, an experiment was performed to investigate the AC signal distortion when the fretting occurs. Incorporating an

understanding of contact impedance behavior demonstrated in the first study, a circuit model is developed to explain the experimental results and the observation in the second study.

4.2 Experimental Configuration

4.2.1 Experimental Samples and Equipment

As the further effort of last two studies, the same testing article, tin plated copper pin header, was used in this experiment. Two pins were placed axially and touched at a small area at tip areas. Figures 2-3 and 2-4 illustrate the pin samples and contact setup. For a sake of the mechanical and electrical setup, a pair of PC boards worked as carriers with pins soldered on. The dynamic control and shaker system described in chapter two was applied to drive the testing articles to produce fretting degradation between them.

Figure 4-1 shows BK Precision 4011A function generator that can produce various waveforms including sine, square, triangle, ±pulse and ±ramp from 0.5 Hz to 5 MHz in 7 ranges. Coarse and fine tunings are available for frequency and power variations. The output voltage amplitude can be up to 20dB. Distortion is less than 3% at 1kHz; symmetry between 0.5 Hz to 100kHz is less than 2% [102].

Figure 4-1: Photograph of BK Precision 4011A Function Generator

As shown in Figure 4-2, an Agilent E3631A DC power supply outputs DC voltages from

0 to ±25V. It can maintain a steady output when load changes occur, with the 0.01% load and line regulation. These two equipments worked as voltage sources for AC and DC signals in the experiment. [103]

Figure 4-2: Photograph of Agilent E3631A 80W Triple Output Power Supply

Figure 4-3: Photograph of LEM LTS 6-NP Current Transducer

As shown in Figure 4-3, an LEM LTS 6-NP current transducer was used for current measurement. Using the Hall effect, the closed loop current transducer can measure in multiple ranges from 0 to ±19.2 A. The accuracy at primary nominal RMS current (I_{PN}), 6 A, at the room temperature can be ±0.2%. The reaction time at 10% and step response time to 90% of I_{PN} are

respectively less than 100 ns and 400 ns. It outputs analog voltages between ±2.5 V. [104]

Figure 4-4 shows NI 9223 DAQ which was applied to record voltages and currents in this study. Four channels of this module simultaneously acquire analog inputs up to 1MS/s, with voltage ranges from ±10V. With an NI cDAQ-9181 1-slot chassis, the recorded data is transferred to a PC through USB connection. This chassis provides good shielding for external magnetic source to guarantee a high quality recording [105].
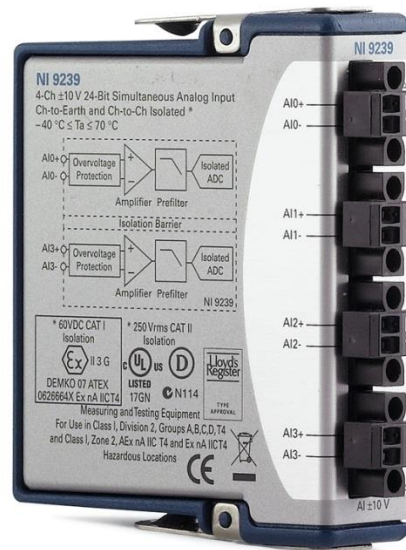
Figure 4-4: Photograph of NI 9223 DAQ

4.2.2 Experimental Setup

As shown in Figure 4-5, a signal generator drove the shaker through an power amplifier to produce the fretting motion between two pins. One of the PC boards where connector pins were soldered was attached on the shaker table that vibrated with the same profile as designed. The other PC board was fixed on the head of the stationary fixture. The testing specification was identical to the last two studies as listed in Table 3-1. The vibrations with various frequencies and amplitudes were applied at the contact interface. The fixture applied a normal force in 1.0 N

between the two sides of contact. The development of contact impedance of the degraded contact and its impact to transmission line were incorporated to understand the effects of fretting motion to signal transfer.
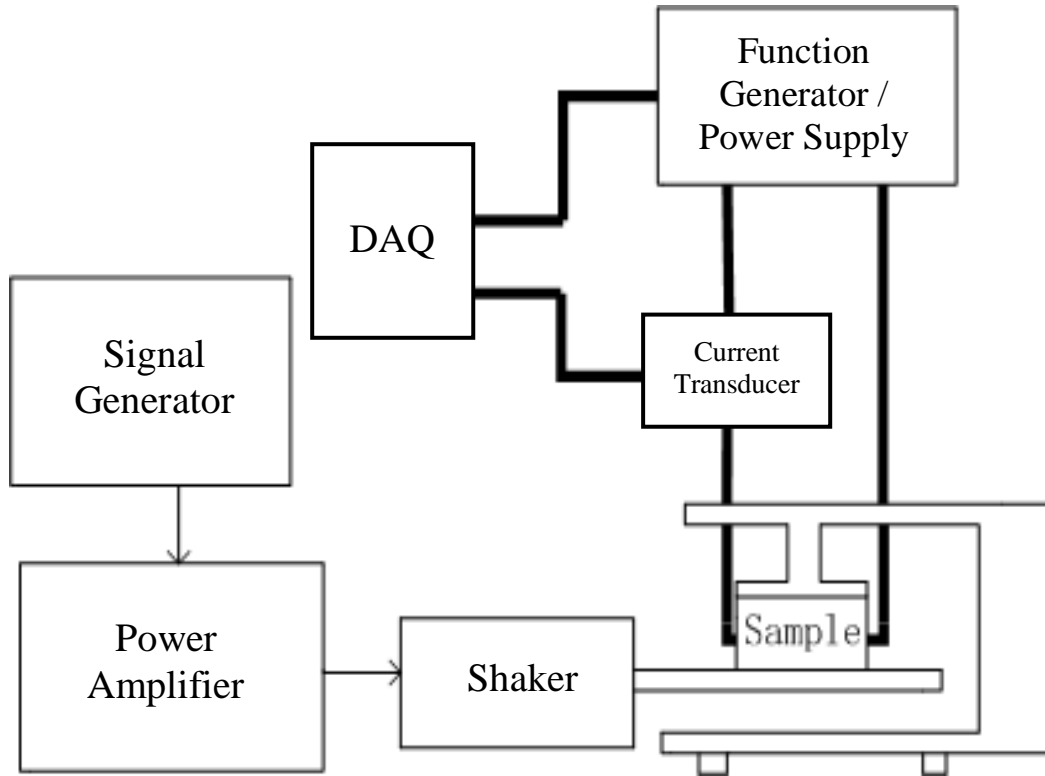
Figure 4-5: Schematic of Experimental Setup

To provide a DC or AC voltage input, the Agilent E3631A power supply or BK Precision A4011A function generator powers a simple circuit involving the contact pair and LTS 6-NP current transducer connected in series. The NI 9223 DAQ simultaneously recorded the current and voltage data. In this study, the transmission line setup was not chosen because de-embedding the behavior of degraded contacts may lead to a loss of accuracy. Using the present configuration, the dynamic property of the degraded contact can be directly acquired by the voltage and current measurement.

4.3 Experimental Results

4.3.1 Effects in DC Principle

In the study in terms of DC principle, electrical resistance is the fundamental quantity. It has been commonly recognized that resistance fluctuates during fretting motion. With a higher resistance, the amplitude of fluctuation generally increases [88]. The oscillation with a relatively large scale tends to occur more frequently with a longer fretting period [106]. At the early stage of the resistance increase, fluctuation takes place with a high resistance at the ends of the fretting track. This is attributed to the fretting mechanism resulting in more accumulation of oxides at ends of the track. But the fluctuation behavior is not uniform for existence of localized mechanical degradation. In addition, these resistance fluctuation disappears if vibration stops [107].
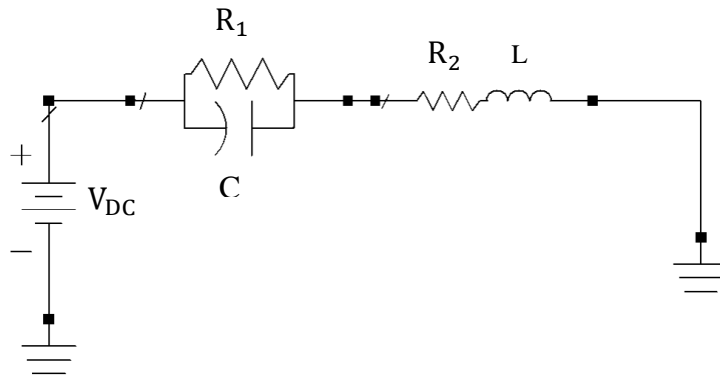
Figure 4-6: Circuit Diagram of DC Testing

Figure 4-6 shows the diagram of the testing with the DC voltage source. R_1 and C describe the contact resistance and capacitance. R_2 and L demonstrate the series resistance and inductance of the lead wire and connector sample. Under DC condition, because of the fluctuation of R_1, the current oscillates and then triggers the reactive effect of C and L. The input single frequency vibrations were applied at 50 Hz and 200 Hz. DAQ's sampling rate was 10 kHz. V_{DC} equals 0.1 volts; the sum of R_2 and R_1 equals 0.74 Ohms; L equals 1.65 uH. Figures 4-7 and

4-8 illustrate the circuit impedances in the frequency and time domains at 50Hz and 200Hz vibration motions. From the time domain results, it is easily found that the oscillatory amplitudes increases as fretting proceeds. Using the fast Fourier transform, FFT, the impedance data from time zero to the timestamp when contact resistance firstly reached 1 Ohms was taken into the frequency domain analysis. From the results, multiple frequency components are observed including the basic frequency of input vibration and its harmonics. The harmonics can be considered the products of the oscillatory impedance which is not a perfect sinusoidal waveform due to the physics of oxidation products distributed in the fretting track. This phenomenon disappeared once fretting motion stopped even if the contact degradation had been serious.
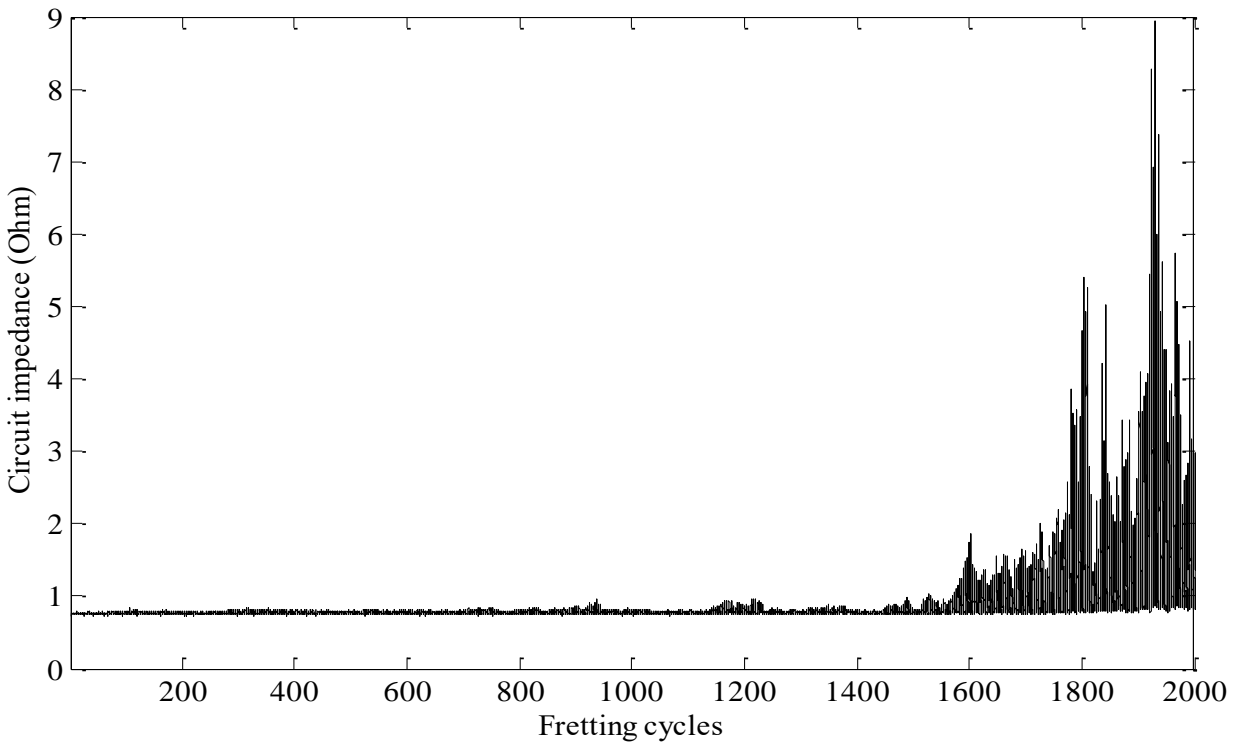
Figure 4-7a: Circuit Impedance during 50 Hz Fretting Motion in Time Domain
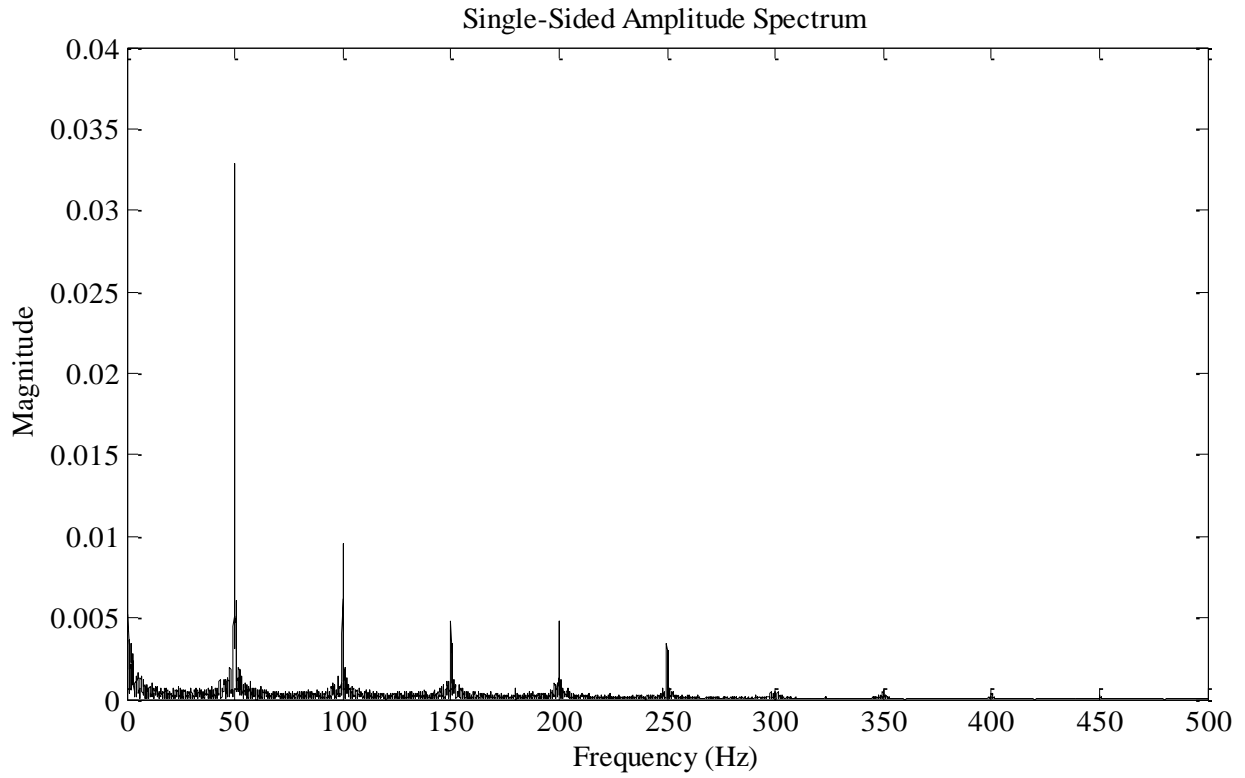
Figure 4-7b: Circuit Impedance during 50 Hz Fretting Motion in Frequency Domain
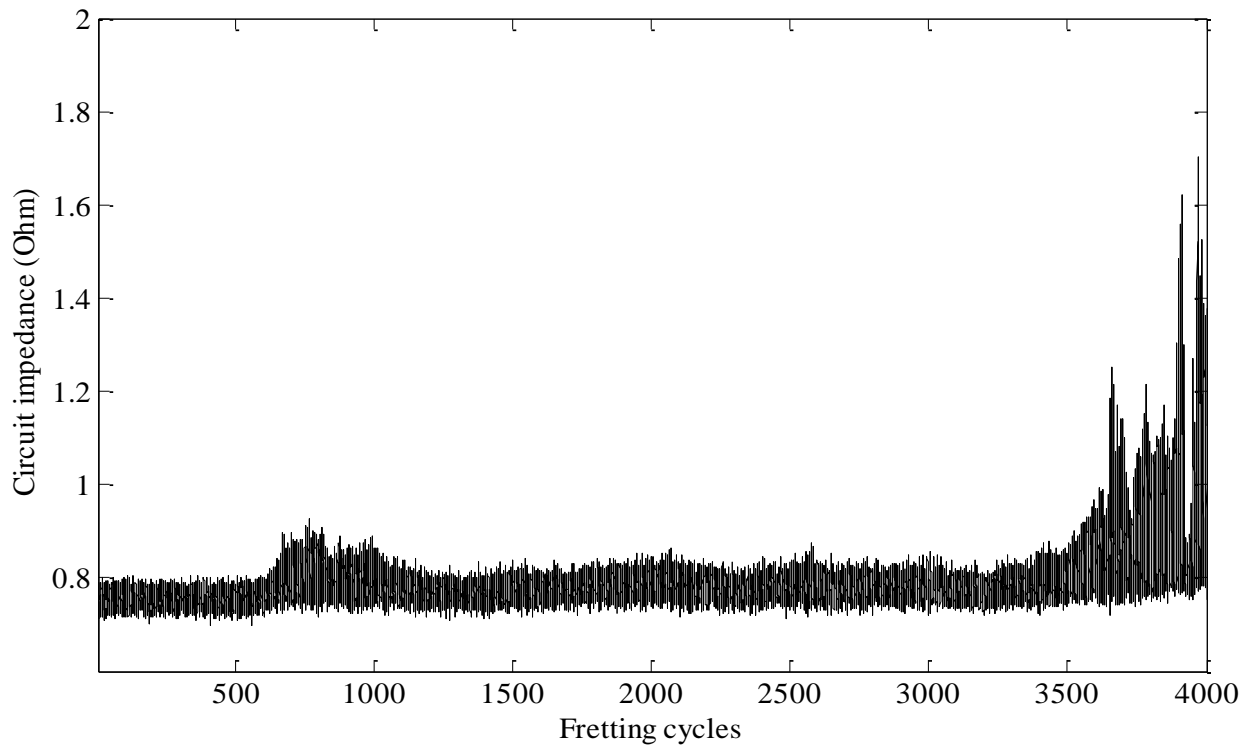
Figure 4-8a: Circuit Impedance during 200 Hz Fretting Motion in Time Domain

100

Single-Sided Amplitude Spectrum
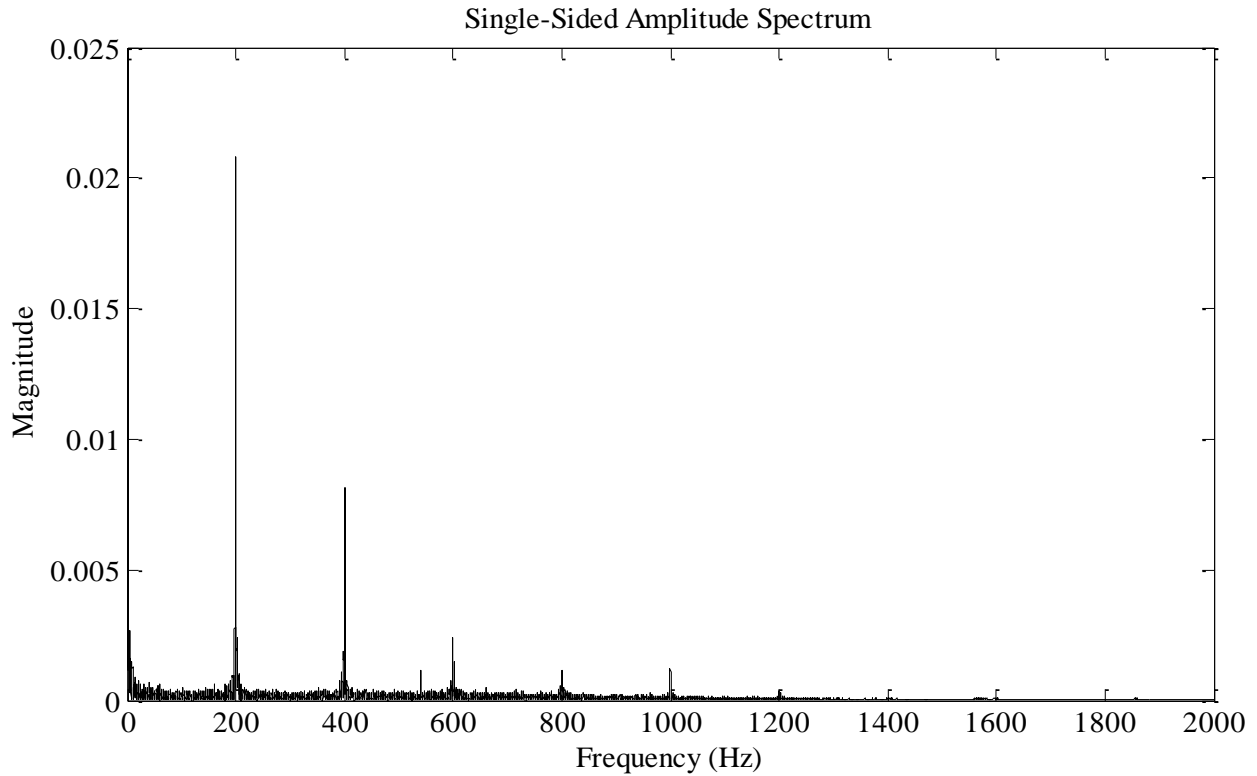
Figure 4-8b: Circuit Impedance during 200 Hz Fretting Motion in Frequency Domain

4.3.2 Effects on AC signals
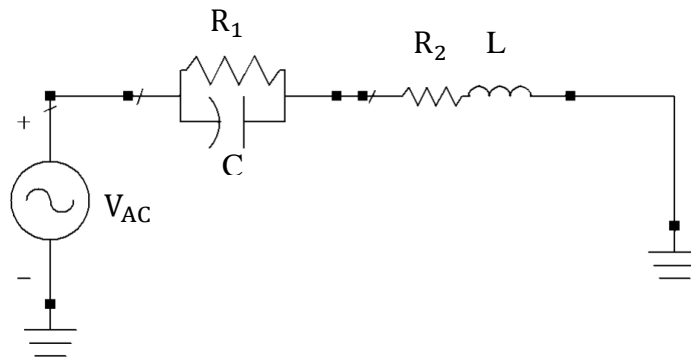
Figure 4-9: Circuit Diagram of AC Testing

Figure 4-9 shows the diagram of the AC testing which includes the same contact and wiring configuration as the DC test. A function generator serves as an AC source providing a single frequency signal at 10 kHz, and the DAQ's sampling rate is 200 kHz. The input single
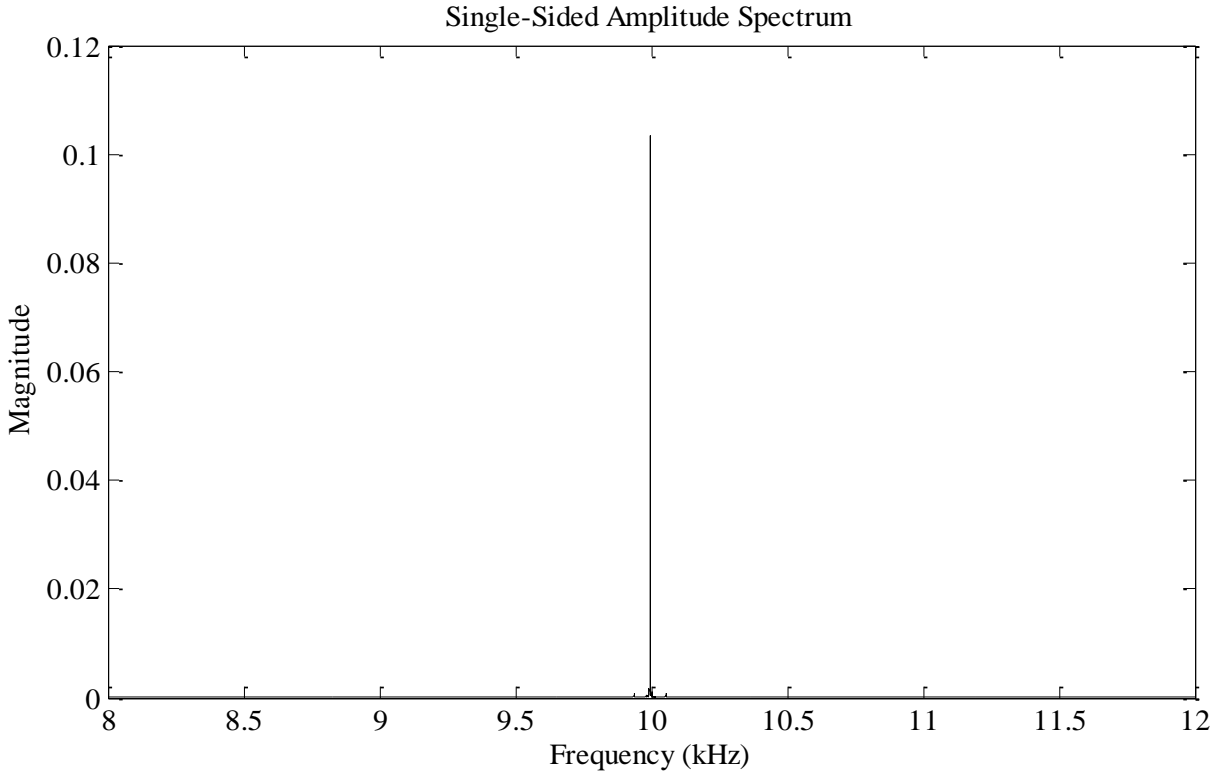
Figure 4-10: Current of Circuit with Fresh Contact in Frequency Domain
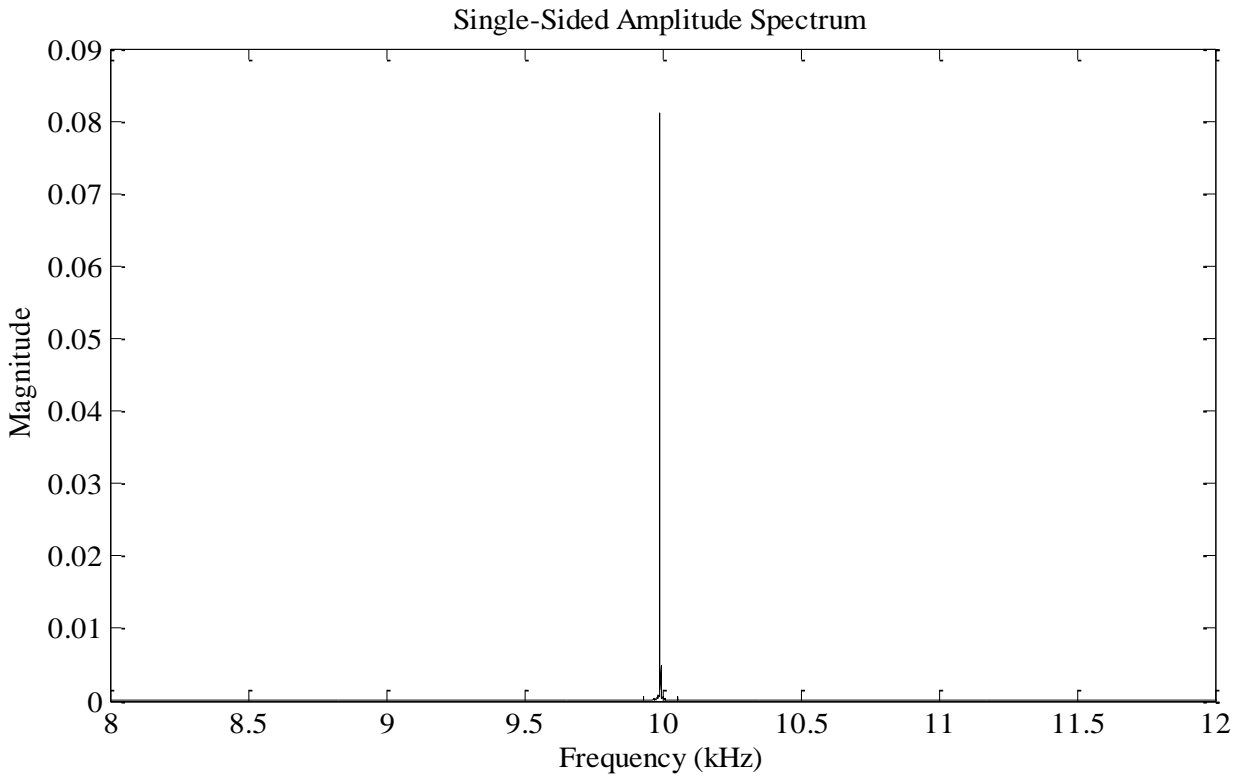
Figure 4-11: Current of Circuit with Stationary Fretted Contact in Frequency Domain
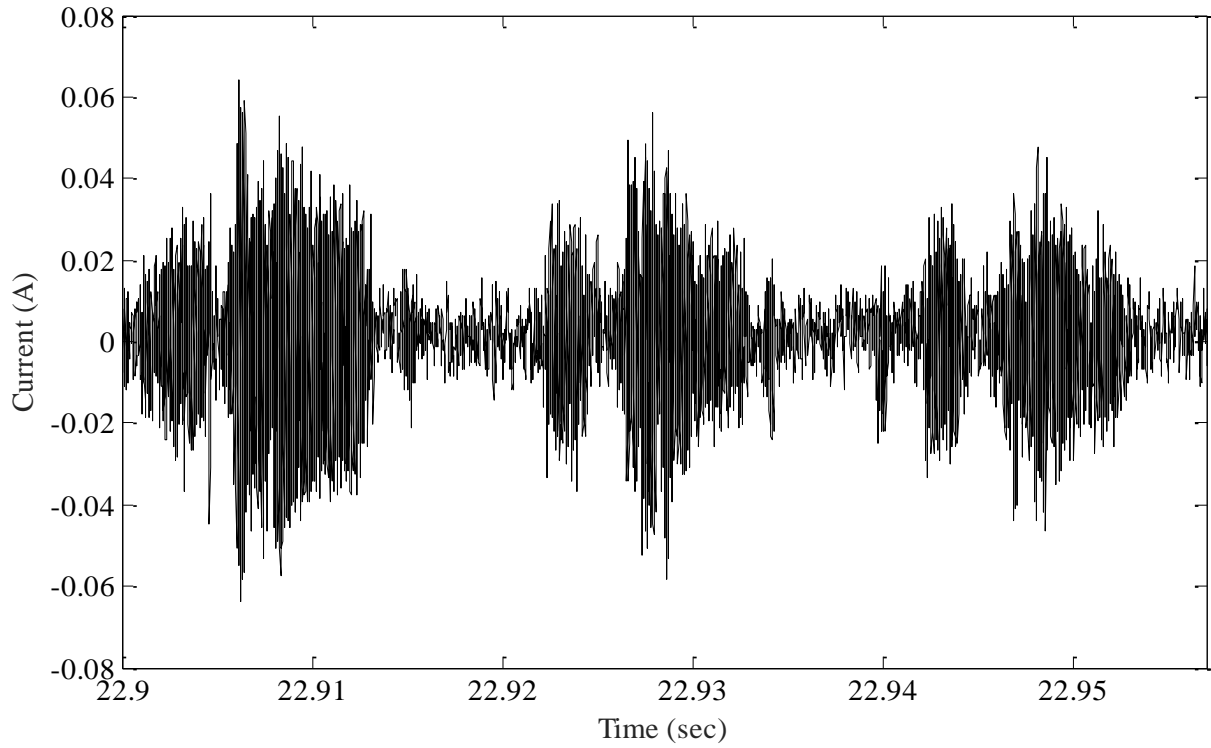
Figure 4-12a: Current of Circuit during 50 Hz Fretting Motion in Time Domain

Single-Sided Amplitude Spectrum
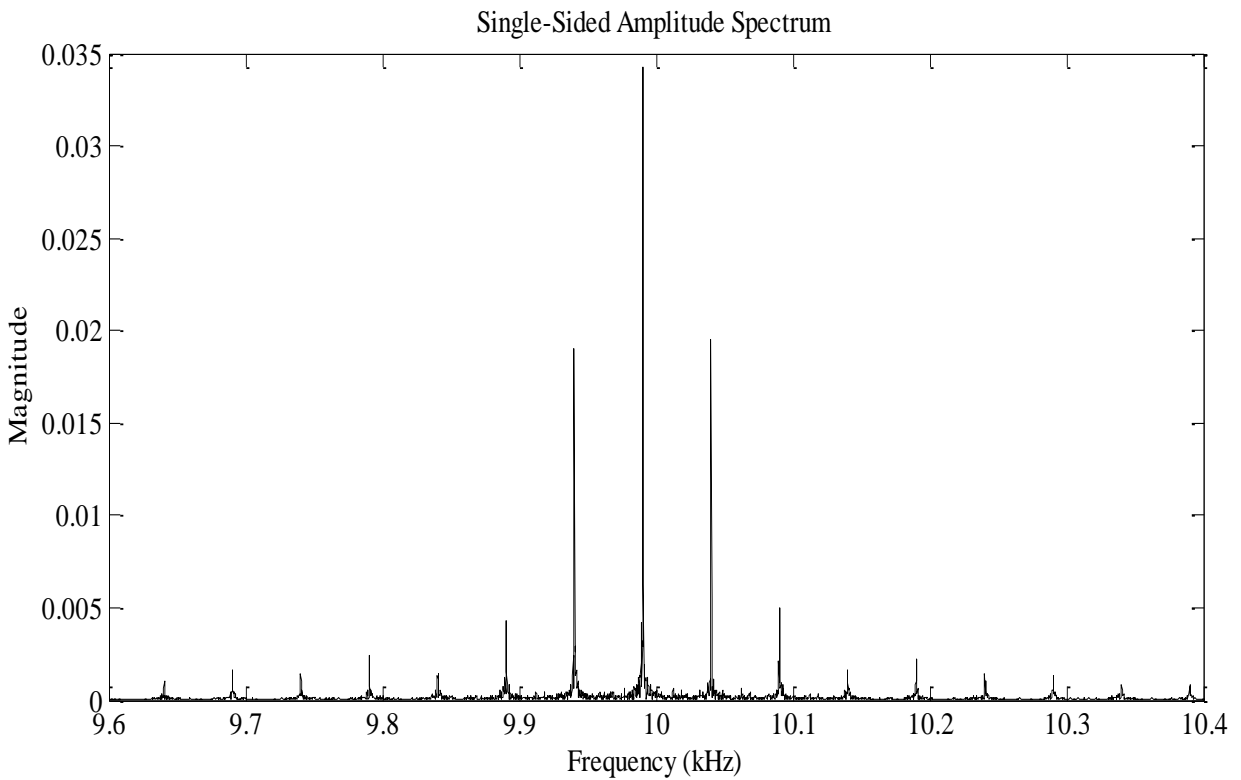
Figure 4-12b: Current of Circuit during 50 Hz Fretting Motion in Frequency Domain
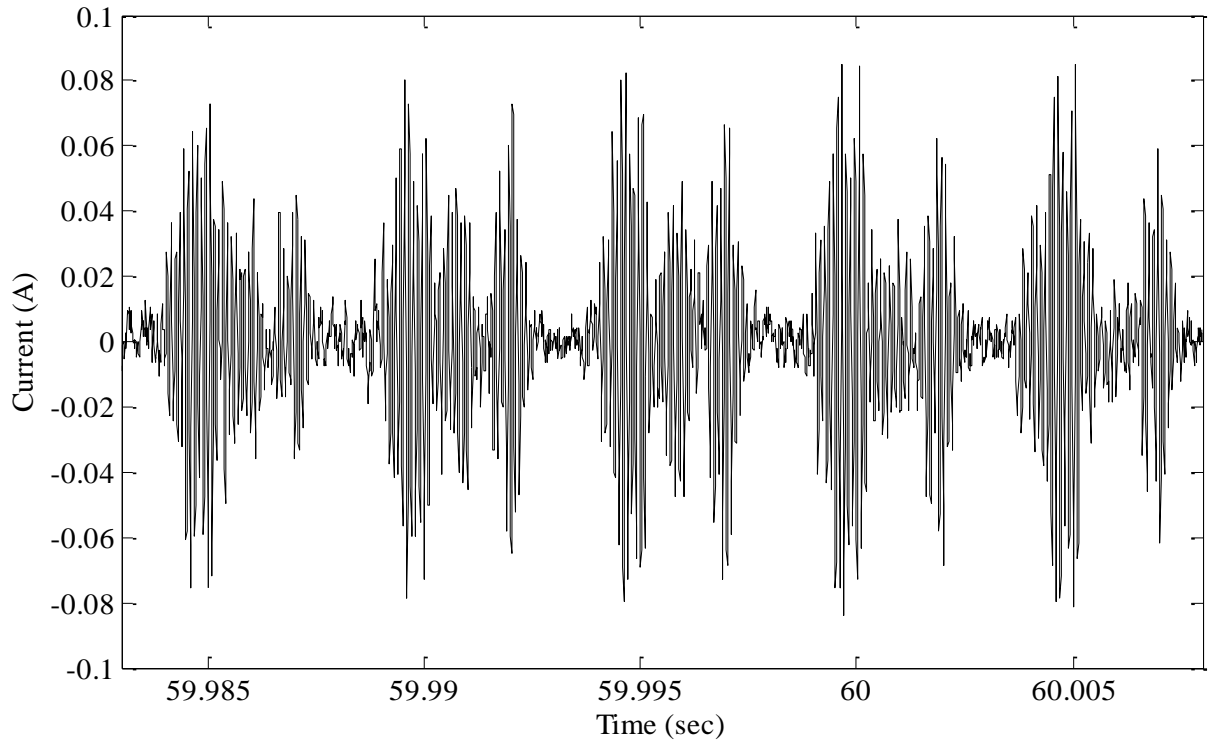
Figure 4-13a: Current of Circuit during 200 Hz Fretting Motion in Time Domain

Single-Sided Amplitude Spectrum
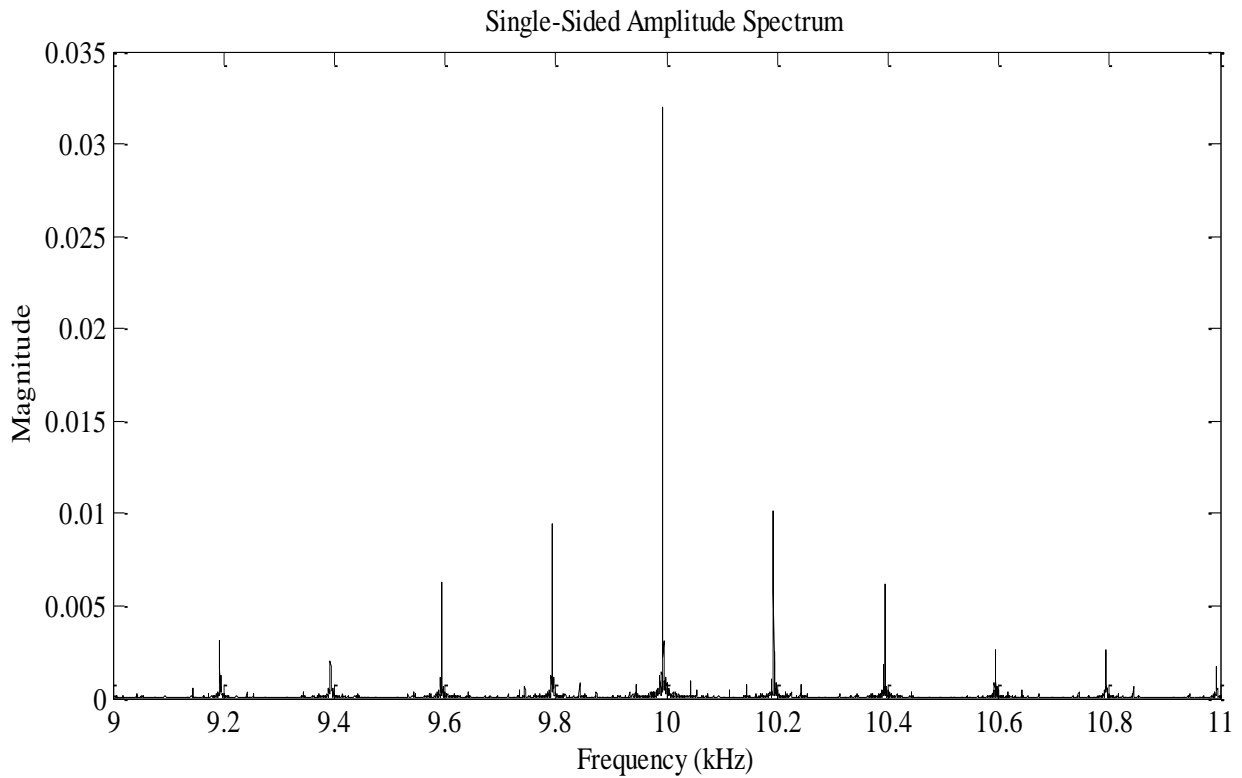
Figure 4-13b: Current of Circuit during 200 Hz Fretting Motion in Frequency Domain

frequency vibrations were applied at 50 Hz and 200 Hz. Figures 4-10 and 4-11 illustrate the currents for the circuit with fresh contact and stationary fretted contact. For these two cases, a single frequency is observed at 10 kHz identical to that of the AC voltage source, but the amplitude decreases as contact resistance increases as a result of fretting corrosion.

Figures 4-12 to 4-13 demonstrated the fluctuation of circuit current under 50 Hz and 200 Hz fretting motion. In the time domain, it is easily found that the oscillatory waves are not perfect sinusoidal curves. As transformed using FFT, the frequency domain results reveal multiple frequency components around the basic signal frequency at 10 kHz. And the differences between each component is the frequency of the input vibration that induced the fretting corrosion. Similar to the impedance oscillation phenomenon in the DC case, this fluctuation also disappears once fretting motion stops, even though the intermittent current could be fairly low due to high contact impedance. Through an inspection and comparison between AC and DC results, one can easily link the circuit impedance oscillation at DC case with the AC signal's multi-frequency effects. Therefore, in the next part, a modeling work will be developed and utilized to explain the mechanism of this fluctuation.

4.4 Model Development

4.4.1 Simulation of DC Case

Based on the layout of the testing circuit as shown in Figures 4-6. The charge at the contact interface is q_C, and V_C denotes the voltage between them. The contact capacitance C is given by

$$C = \frac{q_C}{V_C} \tag{1}$$

Derivative of each side of Equation (1) with respect to time, t, leads to the relationship between the voltage and current, I_C, at the contact.

$$\frac{dq_C}{dt} = \frac{dC}{dt}V_C + C\frac{dV_C}{dt} = I_C \tag{2}$$

The voltage - current relationship of constant inductance, L, is given by

$$V_L = L\frac{dI}{dt} \tag{3}$$

It is easy to find that $V_c = V_{R_1}$, and $V_{R_2} = R_2 I$. According to the previous results, C and R_1 are functions of time; L and R_2 are constants. Matching like components in the preceding relation results in

$$V_{DC} = V_c + V_{R_2} + V_L = V_c + R_2 I + L\dot{I} \tag{4}$$

$$I = I_C + I_{R_1} = \dot{C}(t)V_C + C(t)\dot{V}_C + \frac{V_C}{R_1(t)} \tag{5}$$

The derivative of Equation 4 is given by

$$\dot{V}_C = \dot{V}_{DC} - \dot{I}R_2 - L\ddot{I} \tag{6}$$

Substituting Equations 4 and 6 into Equation 5, we can have

$$CL\ddot{I} + \left[CR_2 + \left(\dot{C} + \frac{1}{R_1}\right)L\right]\dot{I} + \left[1 + \left(\dot{C} + \frac{1}{R_1}\right)R_2\right]I = C\dot{V}_{DC} + (\dot{C} + \frac{1}{R_1})V_{DC} \tag{7}$$

which can be rewritten to lead to the dynamics of circuit impedance as

$$\ddot{Z} + \left(\frac{R_2}{L} - \frac{2\dot{Z}}{Z} + \frac{1}{C}\left(\dot{C} + \frac{1}{R_1}\right)\right)\dot{Z} + \frac{1}{CL}\left(\dot{C} + \frac{1}{R_1}\right)Z^2 - \frac{1}{CL}\left[\left(\dot{C} + \frac{1}{R_1}\right)R_2 + 1\right]Z = 0 \tag{8}$$

If the oscillatory contact resistance is assumed a sinusoidal wave described as

$$R_1 = R_{10} + R_{20}\sin(\omega t) \tag{9}$$

where R_{10} and R_{20} are assumed constant at a short duration of the process of the fretting corrosion. A Simulink model based on Equations 7 and 8 is developed to simulate the circuit

impedance and current behavior, the diagram of which is illustrated in Figure 4-14.
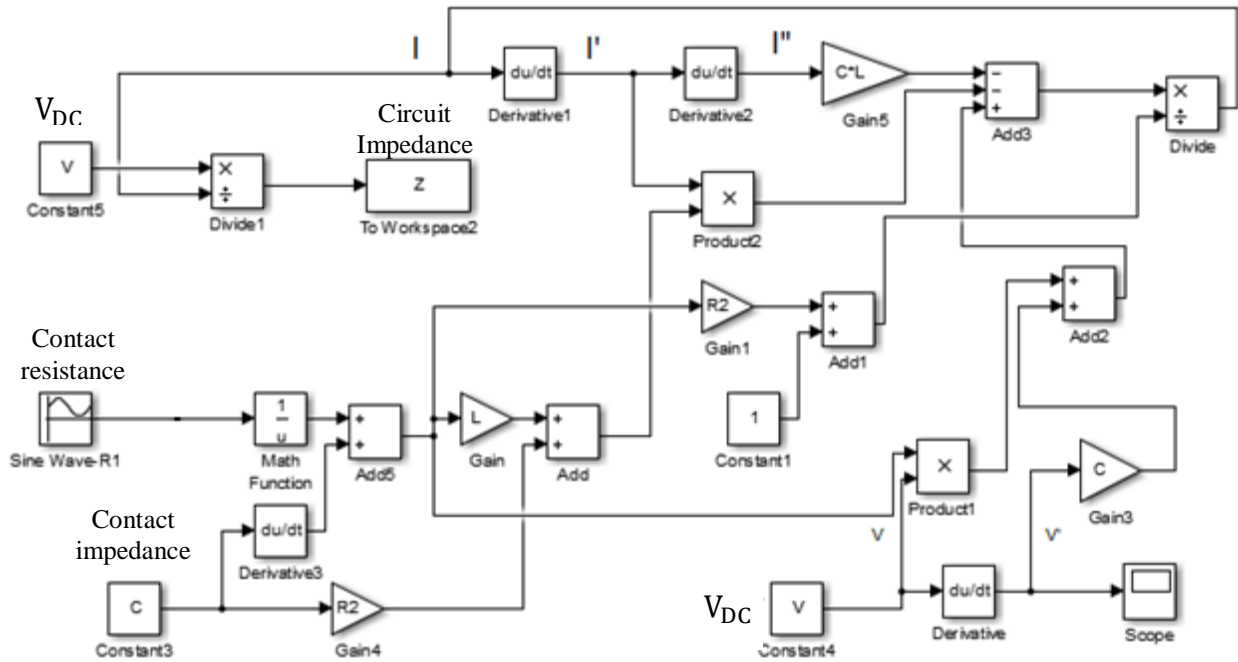
Figure 4-14: Diagram of Simulink Model for DC Case

R_{10} is assumed 1 Ohms and R_{20} is assumed 0.1, 0.2 and 0.3 Ohms. The oscillation frequencies of the contact resistances are 50 Hz and 200 Hz. R_2 and L have the identical values as the experimental setup; C is assumed constant as 5 pF. Based on the study in chapter 2, C changes without dramatic changes while the cycle number is high. Figures 4-15 and 4-16 illustrate the simulated contact impedance in the time and frequency domains. In the figure of the time domain, the circuit impedance oscillates in limited bounds which is determined by R_{20}. The frequency response reveals that the circuit impedance has the basic frequency equaling that of the fluctuation of the contact resistance and harmonics. With a higher scale of the oscillation, the values of all components increase.
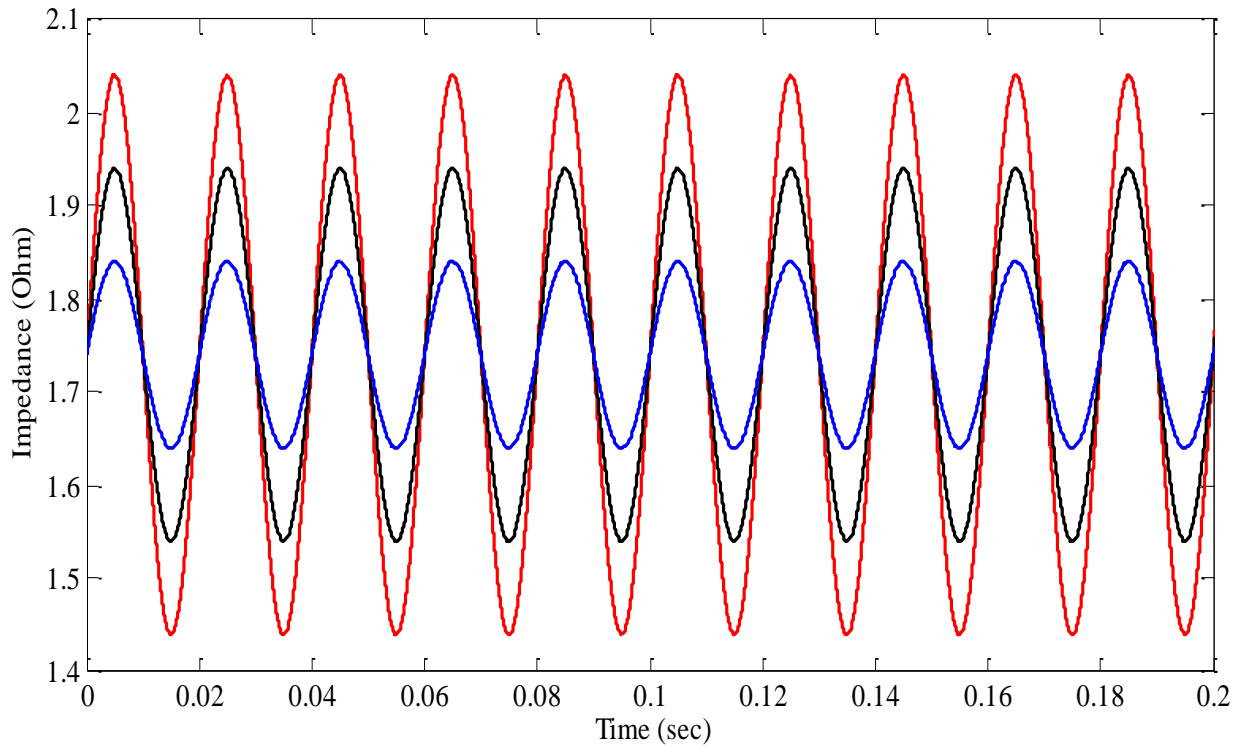
Figure 4-15a: Simulation Impedance Oscillation under 50 Hz Vibration (Time Domain)
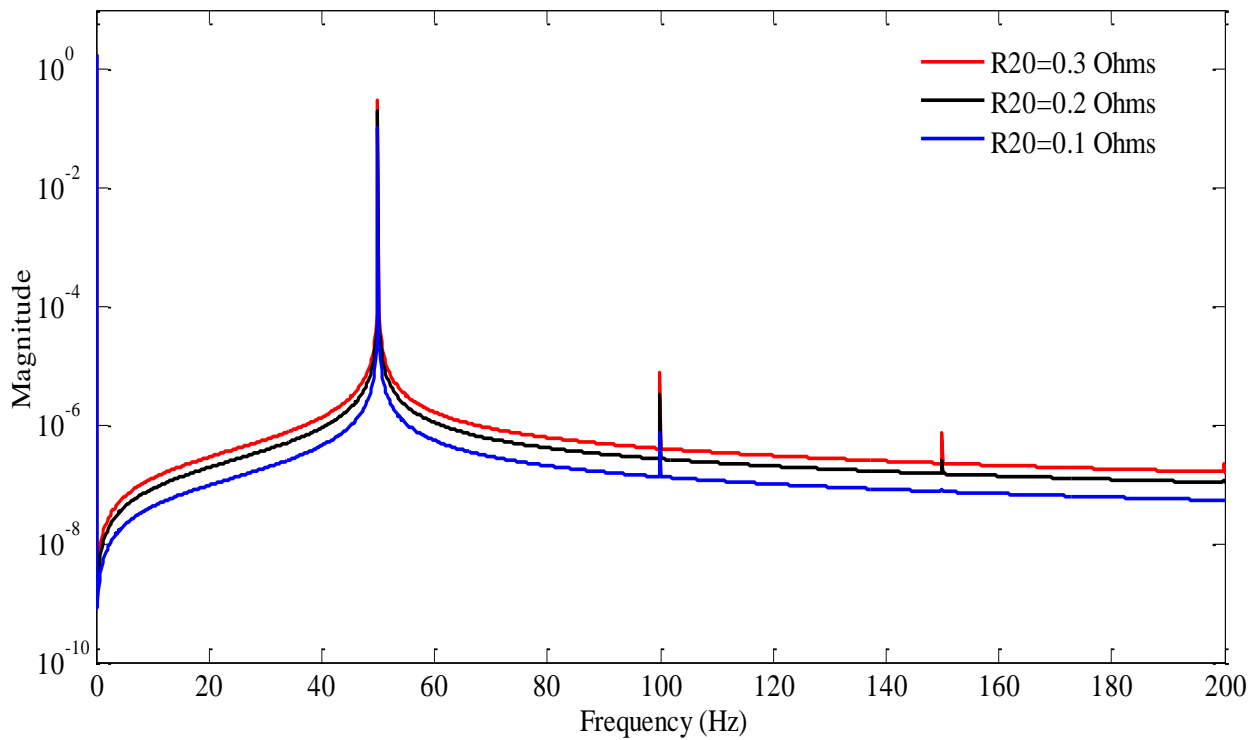
Figure 4-15b: Simulation Impedance Oscillation under 50 Hz Vibration (Frequency Domain)
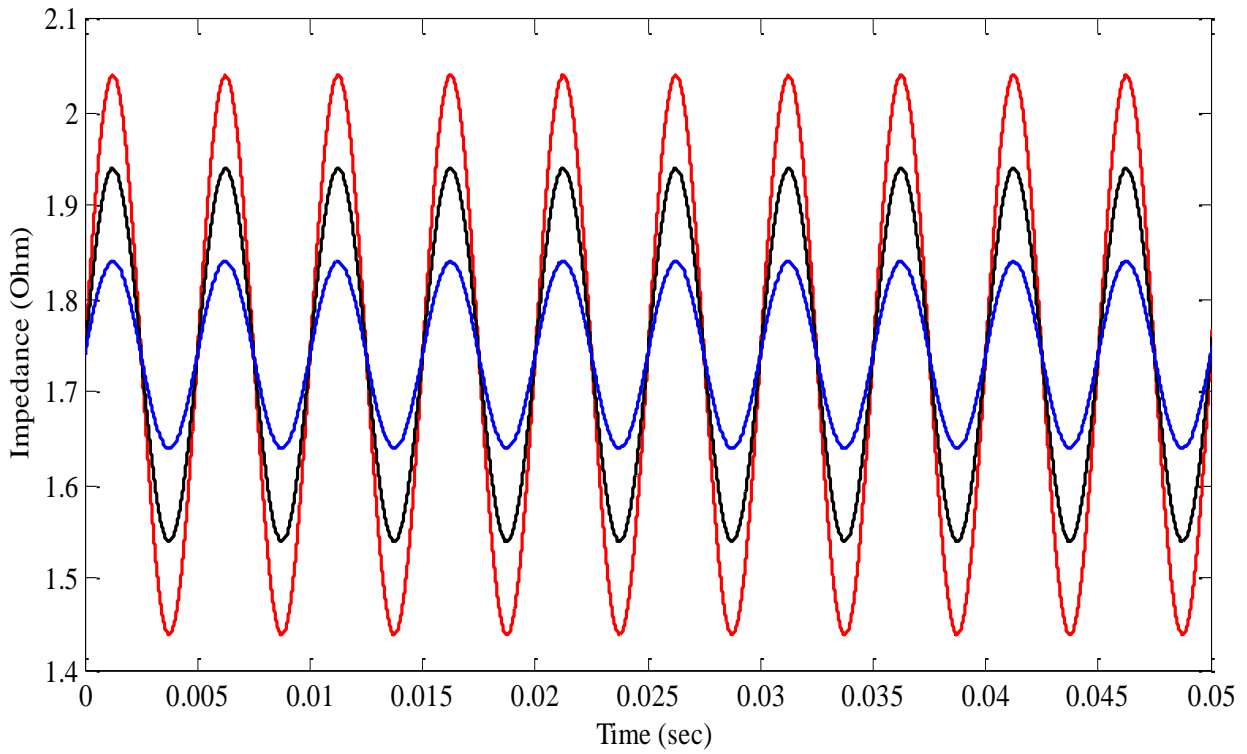
Figure 4-16a: Simulation Impedance Oscillation under 200 Hz Vibration (Time Domain)
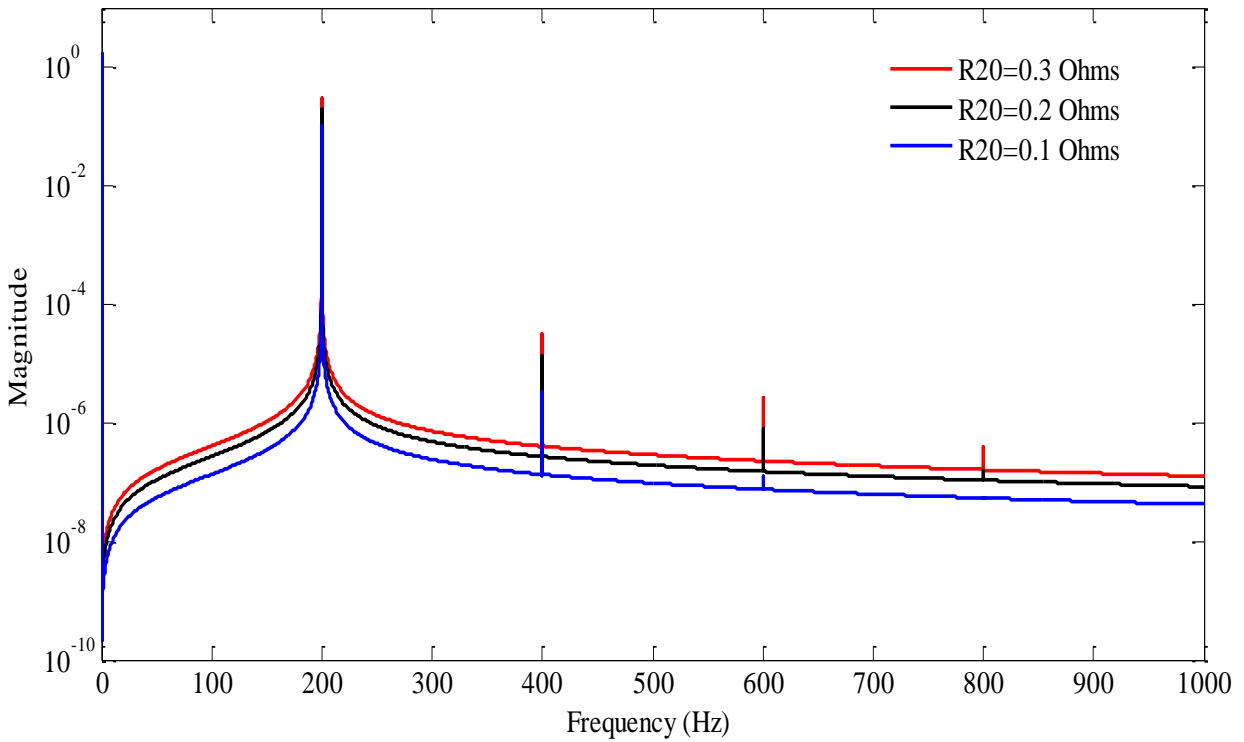
Figure 4-16b: Simulation Impedance Oscillation under 200 Hz Vibration (Frequency Domain)

According to the Simulink results, a series of harmonics are produced by the single frequency oscillation of the contact resistance. This phenomenon could be explained by a solution of the circuit dynamics. The nonlinear second order differential equation, Equation 8, is solved by Natural Decomposition Method (NDM) [111]. The NDM is based on the natural transform method (NTM) and Adomian Decomposition Method (ADM). The natural transform of a function of t, f(t), is expressed as

$$N[f(t)] = R(s,u) = \int_{-\infty}^{\infty} e^{-st} f(ut) dt; \qquad s, u \in (-\infty, \infty) \tag{10}$$

where N is the transform operator; s and u are the natural transform variables. For differential equations where $t \geqslant 0$,

$$N^+[f(t)] = \int_0^{\infty} e^{-st} f(ut) dt \tag{11}$$

is the form we will use. In the simulation, C is assumed constant, and then $\dot{C}$ equals 0. Then Equation 8 is simplified as

$$\ddot{Z} + \left(\frac{R_2}{L} - \frac{2\dot{Z}}{Z} + \frac{1}{CR_1} \right) \dot{Z} + \frac{1}{CLR_1} Z^2 - \frac{1}{CL} \left[\frac{R_2}{R_1} + 1 \right] Z = 0 \tag{12}$$

N transform of it is given by

$$\frac{s^2}{u^2} Z(s,u) - \frac{s}{u^2} Z(0) - \frac{\dot{Z}(0)}{u} + N^+ \left[\left(\frac{R_2}{L} - \frac{2\dot{Z}}{Z} + \frac{1}{CR_1} \right) \dot{Z} + \frac{1}{CLR_1} Z^2 - \frac{1}{CL} \left[\frac{R_2}{R_1} + 1 \right] Z \right] = 0 \tag{13}$$

To rearrange this equation, $Z(s,u)$ is described as

$$Z(s,u) = \frac{1}{s} Z(0) + \frac{u}{s^2} \dot{Z}(0) - \frac{u^2}{s^2} N^+ \left[\left(\frac{R_2}{L} - \frac{2\dot{Z}}{Z} + \frac{1}{CR_1} \right) \dot{Z} + \frac{1}{CLR_1} Z^2 - \left[\frac{R_2}{R_1} + 1 \right] Z \right] \tag{14}$$

where

$$Z(t) = \sum_{n=0}^{\infty} Z_n(t)$$

$$\left(\frac{R_2}{L} - \frac{2\dot{Z}}{Z} + \frac{1}{CR_1}\right)\dot{Z} + \frac{1}{CLR_1}Z^2 - \left[\frac{R_2}{R_1} + 1\right]Z = F(Z) = \sum_{n=0}^{\infty} A_n(t)$$

$A_n(t)$ is an Adomian polynomial which represents the nonlinear term. Based on the circuit model, it is easy to find

$$Z(0) = R_{10} + R_2; \qquad \dot{Z}(0) = 0; \tag{15}$$

Inverse N transform of Equation 15 leads to

$$\sum_{n=0}^{\infty} Z_n(t) = Z(0) - N^{-1}\left[\frac{u^2}{s^2} N^+[A_n(t)]\right] \tag{16}$$

the derivative of which is given by

$$Z_0(t) = Z(0)$$

$$Z_1(t) = -N^{-1}\left[\frac{u^2}{s^2} N^+[A_0(t)]\right] = -N^{-1}\left[\frac{u^2}{s^2} N^+\left[\frac{1}{CLR_1}Z^2(0) - \frac{1}{CL}\left[\frac{R_2}{R_1} + 1\right]Z(0)\right]\right] \tag{17}$$

When $R_{10} \gg R_{20}$,

$$\frac{1}{R_1} \approx r_1 + r_2 \sin(\omega t) \tag{18}$$

where

$$r_1 = \frac{1}{R_{10} - 0.5R_{11}^2/R_{10}}, \qquad r_2 = -r_1 \frac{R_{11}}{R_{10}}$$

When R_{20} is larger,

$$\frac{1}{R_1} = r_1 \sum_{n=0}^{\infty} \sin(n\omega t + \emptyset_n) \tag{19}$$

For a simple derivation, Equation 22 is adopted in this case, and the solution of $Z_1(t)$ is given by

$$Z_1(t) = -\frac{t^2}{2}\left(-\frac{(1 + r_1 R_2)Z(0)}{CL} + \frac{r_1 Z^2(0)}{CL}\right) - \frac{\sin(\omega t)}{\omega^2}\left(\frac{Z^2(0)r_2}{CL} - \frac{R_2 r_2 Z(0)}{CL}\right) \tag{20}$$

$$Z_2(t) = -\boldsymbol{N}^{-1}\left[\frac{u^2}{s^2}\boldsymbol{N}^+[A_1(t)]\right] = -\boldsymbol{N}^{-1}\left[\frac{u^2}{s^2}\boldsymbol{N}^+[Z_1(t)F'(Z_1(t))]\right] \tag{21}$$

where

$$F'(Z) = -\frac{2}{CLR_1}Z - \left(\frac{R_2}{CLR_1} + \frac{1}{CL}\right)$$

The $Z_2(t)$ is obtained as

$$Z_2(t) = -\frac{1}{C^2L^2}\left\{\frac{F_1F_3}{4!}t^4 - \frac{F_2F_3}{\omega^4}sin(\omega t)\right.$$

$$+ \frac{F_1r_2Z(0)}{\omega^3}\left[\frac{2}{\omega}sin(\omega t) - 2t + \frac{\omega^3}{3}t^3 - \frac{\omega^2t^2 - sin(\omega t) + 2\omega t cos(\omega t) - 2\omega t}{\omega^3}\right]$$

$$\left. + \frac{2F_2r_2Z(0)}{\omega^2}\left(t^2 + \frac{cos(2\omega t) - 1}{8\omega^2}\right)\right\} \tag{22}$$

where

$$F_1 = \frac{Z(0)}{CL}(-1 + R_{10}r_1)$$

$$F_2 = \frac{Z(0)r_2R_{10}\,sin(\omega t)}{\omega^2CL}$$

$$F_3 = 1 + r_1R_2 + 2r_1Z(0)$$

Due to the calculation complexity, the components of Z with higher indexes are neglected. From the derivation above, one can see oscillatory components with frequency at ω in $Z_1(t)$ and a 2ω component in $Z_2(t)$. Further work shows that the oscillatory components at frequencies of n ω, n as an positive integer, appear in $Z_n(t)$. Using the Natural Transform Method, the harmonics of impedance oscillation is validated to be induced in the signal frequency input vibration and DC voltage conditions.

Despite the findings above, the oscillation of contact resistance does not necessarily take place at a single frequency. This is also indicated by Figures 4-15 and 4-16 that the magnitudes of harmonics are much lower than the basic components which differs from the experimental

results. Based on Equation 8, the contact resistance is expressed as

$$R_1 = \frac{-\frac{\dot{Z}}{C} - \frac{Z^2}{CL} + \frac{R_2 Z}{CL}}{\ddot{Z} + \left(\frac{R_2}{L} - \frac{2\dot{Z}}{Z} + \frac{\dot{C}}{C}\right)\dot{Z} + \frac{\dot{C}}{CL}Z^2 - \frac{Z}{CL}(\dot{C}R_2 + 1)} \qquad (18)$$

where

$$R_2 = 0.74 - R_1(0) \text{ Ohms}$$

Based on the contact theory, the initial contact resistance, $R_1(0)$, can be estimated by

$$R_1(0) = R_o + \frac{\rho}{nd} \qquad (19)$$

where R_o and ρ/nd respectively denote the resistances envelop constriction and multi-point contribution. ρ denotes the electrical resistivity of the contact material. They are expressed as

$$R_o = \frac{\rho}{\sqrt{(A_n/\pi)}} \qquad (20)$$

$$nd = W(e) <m> \sqrt{(A_r A_n/\pi)} \qquad (21)$$

where A_n denotes the nominal contact area; A_r represents the real contact area; <m> is the mean surface slope; W(e) is the separation distribution function evaluated at e, the separation distance between two contact surfaces. Based on the testing configuration, A_n is 0.144 mm^2; A_r is 0.017 mm^2; W(e) is 4.4336×10^5 m^{-1} ; $\rho \approx 11.5 \times 10^{-8}$ Ohm $\cdot$ m; <m>=0.0121. It's easy to find that R_0 equals 0.537 mOhm and $\frac{\rho}{nd}$ equals 0.767 mOhm; thus $R_1(0)$ equals 1.304 mOhm, and $R_2 \approx 738.696$ mOhm.

Incorporating the above parameter values, contact resistance, R_1, is obtained by Equation 18 under the condition of 50 Hz and 200 Hz fretting motions. Figure 4-17 shows the multiple frequency components of the fluctuation of the contact resistance for these two cases. The magnitudes of all frequency components are marginally lower than that of circuit impedance.
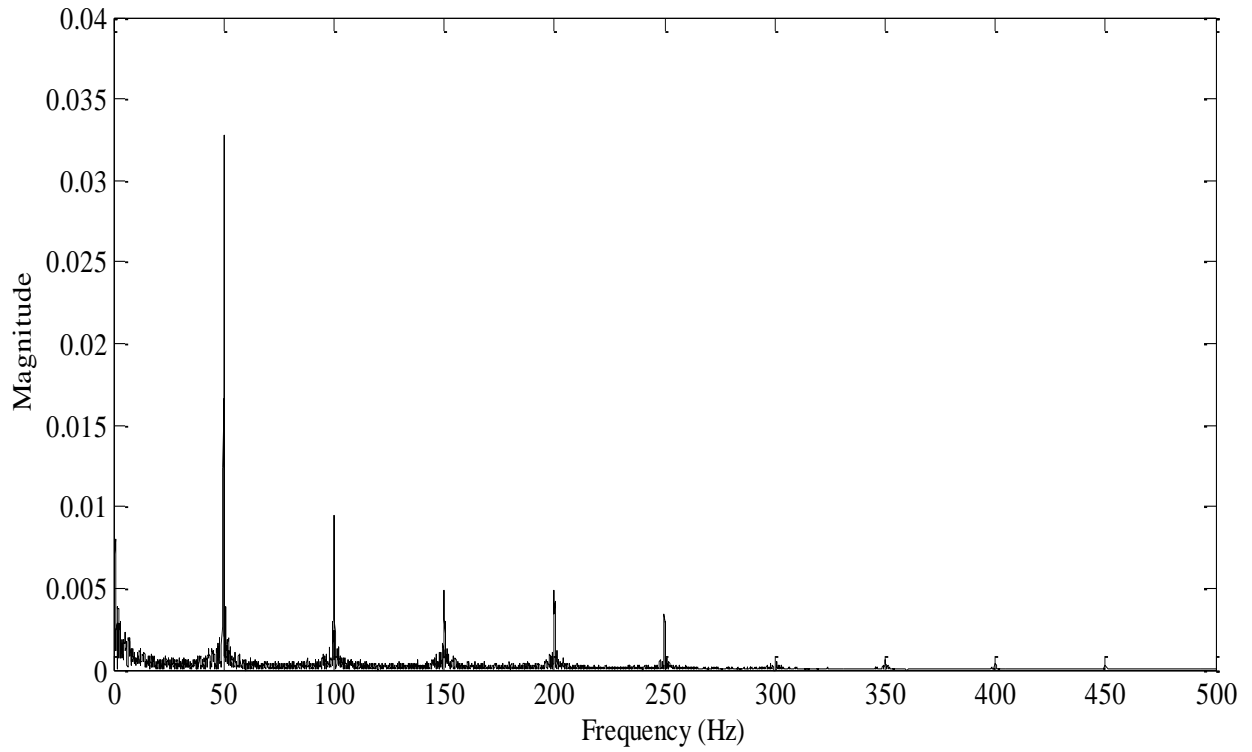
Figure 4-17a: Simulation Contact Resistance Oscillation under 50 Hz Vibration
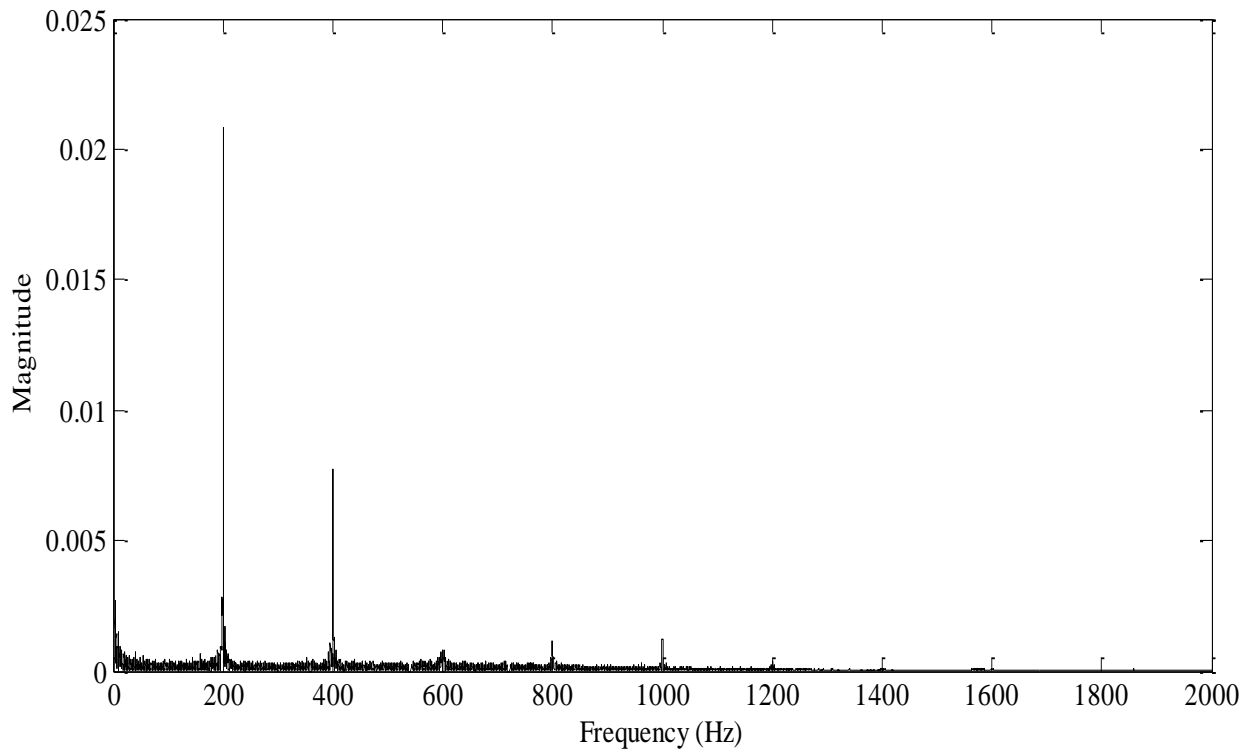
Figure 4-17b: Simulation Contact Resistance Oscillation under 200 Hz Vibration

4.4.2 Simulation of AC Case

The AC circuit configuration is identical to the DC circuit setup, but the AC voltage source. The dynamics of the circuit current can be rewritten from Equation 7 as

$$CL\ddot{I} + \left[CR_2 + \left(\dot{C} + \frac{1}{R_1} \right) L \right] \dot{I} + \left[1 + \left(\dot{C} + \frac{1}{R_1} \right) R_2 \right] I = C\dot{V}_{AC} + \left(\dot{C} + \frac{1}{R_1} \right) V_{AC} \tag{22}$$

As fretting proceeds, contact resistance gradually increases with a higher power of fluctuation. Based on the study of the DC case, during a short period, the average resistance value is assumed constant and it can be described with a Taylor series:

$$R_1 = \frac{r_0}{2} + \sum_{n=1}^{N} r_n \sin(n\omega t + \emptyset_n) \tag{23}$$
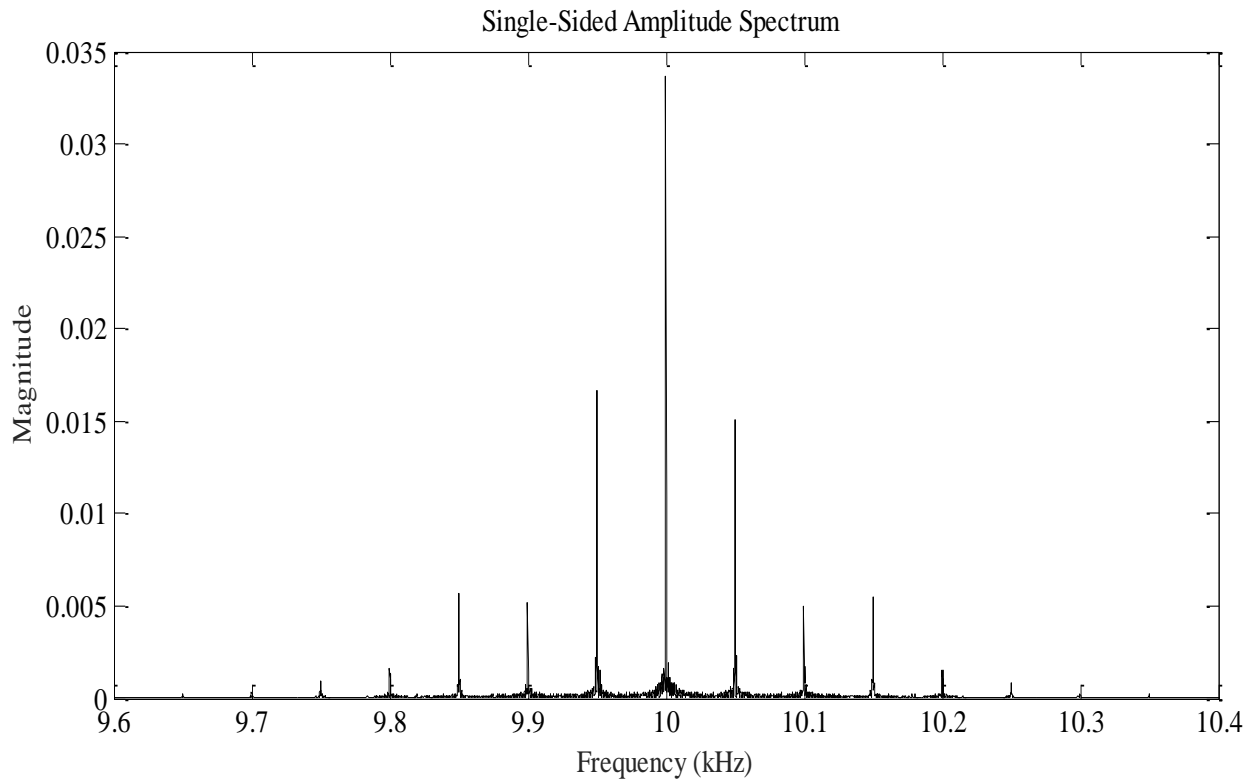
Figure 4-18: Simulation Current Oscillation under 50 Hz Vibration in AC Case

A Simulink model based on Equations 22 and 23 is developed. The layout is close to that's shown in Figure 4-14, but the differences are that the input voltage is at 10 kHz and the contact

115

resistance is with multiple harmonics. Figures 4-18 illustrates the circuit current in the frequency domain with oscillatory contact resistances. From the results, on the two sides of the basic signal frequency, a series of components are located with differences of input vibration's frequency, as observed in the experimental results.
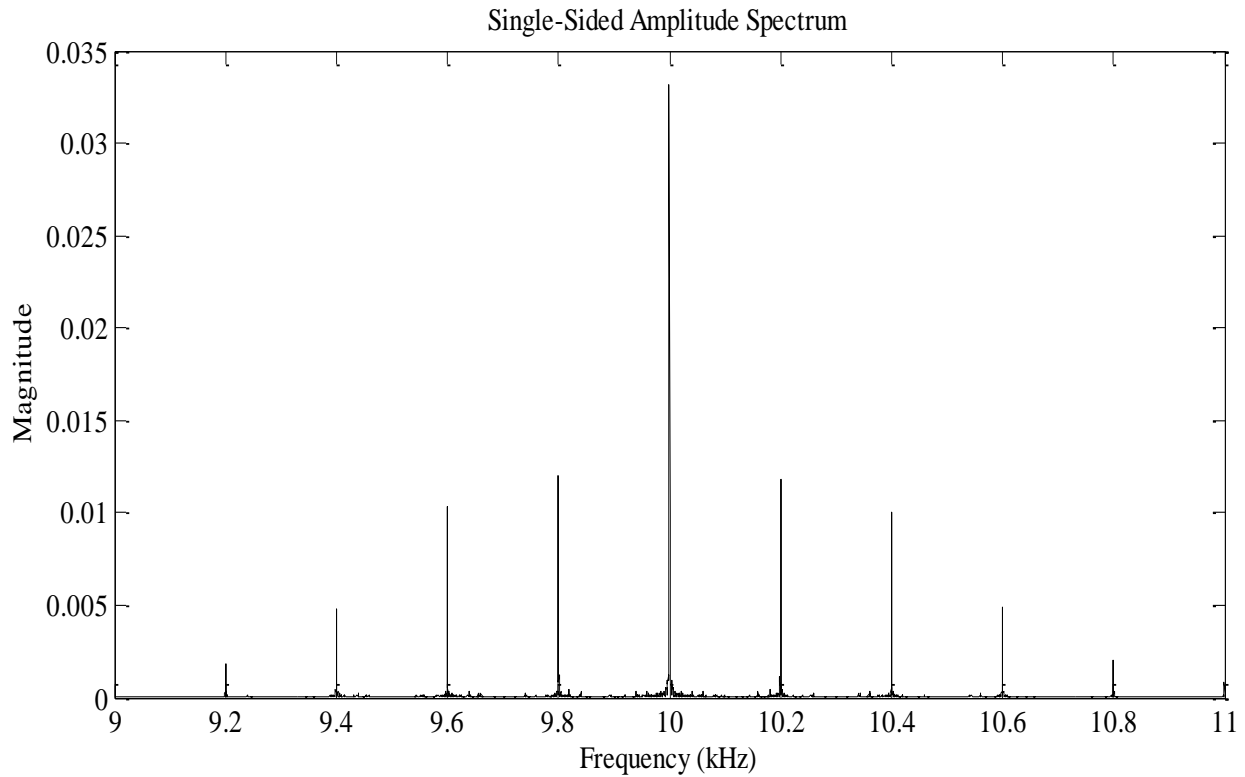
Figure 4-19: Simulation Current Oscillation under 200 Hz Vibration in AC Case

The Equation 22 can be rewritten in a state space format as

$$\begin{bmatrix} \dot{V_C} \\ \dot{I} \end{bmatrix} = \begin{bmatrix} -\dfrac{1}{C(t)}(\dfrac{1}{R_1(t)} + \dot{C}(t)) & \dfrac{1}{C(t)} \\ -\dfrac{1}{L} & -\dfrac{R_2}{L} \end{bmatrix} \begin{bmatrix} V_C \\ I \end{bmatrix} + \begin{bmatrix} 0 \\ \dfrac{1}{L} \end{bmatrix} V_{AC} \tag{24}$$

For a time varying linear system with a general state space representation in the following form

$$\dot{x}(t) = A(t)x(t) + B(t)u(t) \ , \tag{25}$$

the solution is expressed as [108][109]

116

$$x(t) = \Phi(t, t_0)x(t_0) + \int_{t_0}^{t} \Phi(t, \tau)B(\tau)u(\tau)d\tau \tag{26}$$

where $\Phi(t, \tau)$ is the state transition matrix. The most general transition matrix is described using

Peano-Baker series [109]

$$\Phi(t, \tau) = I_0 + \int_{\tau}^{t} A(\sigma_1)d\sigma_1 + \int_{\tau}^{t} A(\sigma_1) \int_{\tau}^{\sigma_1} A(\sigma_2)d\sigma_2 \, d\sigma_1$$

$$+ \int_{\tau}^{t} A(\sigma_1) \int_{\tau}^{\sigma_1} A(\sigma_2) \int_{\tau}^{\sigma_2} A(\sigma_3)d\sigma_3 \, d\sigma_2 \, d\sigma_1 \cdots = I_0 + \sum_{m=1}^{\infty} H_m(t, \tau) \tag{27}$$

where I_0 is an identity matrix. The $H_m(t, \tau)$ is given by

$$H_m(t, \tau) = \int_{\tau}^{t} A(\sigma_1) \int_{\tau}^{\sigma_1} A(\sigma_2) \int_{\tau}^{\sigma_2} A(\sigma_3) \cdots \int_{\tau}^{\sigma_m} A(\sigma_m)d\sigma_m \cdots d\sigma_3 \, d\sigma_2 \, d\sigma_1 \tag{28}$$

$$H_{m+1}(t, \tau) = \int_{\tau}^{t} A(\sigma_1)H_m(\sigma_1, \tau)d\sigma_1 \tag{29}$$

Matching like components in the preceding relation leads to the expression of the current as

$$I(t)$$

$$= \Phi(t, t_0)_{2,1}V_C(t_0) + \Phi(t, t_0)_{2,2}I(t_0) + \int_{t_0}^{t} \Phi(t, \tau)_{2,2} \cdot \frac{1}{L} \cdot V_{AC}(\tau)d\tau . \tag{30}$$

If the input voltage is a sinusoidal signal as

$$V_{AC}(t) = V_0\sin(\omega t), \tag{31}$$

it can be found the initial values of the states as

$$I(t_0) = \dot{I}(t_0) = V_C(t_0) = \dot{V}_C(t_0) = 0 . \tag{32}$$

This assumption helps to simplify Equation (12) into the following form

$$I(t) = \int_{t_0}^{t} \Phi(t, \tau)_{2,2} \cdot \frac{1}{L} \cdot V_{AC}(\tau)d\tau \tag{33}$$

where

$$\Phi(t, \tau)_{2,2} = I_0 + \sum_{m=1}^{\infty} H_m(t, \tau)_{2,2} . \tag{34}$$

To simplify the solution, C is assumed constant and $\dot{C}$ is zero. This is because, in the experiment, FFT was performed for a short duration, and contact capacitance was found to vary slowly as fretting proceeds. The second component of the Peano-Baker series is expressed as

$$H_1(t, \tau) = \int_{\tau}^{t} \begin{bmatrix} -\dfrac{1}{CR_1(\sigma_1)} & \dfrac{1}{C} \\ -\dfrac{1}{L} & -\dfrac{R_2}{L} \end{bmatrix} d\sigma_1 = \begin{bmatrix} \int_{\tau}^{t} -\dfrac{1}{CR_1(\sigma_1)} d\sigma_1 & \dfrac{1}{C}(t - \tau) \\ -\dfrac{1}{L}(t - \tau) & -\dfrac{R_2}{L}(t - \tau) \end{bmatrix} . \tag{35}$$

There is no periodic component in $H_1(t, \tau)_{2,2}$. The third component of the Peano-Baker series is expressed as

$$H_2(t, \tau) = \int_{\tau}^{t} A(\sigma_1) \begin{bmatrix} \int_{\tau}^{\sigma_1} -\dfrac{1}{CR_1(\sigma_2)} d\sigma_2 & \dfrac{1}{C}(\sigma_1 - \tau) \\ -\dfrac{1}{L}(\sigma_1 - \tau) & -\dfrac{R_2}{L}(\sigma_1 - \tau) \end{bmatrix} d\sigma_1$$

$$= \begin{bmatrix} \int_{\tau}^{t} [\dfrac{1}{C^2 R_1(\sigma_1)} \int_{\tau}^{\sigma_1} \dfrac{1}{R_1(\sigma_2)} d\sigma_2 - \dfrac{1}{LC}(\sigma_1 - \tau)] d\sigma_1 & \int_{\tau}^{t} (-\dfrac{1}{C^2 R_1(\sigma_1)} - \dfrac{R_2}{LC})(\sigma_1 - \tau) d\sigma_1 \\ \int_{\tau}^{t} [\dfrac{1}{LC} \int_{\tau}^{\sigma_1} \dfrac{1}{R_1(\sigma_2)} d\sigma_2 + \dfrac{R_2}{L^2}(\sigma_1 - \tau)] d\sigma_1 & \int_{\tau}^{t} (-\dfrac{R_2{}^2}{L^2} - \dfrac{1}{LC})(\sigma_1 - \tau) d\sigma_1 \end{bmatrix} . \tag{36}$$

There is also no periodic component in $H_1(t, \tau)_{2,2}$. The $H_3(t, \tau)_{2,2}$ is expressed as

$$H_3(t, \tau)_{2,2} = \frac{1}{L} \int_{\tau}^{t} \int_{\tau}^{\sigma_1} \left(\frac{1}{C^2 R_1(\sigma_2)} + \frac{R_2{}^3}{L^2} \right) (\sigma_2 - \tau) \, d\sigma_2 d\sigma_1 . \tag{37}$$

With respect to the observed periodic fluctuation of R_1 during fretting motion, using Fourier series, the reciprocal of R_1 can be described as

$$\frac{1}{R_1(t)} = \frac{P_0}{2} + \sum_{n=1}^{N} P_n \sin(\frac{2\pi n}{h} t + \emptyset_n) \tag{38}$$

where P_0 and P_n are considered constant in the short duration. Matching like components in the

118

preceding relation results in

$$H_3(t,\tau)_{2,2}$$

$$= \frac{1}{LC^2} \int_{\tau}^{t} \left\{ \left[\frac{P_0}{4} - \frac{R_2}{2L} \left(\frac{R_2{}^2}{L^2} - \frac{1}{LC} \right) \right] (\sigma_1{}^2 - \tau^2) + \frac{R_2}{L^2C} \left(\frac{1}{2} \sigma_1{}^2 - \tau\sigma_1 - \frac{3}{2}\tau^2 \right) \right.$$

$$- \frac{R_2\tau}{L} \left(\frac{1}{LC} - \frac{R_2{}^2}{L^2} \right) (\sigma_1 - \tau)$$

$$+ \sum_{n=1}^{N} \frac{P_n}{(\frac{2\pi n}{h})^2} \left[\sin\left(\frac{2\pi n}{h}\sigma_1 + \varnothing_n \right) - \sin\left(\frac{2\pi n}{h}\tau + \varnothing_n \right) \right.$$

$$\left. \left. - \frac{h}{2\pi n}\sigma_1\cos\left(\frac{2\pi n}{h}\sigma_1 + \varnothing_n \right) + \frac{h}{2\pi n}\tau\cos\left(\frac{2\pi n}{h}\tau + \varnothing_n \right) \right] \right\} d\sigma_1 \qquad (39)$$

where the periodic components are at the basic frequency and harmonic components of the input vibration that induces fretting motion. $H_3(t,\tau)_{2,2}$ is assumed the addition of $H_3(t,\tau)_{2,2[1]}$ and $H_3(t,\tau)_{2,2[2]}$ and all trigonometric components are in the second one. This leads to

$$\int_{t_0}^{t} H_3(t,\tau)_{2,2} \cdot \frac{1}{L} \cdot V(\tau)d\tau = \int_{t_0}^{t} (H_3(t,\tau)_{2,2[1]} + H_3(t,\tau)_{2,2[2]}) \cdot \frac{1}{L} \cdot V_{AC}(\tau)d\tau \qquad (40)$$

where

$$\int_{t_0}^{t} H_3(t,\tau)_{2,2[2]} \cdot \frac{1}{L} \cdot V_{AC}(\tau)d\tau$$

$$= \frac{V_0}{L^2C^2} \sum_{n=1}^{N} \frac{P_0}{(\frac{2\pi n}{h})^2} \left\{ A_1 \sin\left[\left(\frac{2\pi n}{h} + \omega \right)t + \varnothing_n \right] + A_2 \cos\left[\left(\frac{2\pi n}{h} + \omega \right)t + \varnothing_n \right] \right.$$

$$- A_3 \sin\left[\left(-\frac{2\pi n}{h} + \omega \right)t - \varnothing_n \right] + A_4\cos\varnothing_n + A_5\sin\varnothing_n$$

$$\left. + A_6 \cos\left[\left(-\frac{2\pi n}{h} + \omega \right)t - \varnothing_n \right] - \frac{t}{\omega}\sin\left[\frac{2\pi n}{h}t + \varnothing_n \right] + \frac{h}{\omega nt}\cos\left[\frac{2\pi n}{h}t + \varnothing_n \right] \right\}$$

and where

$$A_1 = [\frac{t}{2\omega} - \frac{t}{2\left(\frac{2\pi n}{h} + \omega\right)} - \frac{\pi n t}{h\left(\frac{2\pi n}{h} + \omega\right)^2}]$$

$$A_2 = \{\frac{h}{2n\omega\pi} - \frac{\frac{h}{2\pi n} + \frac{\pi n t^2}{h}}{\frac{2\pi n}{h} + \omega} + \frac{1}{\left(\frac{2\pi n}{h} + \omega\right)^2} + \frac{\pi n\left[\left(\frac{2\pi n}{h} + \omega\right)^2 t^2 + \frac{4\pi n\omega t^2}{h} + \omega^2 t^2 - 2\right]}{h\left(\frac{2\pi n}{h} + \omega\right)^3}\}$$

$$A_3 = [\frac{t}{2\omega} + \frac{t}{2\left(\frac{2\pi n}{h} + \omega\right)} - \frac{\frac{3\pi n}{h} t}{\left(\frac{2\pi n}{h} + \omega\right)^2}]$$

$$A_4 = [-\frac{h}{2\pi n\left(\frac{2\pi n}{h} + \omega\right)} + \frac{4\pi n}{h\left(\frac{2\pi n}{h} - \omega\right)^3}]$$

$$A_5 = -\frac{t}{2\left(\frac{2\pi n}{h} + \omega\right)}$$

$$A_6 = \{\frac{h}{2\omega\pi n} + \frac{\frac{h}{2\pi n} + \frac{\pi n t^2}{h}}{\frac{2\pi n}{h} - \omega} + \frac{1}{\left(\frac{2\pi n}{h} - \omega\right)^2} + \frac{\pi n\left[\left(\frac{2\pi n}{h}\right)^2 t^2 - \frac{4\pi n\omega t^2}{h} + \omega^2 t^2 - 2\right]}{h\left(\frac{2\pi n}{h} - \omega\right)^3}\}$$

The periodic components are at the voltage frequency, ω, and the around it with differences in

$\frac{2\pi n}{h}$ which are basic and harmonic frequencies of input vibration frequency. Based on the

derivation above, this influence of fretting motion is involved in $H_m(t, \tau)_{2,2}$ for m is larger than

3.

This solution matches the inter-modulation effects observed in the frequency behavior of

current in the experiment part. This phenomenon also implies that the low pass filter is not able

to eliminate the low frequency interference, because it is not an electrical signal. Due to the

fretting motion, oscillatory contact resistance impacts the frequency behavior of the transmission

line, and then distorts the transferred signals no matter which frequencies they are at.

4.5 Summary and Conclusion

In this study, a series of experimental and modeling work has been performed for an understanding of the impact of fretting motion to signal transfer. For the DC principle, fretting motion brings about the fluctuation of contact resistance which distorts the DC signal through producing an oscillation of contact resistance at the basic and harmonic frequencies of the input vibration. For the AC signal, fretting motion results in various inter-modulation components around the frequency of transferred signals. The analytical solution of the testing circuit has validated the experimental findings.

The understanding naturally lends itself to a fault detection strategy of electrical connectors and interconnections that are undergoing vibration induced fretting corrosion. The distortion behavior is characterized by additional tones in the frequency domain of which the profile is determined by the properties of relative motion at the contact interface. Compared to stationary degraded contacts, impact of fretting motion is not limited in the low frequency range, but at the spectrum near the transferred signal. Due to the inter-modulation effects, some inter-modulation components appear around the signal frequencies no matter how high they are. In addition, the frequency differences between them are relatively low because the mechanical vibration is often at the frequencies much lower than electrical transmission. This inter-modulation effect cannot be diminished by a low pass filter because, rather than a disturbing signal, the oscillating resistance is the key of the interference. On account of the occurrence of the interrupting behavior at the very early stage of the increase of contact resistance, the targeted acquisition is in favor of a timely failure diagnosis.

CHAPTER 5   CONCLUSIONS AND RECOMMENDATIONS

A study of the high frequency behavior of the electrical contacts subjected to fretting degradation has been described in this dissertation. Experimental analysis accompany with corresponding modeling validations was performed to evaluate the impact of the degraded contacts to high frequency data transmission. The dissertation consists of three chapters.

First of all, a research on contact impedance development in the electrical contact under vibration induced fretting corrosion was introduced. In the contact of a pair of tin coated copper connector pins, the contact impedance was measured at various degradation levels. With a higher contact resistance, capacitive characteristics gradually showed up with a high-pass filter performance whose cut-off frequency tended to decrease. Using the RC parallel circuit, the effective contact capacitance was extracted and was found in a decreasing fashion with a longer fretting period. Incorporating acquired surface parameters experimentally, a statistical tribology model was proposed to account for the development of capacitance. The finding validated that , due to the build-up of the insulating layer between two sides of the contact surfaces, increased resistance and decreased capacitance influenced the data transmission at the low frequency range.

In the second part, the influence of degraded contacts to high frequency data transmission line was investigated. A microstrip based transmission configuration involving contacts was designed for an experimental study. It was found that the influence fretting corrosion was significantly at the low frequency spectrum. Incorporating the information of contact impedance in the first study, a network model was proposed to account for the testing results. The network with a fresh contact was optimized to match the original testing circuit. After comparison, a well

correlation between the experimental and modeling results was achieved.

In the third part, an investigation of fretting motion induced effects was performed based on the DC and AC principles. Due to the non-uniformly distributed oxidation products in the fretting track, the higher electrical resistance has been noticeable at the ends of the fretting area. During the fretting motion, resistance oscillates periodically at the basic and harmonic frequency of the input vibration. The fretting motion caused the inter-modulation effect between the transferred signal and the input vibration. Inter-modulation components were observed around the frequency of transmitted signals. A circuit model was developed according to the testing configuration. The analytic solution of the dynamic circuit system validated that this phenomenon resulted from the resistance oscillation. In addition, the analytical solution of dynamic contact impedance was well correlated with the disturbance observed in the second study.

There is certainly a great deal of fertile ground for further studies on the topics of the high frequency performance of electrical contacts subjected to vibration-induced fretting corrosion. Some suggestions for future work in this area are:

- Investigation of the influence of triboogical and coating parameters on the development of contact impedance.
- Study of the influence of various parameters, such as fretting amplitude, normal force, frequency on the contact impedance.
- High frequency behavior of a connector system considering the contact geometry, housing design, cable design, etc..
- Study of the contact impedance and impact to high frequency data transmission of electrical contacts subjected to rotary fretting motion.

- Contact capacitance behavior at difference locations of the fretting track.

REFERENCES

[1]   ASM Handbook, Vol.13 "Corrosion", ASM International, 1987

[2]   M. G. Fontana, Corrosion Engineering, McGraw-Hill Book, New. York, 1986

[3]   J. Williams, Engineering Tribologhy, New York: Cambridge University Press, 2005

[4]   C. Lipson and L. V. Colwell; Handbook of mechanical wear: wear, frettage, pitting, cavitation, corrosion; University of Michigan Press, 1961; p. 449.

[5]   R. B. Waterhouse, "Fretting Corrosion", Oxford Pergamon Press, USA.1972

[6]   I-Ming Feng and H. Uhlig, Journal of Applied Mechanics, 21, 395 (1954)

[7]   M. D. Bryant, "Resistance Buildup in Electrical Connectors Due to Fretting Corrosion of Rough Surfaces", IEEE Transactions on Components, Packaging And Manufacturing Technology, Part A, vol. 17, 1994, pp. 86-95

[8]   Sakmann, B. W., and B. G. Rightmire. "An Investigation of Fretting Corrosion under Several Conditions of Oxidation." (1948).

[9]   E.M. Bock and J.H. Whitley, "Fretting Corrosion in Electric Contacts", Proceedings of Holm Conference on Electrical Contacts, 1974, pp. 128-138.

[10]   Freitag, W., "Lubricants for Separable Connectors," Parts, Hybrids, and Packaging, IEEE Transactions on , vol.13, no.1, pp.72,78, Mar 1977

[11]   Antler, M., "Fretting Corrosion of Solder-Coated Electrical Contacts," Components, Hybrids, and Manufacturing Technology, IEEE Transactions on , vol.7, no.1, pp.129,138, Mar 1984

[12]   Antler, M., "Effect of Fretting on the Contact Resistance of Palladium Electroplate Having a Gold Flash, Cobalt-Gold Electroplate, and DG R156," Components, Hybrids, and Manufacturing Technology, IEEE Transactions on , vol.7, no.4, pp.363,369, Dec 1984

[13]   Braunovic, M., "Evalutation of Different Types of Contact Aid Components for Aluminum-to-Aluminum Connectors and Conductors," Components, Hybrids, and Manufacturing Technology, IEEE Transactions on , vol.8, no.3, pp.313,320, Sep 1985

[14]   Braunovic, M., "Fretting in Ni-coated aluminum conductors," Components, Hybrids, and Manufacturing Technology, IEEE Transactions on , vol.14, no.2, pp.327,336, Jun 1991

[15]   Antler, M.; Sproles, E., "Effect of Fretting on the Contact Resistance of Palladium," Components, Hybrids, and Manufacturing Technology, IEEE Transactions on , vol.5, no.1, pp.158,166, Mar 1982

[16]   Antler, M., "Survey of Contact Fretting in Electrical Connectors," Components, Hybrids, and Manufacturing Technology, IEEE Transactions on , vol.8, no.1, pp.87,104, Mar 1985

[17]   Y. Shibata et al., "Detailed analysis of contact resistance of fretting corrosion track for the tin plated contacts," 26th International Conference on Electrical Contacts (ICEC 2012), Beijing, 2012, pp. 228-232.doi: 10.1049/cp.2012.0652

[18]   Ambier, J.; Perdigon, P., "Fretting Corrosion of Separable Electrical Contacts," Components, Hybrids, and Manufacturing Technology, IEEE Transactions on, vol.8, no.1, pp.197,201, Mar 1985

[19]   R. D. Malucci, "Impact of fretting parameters on contact degradation," Electrical Contacts - 1996. Proceedings of the Forty-Second IEEE Holm Conference on Electrical Contacts. Joint with the 18th International Conference on Electrical Contacts, Chicago, IL, USA, 1996, pp. 395-403.

[20]   Ed P. Slade, "Electrical Contacts: Principles and Applications", Chapter 6, 1990

[21]   S. Hannel S. Fouvry. Ph. Kaaspa, L. Vincent 'The Fretting Sliding Transition as a Criterion for Electrical Contact Performance', Wear, vol. 249, 2001, 761-770

[22]   Y. Park, T.S.N. S. Narayanan, K. Lee, "Effect of Temperature on the Fretting Corrosion of Tin Plated Copper Alloy Contacts", Wear, vol. 262, 2007, pp. 320–330

[23]   Aukland, N.; Hardee, H.; Wehr-Aukland, A.; Lees, P., "A comparison of a clad material (65Au21Pd14Ag) and an electroplated gold over palladium material system under fretting conditions at elevated temperatures," Electrical Contacts, 1999. Proceedings of the Forty-Fifth IEEE Holm Conference on , vol., no., pp.213,224, 4-6 Oct. 1999

[24]   Ji Wu; Pecht, M., "Fretting corrosion studies for lead-free alloy plated contacts," Electronics Packaging Technology Conference, 2002. 4th , vol., no., pp.20,24, 10-12 Dec. 2002

[25]   "Chemistry of Oxygen". Chemwiki UC Davis. Retrieved 2016-05-01

[26]   J. Song, C. Koch, and L. Wang, "Correlation betweenWear Resistance and Lifetime of Electrical Contacts", Hindawi Publishing Corporation Advances in Tribology, vol. 2012, pp. 9.

[27]   Mottine, J.; Reagor, B.T., "Investigation of Fretting Corrosion at Dissimilar Metal Interfaces in Socketed IC Device Applications," Components, Hybrids, and Manufacturing Technology, IEEE Transactions on , vol.7, no.1, pp.61,68, Mar 1984

[28]   Mottine, J.; Reagor, B.T., "The Effect of Lubrication on Fretting Corrosion at Dissimilar Metal Interfaces in Socketed IC Device Applications," Components, Hybrids, and Manufacturing Technology, IEEE Transactions on , vol.8, no.1, pp.173,181, Mar 1985

[29]   Bock, E., "Mateability of tin to gold, palladium, and silver," Electronic Components and

Technology Conference, 1990. ., 40th , vol., no., pp.840,844 vol.1, 20-23 May 1990

[30]   Sproles, E.; Drozdowicz, M., "Comparison of the Stability of Gold and Palladium Alloy Connector Contacts Subjected to Vibration," Components, Hybrids, and Manufacturing Technology, IEEE Transactions on , vol.9, no.4, pp.480,484, Dec 1986

[31]   Shirakawa, R.; Suzuki, S.; Matsuda, A.; Shibata, N., "Cd-free silver alloy for sliding contact," Electrical Contacts, 1992., Proceedings of the Thirty-Eighth IEEE Holm Conference on , vol., no., pp.119,124, 18-21 Oct. 1992

[32]   Lee, A.; Mamrick, M., "Fretting corrosion of Tin-plated copper alloy," Components, Hybrids, and Manufacturing Technology, IEEE Transactions on , vol.10, no.1, pp.63,67, Mar 1987

[33]   X. Lin, L. Xu, Y. Shao, G. Luo, H. Zhang "Research on Fretting Resistance and Fretting Wear Property of Ni-Au Contact Pair", Proceedings of Holm Conference on Electrical Contacts, vol. 57, 2011, pp. 11-14

[34]   Braunovic, M.; Trudeau, M.L.; He, A., "Effect of ion-implantation on the contact resistance of copper and silver-copper electrical contacts under fretting conditions," Electrical Contacts, 1994. Proceedings of the Fortieth IEEE Holm Conference on Electrical Contacts , vol., no., pp.195,210, 17-19 Oct. 1994

[35]   Braunovic, M.; Trudeau, M.; Bryden, K.; Ying, J.Y., "Contact resistance behavior of nanocrystalline copper and palladium films under fretting conditions," Electrical Contacts, 1995., Proceedings of the Forty-First IEEE Holm Conference on , vol., no., pp.71,82, 2-4 Oct. 1995

[36]   Trudeau, M.L.; Braunovic, M.; Bryden, K.J.; Ying, J.Y., "Fretting studies of nanocrystalline Pd, Pd-Ag and Pd-Y films," Electrical Contacts, 1996. Proceedings of the

Forty-Second IEEE Holm Conference on ??. Joint with the 18th International Conference on Electrical Contacts , vol., no., pp.383,394, 16-20 Sept. 1996

[37]   S. Fouvry, P. Jedrzejczyk, P. Chalandon, "Introduction of an Exponential Formulation to Quantify the Electrical Endurance of Micro-contacts Enduring Fretting Wear: Application to Sn, Ag and Au Coatings", Wear, vol. 271, 2011, pp. 1524– 1534

[38]   T. Ito, S. Sawada, Y. Hattori, Y. Saitoh, T. Tamai and K. Iida, "Microscopy Study of Fretting Corrosion Caused by the Tin Plating Thickness," 2008 Proceedings of the 54th IEEE Holm Conference on Electrical Contacts, Orlando, FL, 2008, pp. 294-300.

[39]   Braunovic, M.; McIntyre, N.; Chauvin, W.; Aitchison, I., "Surface Analysis of Fretting Damage in Electrical Contacts of Aluminum with different Contact Materials," Components, Hybrids, and Manufacturing Technology, IEEE Transactions on , vol.7, no.1, pp.96,106, Mar 1984

[40]   T. Ito, M. Matsushima, K. Takata and Y. Hattori, "Factors Influencing the Fretting Corrosion of Tin Plated Contacts," Electrical Contacts - 2006. Proceedings of the 52nd IEEE Holm Conference on Electrical Contacts, Montreal, QC, 2006, pp. 267-272.

[41]   T. Ito, Y. Nomura and Y. Hattori, "Three-Dimensional Structural Study of Tin Plated Fretting Contacts," 2009 Proceedings of the 55th IEEE Holm Conference on Electrical Contacts, Vancouver, British Columbia, Canada, 2009, pp. 319-323.

[42]   Swingler, J.; McBride, J.W., "Fretting corrosion studies of an extrinsic conducting polymer and tin interface," Electrical Contacts, 2001. Proceedings of the Forty-Seventh IEEE Holm Conference on , vol., no., pp.215,219, 2001

[43]   Lam, L.; McBride, J.W.; Swingler, J., "The fretting characteristics of intrinsically conducting polymer contacts," Electrical Contacts, 2005. Proceedings of the Fifty-First

IEEE Holm Conference on , vol., no., pp.196,203, 26-28 Sept. 2005

[44]   Heaton, C.E.; McCarthy, S.L., "High cycle fretting corrosion studies on tin-coated contact materials," Electrical Contacts, 2001. Proceedings of the Forty-Seventh IEEE Holm Conference on , vol., no., pp.209,214, 2001

[45]   D. Gagnon and M. Braunovic, "Fretting in copper-to-copper contacts under AC and DC current conditions," in IEEE Transactions on Components and Packaging Technologies, vol. 24, no. 3, pp. 378-383, Sep 2001

[46]   R. D. Malucci, "Multispot Model of Contacts Based on Surface Features", Electric Contacts- 1990, IEEE- HOLM, Montreal, 1990, p.625

[47]   R. D. Malucci, "Dynamic Model of Stationary Contacts Based on Random Variations of Surface Features," Components, Hybrids, and Manufacturing Technology, IEEE Transactions on , vol.15, no.3, June 1992

[48]   R. D. Malucci, "Making Contact to Aged Surfaces," Components, Hybrids, and Manufacturing Technology, IEEE Transactions on , vol.16, no.4, June 1993

[49]   R. D. Malucci, "The effects of wipe on contact resistance of aged surfaces," Proceedings of IEEE Holm Conference on Electrical Contracts, 1994, pp. 131-144.

[50]   R. D. Malucci, "Accelerated testing of tin-plated copper alloy contacts," in IEEE Transactions on Components and Packaging Technologies, vol. 22, no. 1, pp. 53-60, Mar 1999.

[51]   F. Xie, Thesis "A Study of Electrical Connector Performance in Fretting", Auburn University, 2003

[52]   G Villeneuve, D. Kulkami, P. Batnagel and D. Berry, "Dynamic Finite Element Analysis Simulation of the Terminal Crimping Process", Electrical Contacts, 1996, Proceedings of

the Forty- Second IEEE Holm Conference Joint with the 18th International Conference on Electrical Contacts, Sept. 1996, pp. 156-172

[53]   A. Monnier, B. Froidurot, C. Jarrige, R. Meyer and P. Teste, "A Mechanical Electrical, Thermal Coupled- field Simulation of a Sphere- plane Electrical Contact", Electrical Contacts, 2005. Proceedings of the Fifthy- First IEEE Holm Conference on Sept. 26- 28, 2005, pp: 224-231

[54]   J. Swingler, J.W. Bride, and C. Maul, "The Degradation of Road Tested Automotive Connectors", IEEE Transactions on Components and Packaging Technology (CPMT), 2000, 23(1), p. 157- 164

[55]   Van Dijk, Piet, and M. van Meijl. "Contact Problems due to Fretting and their Solution." AMP Journal of Technology 5 (1996): 14ff.

[56]   G. T. Flowers, F. Xie, and M. J. Bozack, Robert D. Malucci "Vibration Thresholds for Fretting Corrosion in Electrical Connectors" IEEE Transactions on Components and Packaging Technologies, vol.27, 2004, pp.65-71.

[57]   G. T. Flowers, F. Xie, M. J. Bozack, X. Hai, B. I. Rickett, and R. D. Malucci," A Study of the Physical Characteristics of Vibration-Induced Fretting Corrosion" . Proceedings of Holm Conference on Electrical Contacts, vol. 50, 2004, pp 31-319.

[58]   F. Xie et al., "Analysis and Prediction of Vibration-Induced Fretting Motion in a Blade/Receptacle Connector Pair," in IEEE Transactions on Components and Packaging Technologies, vol. 32, no. 3, pp. 585-592, Sept. 2009.

[59]   C. Chen, G. T. Flowers, M, J. Bozack, J. Suhling, B.I. Rickett; B.J. Malucci, C. Manlapaz, "Modeling and Analysis of a Blade/Receptacle Pair for the Prediction of Vibration-Induced

Fretting Degradation" Proceedings of Holm Conference on Electrical Contacts, vol. 54, 2008, pp: 276-283

[60]   C. Chen, G. T. Flowers, M. J. Bozack; J. Suhling, "Modeling and Analysis of a Connector System for the Prediction of Vibration-induced Fretting Degradation", Proceedings of Holm Conference on Electrical Contacts, vol. 55, 2009, pp. 131-137

[61]   J. Gao, C. Chen, G.T. Flowers, R.L. Jackson and M.J. Bozack "The Influence of Particulate Contaminants on Vibration- Induced Fretting Degradation in Electrical Connectors", Proceedings of Holm Conference on Electrical Contacts, vol. 56, 2010, pp. 1-5

[62]   J. Gao, C. Chen, G.T. Flowers, R.L. Jackson and M.J. Bozack "The Influence of Particulate Contaminants on Vibration- Induced Fretting Degradation in Electrical Connectors", Proceedings of Holm Conference on Electrical Contacts, vol. 56, 2010, pp. 1-5

[63]   F. Zhang and G. T. Flowers, "Fretting corrosion in electric connectors induced by axial vibration," 2014 IEEE 60th Holm Conference on Electrical Contacts (Holm), New Orleans, LA, 2014, pp. 1-8.

[64]   L. Lam, J. W. McBride, C. Maul and J. K. Atkinson, "Displacement Measurement at the Connector Contact Interface Employing a Novel Thick Film Sensor", Electrical Contacts, 2005. Proceedings of the Fifty- First IEEE Holm Conference on 26-28, 2005 pp: 89-96

[65]   R. Fu, S. Choe, R. L. Jackson, G. T. Flowers. "Experimental Study of the Vibration-induced Fretting of Silver-plated High Power Automotive Connectors", Proceedings of Holm Conference on Electrical Contacts, vol. 56, 2010, pp. 4-7

[66]   S. V. Angadi, W. E. Wilson, R. L. Jackson, G. T. Flowers, B.I. Rickett "A Multi-physics Finite Element Model of an Electrical Connector Considering Rough Surface Contact", Proceedings of Holm Conference on Electrical Contacts ,vol. 54 ,2008, pp. 168-177.

[67]   C. T. Dervos and J. M. Michaelides, "The effect of contact capacitance on current-voltage characteristics of stationary metal contacts," in IEEE Transactions on Components, Packaging, and Manufacturing Technology: Part A, vol. 21, no. 4, pp. 530-540, Dec. 1998.

[68]   R. D. Malucci, "High frequency considerations for multi-point contact interfaces," Proceedings of the Forth-Seventh IEEE Holm Conference on Electrical Contacts (IEEE Cat. No.01CH37192), Montreal, Que., 2001, pp. 175-185.

[69]   R. D. Malucci, "The impact of contact resistance on high speed digital signal transmission," Proceedings of the Forty-Eighth IEEE Holm Conference on Electrical Contacts, 2002, pp. 212-220.

[70]   R. D. Malucci and A. P. Panella, "Wave Propagation and High Frequency Signal Transmission across Contact Interfaces," Electrical Contacts - 2006. Proceedings of the 52nd IEEE Holm Conference on Electrical Contacts, Montreal, QC, 2006, pp. 199-206.

[71]   R. D. Malucci and A. P. Panella, "Contact Physics of Capacitive Interconnects," in IEEE Transactions on Components, Packaging and Manufacturing Technology, vol. 3, no. 3, pp. 377-383, March 2013.

[72]   Timsit, Roland S. "High speed electronic connectors: A review of electrical contact properties."IEICE transactions on electronics 88, no. 8 (2005): 1532-1545.

[73]   Dervos, C.T.; Novakovic, J.; Vassiliou, P., "Electroless Ni-B and Ni-P coatings with high-fretting resistance for electrical contact applications," Electrical Contacts, 2004. Proceedings of the 50th IEEE Holm Conference on Electrical Contacts and the 22nd

International Conference on Electrical Contacts , vol., no., pp.281,288, 20-23 Sept. 2004

[74] Ji Wu; Pecht, M.G., "Contact resistance and fretting corrosion of lead-free alloy coated electrical contacts," Asian Green Electronics, 2004. AGEC. Proceedings of 2004 International IEEE Conference on the , vol., no., pp.127,135, 2004

[75] Xin Wang; Xueyan Lin; Weimin Yang, "The Research of The Gold Plating Product's Fretting Characteristic," Information Acquisition, 2006 IEEE International Conference on , vol., no., pp.1244,1247, 20-23 Aug. 2006

[76] R.D. Malucci, "Fretting Corrosion Degradation, Threshold Behavior and Contact Instability", Ragnal Holm Scientific Achievement Award Address, Proceedings of the 49th IEEE Holm Conference on Electrical Contacts, pp. 1-15, Washington, D.C., September 8-10, 2003

[77] Zhang Hao; Gao Jinchun; Yu Cuiping; Chen Chen, "Wavelet analysis for the fault detection in electrical connectors," Electrical Contacts (ICEC 2012), 26th International Conference on , vol., no., pp.301,305, 14-17 May 2012

[78] Jinchun Gao; Hao Zhang; Rui Ji; Chen Chen; Gang Xie; Cuiping Yu, "Fault Detection of Electrical Connectors in RF Circuits Using a Wavelet Transform Approach,"Holm Conference on Electrical Contacts (HOLM) , 2013 IEEE 59th , vol., no., pp.1,6, 22-25 Sept. 2013

[79] Rui Ji; Jinchun Gao; Gang Xie; Flowers, G.T.; Chen Chen, "A fault diagnosis method of communication connectors in wireless receiver front-end circuits," Electrical Contacts (Holm), 2014 IEEE 60th Holm Conference on , vol., no., pp.1,6, 12-15 Oct. 2014

[80] R. Ji, J. Gao, G. Xie, G. T. Flowers and Q. Jin, "The impact of coaxial connector failures on high frequency signal transmission," 2015 IEEE 61st Holm Conference on Electrical

Contacts (Holm), San Diego, CA, 2015, pp. 298-303.

[81]   Agilent 4294A High Precision Impedance Analyzer Operation Manual, Fifth Edition, March 2002.

[82]   Laser Vibrometer User Manual, Controller OFV-2610/2620, Sensor Head OFV-353, POLYTEC Co., Germany

[83]   HP 35665A Dynamic Signal Analyzer Installation and Verification Guide, Hewlett-Packard Company, USA, 1991

[84]   Y. Kimura, " Estimation of the number and mean area of real contact points on the basis of surface profiles," Wear, vol. 15, pp. 47-55, 1970.

[85]   J. Tripp and S. Garte, "The Gas-Tightness of Separable Base Metal Electric Contacts," in IEEE Transactions on Components, Hybrids, and Manufacturing Technology, vol. 4, no. 1, pp. 85-92, Mar 1981. doi: 10.1109/TCHMT.1981.1135778

[86]   M. Braunovic, V. V. Konchits and N. K. Myshkin, Electrical Contacts: Fundamentals Applications and Technology, 2006, CRC Press.

[87]   Sauger, E., S. Fouvry, L. Ponsonnet, Ph Kapsa, J. M. Martin, and L. Vincent. "Tribologically transformed structure in fretting." Wear 245, no. 1 (2000): 39-52.

[88]   R. D. Malucci, "Characteristics of films developed in fretting experiments on tin plated contacts," in IEEE Transactions on Components and Packaging Technologies, vol. 24, no. 3, pp. 399-407, Sep 2001. doi: 10.1109/6144.946486

[89]   S. Noël, D. Alamarguy, L. Baraton and P. Laurat, "Influence of contact interface composition on the electrical and tribological properties of nickel electrodeposits during fretting tests," Electrical Contacts (ICEC 2012), 26th International Conference on, Beijing, 2012, pp. 221-227.

[90]   R. Brahimi, Y. Bessekhouad, N. Nasrallah, M. Trari, "Visible light CrO4(2-) reduction using the new CuAlO2/CdS hetero-system," Journal of Hazardous Materials, 219-220 (2012) 19-25

[91]   N.H. Winchell and A.N. Winchell, "Elements of optical mineralogy: an introduction to microscopic petrography. Part 2: description of minerals, with special reference to their optical and microscopic characters", 2nd. Ed., New York: Wiley, 1927

[92]   W. E. Boggs, P. S. Trozzo and G. E. Pellissier, "The Oxidation of Tin: II . The Morphology and Mode of Growth of Oxide Films on Pure Tin", J. Electrochem. Soc. 1961 108(1): 13-24; doi:10.1149/1.2428003

[93]   Peddada, Srikanth. "Signal Integrity Analysis of Transmission Lines in Anisotropic Substrates for High-Speed Data Transmission." PhD diss., Auburn University, 2013.

[94]   Walt Kester. "Tips about PCB design: Part 2 - Single-card grounding for multicard systems" ; Embedded cracking the code to systems development, 2008.

[95]   Symmetric Stripline Analysis/Synthesis calculator, Dan McMahill,CGI,2001-2009.

[96]   Brian C. Wadell." Introduction to Common Printed Circuit Transmission Lines" . Artech House, Maxim Integrated Products. ISBN 0-89006-436-9,2003.

[97]   http://en.wikipedia.org/wiki/Scattering_parameters

[98]   David M. Pozar, 4th edition "Microwave Engineering", Wiley publications, ISBN :9780470631553, 2012.

[99]   Basics, Agilent Network Analyzer. "Agilent Technologies." Inc., USA (2004): 1-94.

[100] The Basics of Signal integrity, Part I, Transmission line effects, Altera Corporation.

[101] R. Enquebecq et al., "Effect of fretting wear damage in RF connectors subjected to vibration: DC contact resistance and phase-noise response," 2015 IEEE 61st Holm Conference on Electrical Contacts (Holm), San Diego, CA, 2015, pp. 22-28.

[102] http://www.bkprecision.com/products/signal-generators/4011A-5-mhz-function-generator.html

[103] http://www.keysight.com/en/pd-836433-pn-E3631A/80w-triple-output-power-supply-6v-5a-25v-1a?cc=US&lc=eng

[104] http://www.lem.com/hq/en/component/option,com_catalog/task,displaymodel/id,90.37.09.000.0/

[105] http://sine.ni.com/nips/cds/view/p/lang/en/nid/209139

[106] E. Carvou and N. Ben Jemaa, "Statistical Study of Voltage Fluctuations in Power Connectors During Fretting Vibration," in IEEE Transactions on Components and Packaging Technologies, vol. 32, no. 2, pp. 268-272, June 2009.doi: 10.1109/TCAPT.2009.2019633

[107] S. E. Mossouess et al., "Analysis of temporal and spatial contact voltage fluctuation during fretting in automotive connectors," ICEC 2014; The 27th International Conference on Electrical Contacts, Dresden, Germany, 2014, pp. 1-5.

[108] Baake, M.; Schlaegel, U. (2011). "The Peano Baker Series". Proceedings of the Steklov Institute of Mathematics. 275. pp. 155–159.

[109] Brogan, W.L. (1991). Modern Control Theory. Prentice Hall. ISBN 0-13-589763-7.

[110] Arfken, G. Mathematical Methods for Physicists, 3rd ed. Orlando, FL: Academic Press, pp. 440-445, 1985.

[111] Rawashdeh, M., and Shehu Maitama. "Solving nonlinear ordinary differential equations

using the NDM." *Journal of Applied Analysis and Computation* 5, no. 1 (2015): 77-88.